NATIONAL AERONAUTICS AND SPACE ADMINISTRATION

Technical Report 32-1331

An Ambiguity in the Orbit Determination of Planetary Flyby Trajectories

W. E. Bollman

JET PROPULSION LABORATORY
CALIFORNIA INSTITUTE OF TECHNOLOGY
PASADENA, CALIFORNIA

November 1, 1968

NATIONAL AERONAUTICS AND SPACE ADMINISTRATION

Technical Report 32-1331

An Ambiguity in the Orbit Determination of Planetary Flyby Trajectories

W. E. Bollman

JET PROPULSION LABORATORY
CALIFORNIA INSTITUTE OF TECHNOLOGY
PASADENA, CALIFORNIA

November 1, 1968

TECHNICAL REPORT 32-1331

Prepared Under Contract No. NAS 7-100
National Aeronautics & Space Administration

Preface

The work described in this report was performed by the Systems Division of the Jet Propulsion Laboratory.

Acknowledgments

This investigation was accomplished for a master's thesis while the author was employed by the Jet Propulsion Laboratory, which supported the work. The author is indebted to Dr. B. D. Tapley of the University of Texas at Austin for supervising the research and to Dr. W. Fowler and Dr. P. Russell for serving on the thesis committee. The author would like to thank several employees of the Jet Propulsion Laboratory for their assistance: Mr. E. Cutting and Mr. F. Sturms for supporting the study; Dr. J. F. Jordan for his assistance regarding the theoretical work; Mr. N. Haynes, Mr. D. Curkendall, and Mr. T. Duxbury for their suggestions regarding the theoretical work; Mrs. B. Paulson and Mrs. H. Ling for their assistance with the computer programs; and Miss M. Beckwith for her plotting assistance.

Contents

Contents (contd)

Figures

Contents (contd)

Figures (contd)

Contents (contd)

Figures (contd)

Contents (contd)

Figures (contd)

Abstract

As new space missions from earth to the planets are designed, the requirements for accurately estimating the trajectory in flight will in general increase to complement the more complex scientific desires. Conventional methods of in-flight orbit determination, such as two-way-doppler and range measurements from one or more ground tracking stations, have demonstrated the high accuracy that can be achieved. Traditionally the accuracy of orbit estimation becomes very good near the planet when the spacecraft speeds up under the planet's gravitational attraction and thus as the doppler changes are magnified. The purpose of this study is to analyze the geometrical properties of spacecraft doppler measurements made near a planet and to show that under certain situations an orbit-determination program could converge to an incorrect solution for the planet-centered inclination of the spacecraft hyperbolic orbital plane. Ways of correcting the situation are also presented.

An Ambiguity in the Orbit Determination of Planetary Flyby Trajectories

I. Introduction

The primary concern in the determination of the orbit of a spacecraft during a mission is to estimate the miss vector and the time that the spacecraft will fly by the planet. The knowledge of these parameters is important to the success of the mission if precision-pointing instruments aboard the spacecraft are to scan the planet. An initial uncertainty of the spacecraft's position and velocity in heliocentric space prior to planet arrival will result in a position uncertainty as the spacecraft passes the planet. Figure 1 demonstrates this position uncertainty. As the spacecraft approaches the planet and speeds up under the planet's gravitational influence, the orbit determination of the spacecraft's near-planet trajectory becomes more accurate. This occurs because the velocity of the spacecraft is changing more rapidly at this time, which in turn causes the scalar speed (range rate) between the earth and the spacecraft, and thus the doppler-frequency measurement, to change more rapidly.

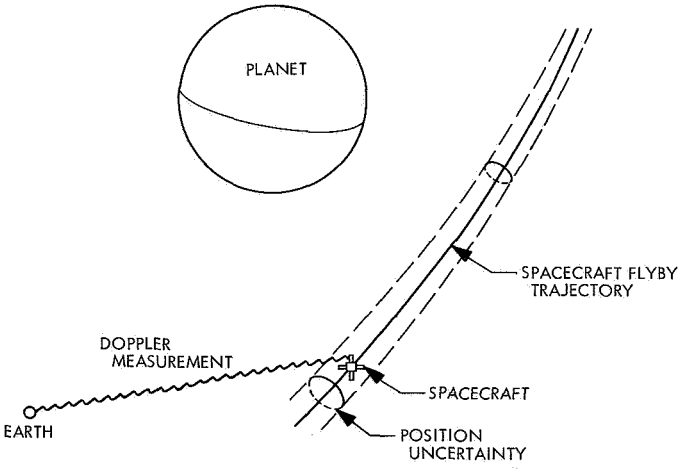

Fig. 1. Description of flyby pass

During the investigation of geometrical properties of trajectories near a target planet, dual solutions for the planet-centered inclination of the spacecraft's flyby trajectory plane have been found that will produce a near-identical doppler time history as well as earth-to-spacecraft range time history past the planet. In other words, for every planet-centered trajectory inclination or orientation that is selected for the spacecraft's ballistic flyby at the planet, another inclination can be found (but with the other orbital elements being the same) that will produce a near-identical time history of the doppler and earth-to-spacecraft range past the planet. For identification purposes let us define the other inclination as the "image" inclination. Prior to this investigation, it was thought that every trajectory that passed the planet has a unique doppler and earth-to-spacecraft range time history past the planet. The parameter time histories

are identical for the two inclinations if the vector from the earth-based observer to the spacecraft is held fixed. Allowing the position vector to vary realistically, for a spacecraft that approaches the target planet and for displacements of the spacecraft that result from rotating the trajectory plane, produces a range-rate time history slightly different for the two inclinations. The difference depends on the approach geometry of the spacecraft near the planet. The range time history of the two inclinations is still the same to within the expected accuracy of the measurements. The dual solutions of inclination for a given range and range-rate time history are symmetric about a plane that contains the earth, the planet, and the approach asymptote of the near-planet trajectory, as shown in Fig. 2. In this figure the trajectory inclination is measured from the plane that contains the approach asymptote and the direction to the earth.

The direct implications of the dual solutions are that an orbit-determination procedure using doppler measurements and/or range measurements might converge to the incorrect image solution for the planet-centered inclination of the trajectory plane. This could happen if the initial estimated flyby trajectory is located such that the *a priori* dispersions of inclination encompass both the image and the nominal inclination. The derivations for the dual solutions of the trajectory-plane inclination for a given doppler and earth-to-spacecraft range time history are given in the subsequent discussions.

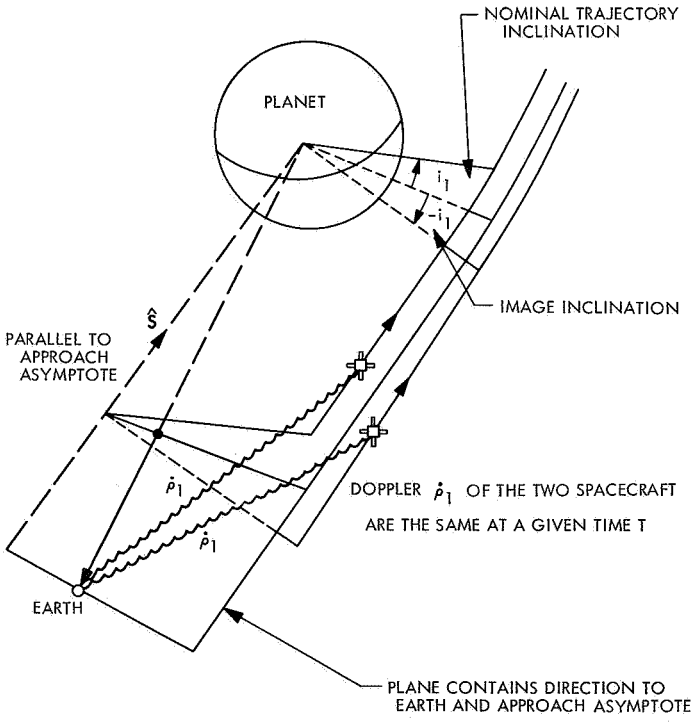

Fig. 2. Description of dual solutions for inclination

Simplifying assumptions are made to the geometry of the doppler observable to enable the partial differentiation to be easily managed. For an example problem, these partial derivatives are then used in a recursive orbit-determination program to show that incorrect convergence to the trajectory image inclination can result under certain situations. A spacecraft-centered angular measurement is then taken in conjunction with the doppler measurement to show that correct convergence results. Other means of assuming a correct convergence are also discussed. The numerical results are obtained for the example trajectory by using an IBM 1620 digital computer.

II. Derivation of Observables

For radar observations, the basic measurement is an integrated doppler-frequency shift. This measurement can be converted to the range rate $\dot{\rho}$ of the spacecraft with respect to the observer on earth (Ref. 1). Hence in this study the range rate will be considered as an observable.[1]

A second observable used in the study is the spacecraft angle β between the direction to a star and the planet as measured by an on-board sensor. The star Canopus is used as the reference star for the angular measurement. The literature (Refs. 2 and 3) indicates that two angular components could be measured for approach guidance. The angle between the sun and the planet, called the cone angle, could be taken as one measurement type; the angle between two planes, one plane containing the sun-to-spacecraft-to-Canopus vector and the other plane containing the sun-to-spacecraft-to-planet vector, called the clock angle, as the second measurement type. It is assumed that the spacecraft is oriented by a two-axis sun sensor that points the roll axis toward the sun, and by a single-axis star sensor that acquires the star Canopus and holds the spacecraft fixed in roll. Another optical device that finds the center of the visible disk of the target planet completes the measurement system. For simplicity and for the purposes of this study, only one type of angular measurement—the spacecraft-centered angle between the star Canopus and the target planet—is used. This angle differs from the two angles previously described. However, the conclusion of the study should not change with the substitution or inclusion of one or more types of angular measurement. Figure 3 shows the graphical explanation of the two observables used in this report.

[1]The terms *observable* and *measurement* are assumed to be interchangeable in this report.

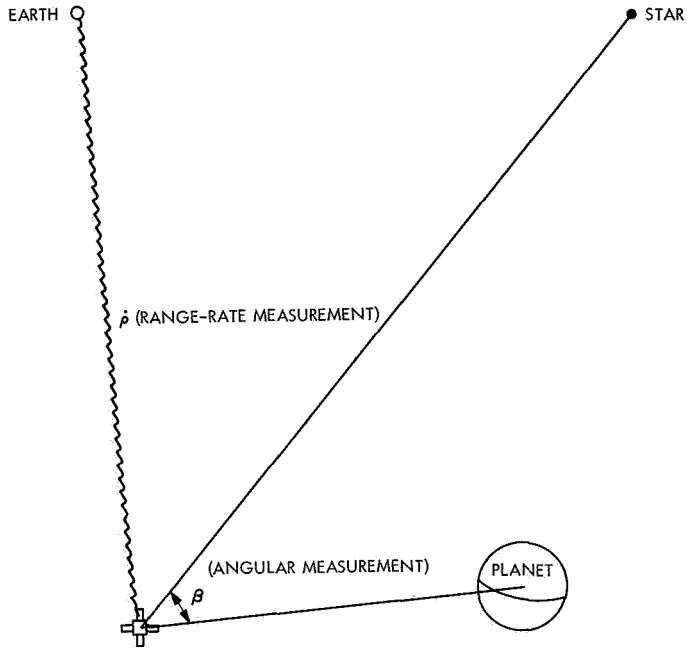

Fig. 3. Description of the observables

A. Simplified Range-Rate Computation

The range rate between an earth-based observer and the spacecraft can be expressed as

$$\dot{\rho} = \mathbf{V}_{S/E} \cdot \hat{\boldsymbol{\rho}} \tag{1}$$

where

$$\mathbf{V}_{S/E} = -\mathbf{V}_E + \mathbf{V}$$

Since

$$\mathbf{V}_{S/E} = -\mathbf{V}_E + \mathbf{V}_P + \mathbf{V}_{S/P}$$

it follows that

$$\dot{\rho} = (-\mathbf{V}_E + \mathbf{V}_P + \mathbf{V}_{S/P}) \cdot \hat{\boldsymbol{\rho}}$$

where

$\mathbf{V}_{S/E}$ = velocity of the spacecraft with respect to the observer on earth

$\mathbf{V}_E$ = heliocentric velocity of an observer on earth at a given time

$\mathbf{V}$ = heliocentric velocity of the spacecraft

$\mathbf{V}_P$ = heliocentric velocity of the center of Mars at a given time

$\mathbf{V}_{S/P}$ = velocity of the spacecraft with respect to the center of the planet at a given time

$\hat{\boldsymbol{\rho}}$ = the unit vector from an observer on earth to the spacecraft at a given time

Figures 4 and 5 show the graphical explanations of range rate and some of the defined vectors.

1. The observer-to-spacecraft direction vector. The direction $\hat{\boldsymbol{\rho}}$ from an earth-based observer to the spacecraft near the planet can be expressed in terms of a coordinate system $\hat{\mathbf{R}}, \hat{\mathbf{S}}, \hat{\mathbf{T}}$ used at the Jet Propulsion Laboratory (Ref. 4).

The unit vector $\hat{\mathbf{S}}$ is along the approach asymptote of the spacecraft's hyperbolic conic with respect to the planet. For a given launch date at earth and arrival date

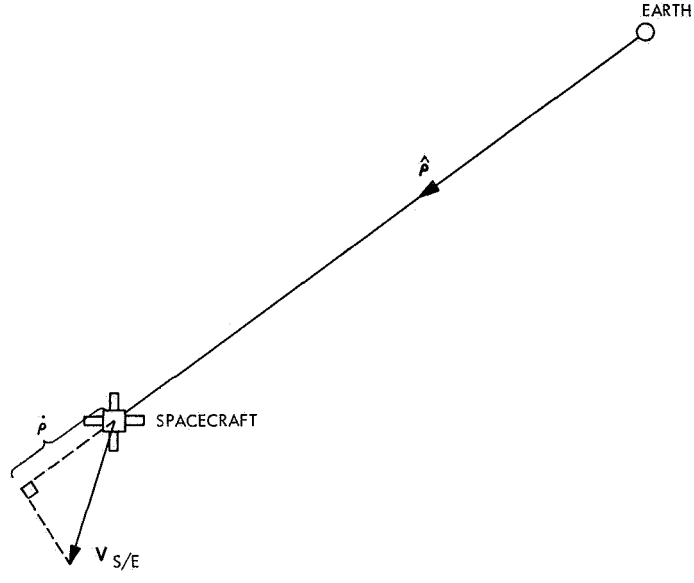

Fig. 4. Description of range rate

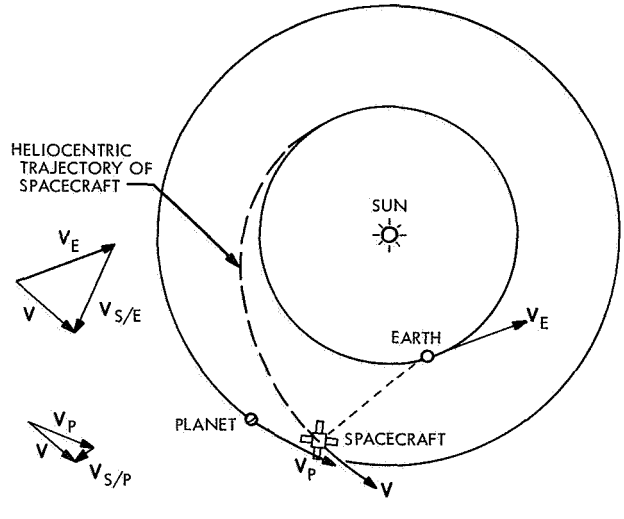

Fig. 5. Heliocentric view of spacecraft

at the planet, the direction of $\hat{\mathbf{S}}$ is almost constant, independent of the orientation of the spacecraft's trajectory plane with respect to the encounter planet. Appendix A reveals more information on the definition of $\hat{\mathbf{S}}$.

The unit vector $\hat{\mathbf{T}}$ is in a plane perpendicular to $\hat{\mathbf{S}}$ and is parallel to a given plane (such as the ecliptic) and is given by

$$\hat{\mathbf{T}} = \frac{\hat{\mathbf{S}} \times \hat{\mathbf{P}}}{|\hat{\mathbf{S}} \times \hat{\mathbf{P}}|}$$

where $\hat{\mathbf{P}}$ is along the ecliptic north pole, and

$$\hat{\mathbf{R}} = \hat{\mathbf{S}} \times \hat{\mathbf{T}}$$

The observer-to-spacecraft direction $\hat{\boldsymbol{\rho}}$ can then be expressed in the $\hat{\mathbf{R}}, \hat{\mathbf{S}}, \hat{\mathbf{T}}$ system as

$$\hat{\boldsymbol{\rho}} = (\hat{\boldsymbol{\rho}} \cdot \hat{\mathbf{S}})\hat{\mathbf{S}} + (\hat{\boldsymbol{\rho}} \cdot \hat{\mathbf{T}})\hat{\mathbf{T}} + (\hat{\boldsymbol{\rho}} \cdot \hat{\mathbf{R}})\hat{\mathbf{R}} \tag{2}$$

From Fig. 6 the following definitions are readily obtained:

$$\left.\begin{aligned} \hat{\boldsymbol{\rho}} \cdot \hat{\mathbf{S}} &= -\cos \zeta_E \\ \hat{\boldsymbol{\rho}} \cdot \hat{\mathbf{T}} &= \sin \zeta_E \cos \eta_E \\ \hat{\boldsymbol{\rho}} \cdot \mathbf{R} &= \sin \zeta_E \sin \eta_E \end{aligned}\right\} \tag{3}$$

Substituting Eqs. (3) into Eq. (2) yields

$$\hat{\boldsymbol{\rho}} = -\cos \zeta_E \hat{\mathbf{S}} + \sin \zeta_E \cos \eta_E \hat{\mathbf{T}} + \sin \zeta_E \sin \eta_E \hat{\mathbf{R}} \tag{4}$$

As shown in Fig. 6, the angles ζ_E and η_E define the direction from the observer to the spacecraft in the approach-asymptote coordinate system. The parameters vary only slightly with time when the spacecraft is in the near vicinity of the planet.

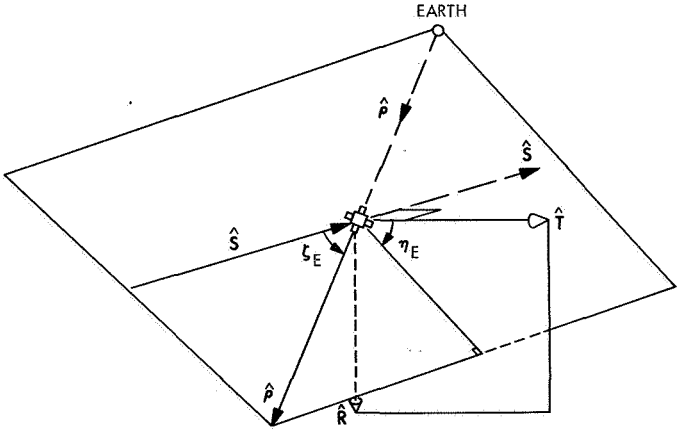

Fig. 6. Description of earth's direction

2. Velocity of spacecraft with respect to the planet. The velocity of the spacecraft with respect to the target planet is assumed to be that resulting from two-body motion. This is an approximation, which becomes more accurate as the spacecraft nears the planet. The velocity $\mathbf{V}_{S/P}$ is then the time derivative of the radius vector $\mathbf{r}$ from the target planet to the spacecraft.

The radius of the spacecraft from the target planet for two-body celestial mechanics can be expressed as

$$\mathbf{r} = -r \cos \alpha \hat{\mathbf{S}} + r \sin \alpha \hat{\mathbf{b}} \tag{5}$$

where

r = distance from planet center to the spacecraft

α = the planet-centered angle from a planet-centered unit vector (parallel to $-\hat{\mathbf{S}}$) to $\mathbf{r}$

$\hat{\mathbf{S}}$ = direction of the approach asymptote

$\hat{\mathbf{b}}$ = a unit vector along $\mathbf{b}$, i.e., $\dfrac{\mathbf{b}}{|\mathbf{b}|}$

$\mathbf{b}$ = the perpendicular vector (called the miss parameter) from planet center to $\hat{\mathbf{S}}$ and lies in the trajectory plane of the spacecraft with respect to the target planet

Figure 7 describes some of these hyperbolic parameters.

The distance r, as derived in Appendix B, is given as

$$r = \frac{b^2}{a\left(1 + \dfrac{b}{a}\sin \alpha - \cos \alpha\right)} \tag{6}$$

where

a = semimajor axis of the hyperbolic orbit and is equal to μ/V_∞^2

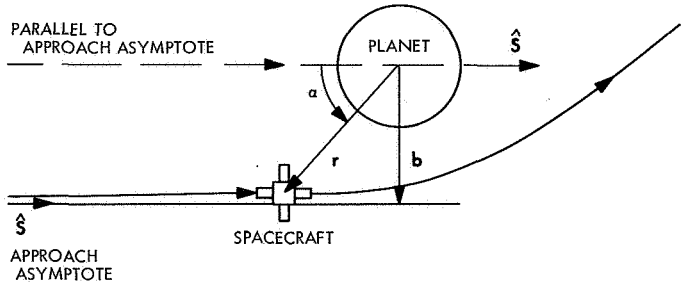

Fig. 7. Description of hyperbolic parameters

μ = gravitational constant of planet

V_∞ = hyperbolic excess speed of the spacecraft with respect to the planet (described more fully in Appendix A)

$b = |\mathbf{b}|$, semiminor axis of the hyperbolic orbit (also referred to as the miss parameter)

The velocity $\mathbf{V}_{S/P}$ can be derived by taking the time derivative of $\mathbf{r}$ in Eq. (5) as follows:

$$\mathbf{V}_{S/P} = \dot{\mathbf{r}} = \hat{\mathbf{S}}(-\dot{r}\cos\alpha + r\dot{\alpha}\sin\alpha) + \hat{\mathbf{b}}(\dot{r}\sin\alpha + r\dot{\alpha}\cos\alpha) \tag{7}$$

The expressions for $\dot{r}$ and $\dot{\alpha}$ can be obtained from

$$r^2\dot{\alpha} = bV_\infty$$

which is the angular momentum equation, and from

$$\dot{r} = \frac{dr}{d\alpha}\dot{\alpha}$$

where

$$\frac{dr}{d\alpha} = -\frac{ar^2}{b^2}\left(\frac{b}{a}\cos\alpha + \sin\alpha\right)$$

which is obtained by taking the derivative of Eq. (6). Substituting these expressions into Eq. (7) yields

$$\mathbf{V}_{S/P} = \left(V_\infty + \frac{\mu}{bV_\infty}\sin\alpha\right)\hat{\mathbf{S}} + \frac{\mu}{bV_\infty}(\cos\alpha - 1)\hat{\mathbf{b}} \tag{8}$$

where

$$\hat{\mathbf{b}} = \cos\theta\hat{\mathbf{T}} + \sin\theta\hat{\mathbf{R}} \tag{9}$$

The angle θ is measured from the $\hat{\mathbf{T}}$ axis clockwise to $\hat{\mathbf{b}}$. Hence, θ gives the orientation of the trajectory plane, as shown in Fig. 8. Substituting Eq. (9) into (8) yields

$$\mathbf{V}_{S/P} = \left(V_\infty + \frac{\mu}{bV_\infty}\sin\alpha\right)\hat{\mathbf{S}} + \frac{\mu}{bV_\infty}(\cos\alpha - 1)\cos\theta\hat{\mathbf{T}} + \frac{\mu}{bV_\infty}(\cos\alpha - 1)\sin\theta\hat{\mathbf{R}} \tag{10}$$

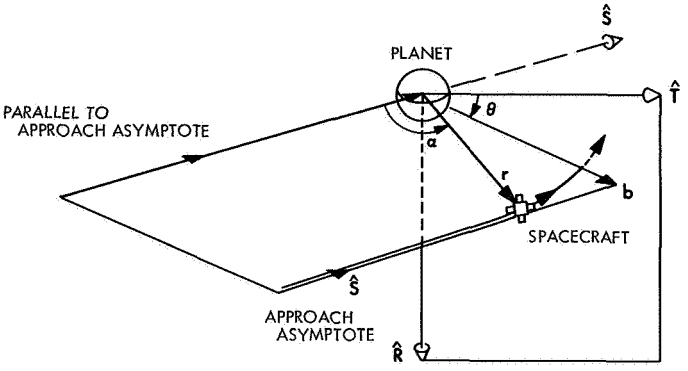

Fig. 8. Description of trajectory-plane orientation

3. ***Simplified range-rate equation.*** As previously shown, the range rate can be expressed as

$$\dot{\rho} = (-\mathbf{V}_E + \mathbf{V}_P)\cdot\hat{\boldsymbol{\rho}} + \mathbf{V}_{S/P}\cdot\hat{\boldsymbol{\rho}} \tag{11}$$

Substituting Eqs. (4) and (10) into (11) yields

$$\dot{\rho} = (-\mathbf{V}_E + \mathbf{V}_P)\cdot\hat{\boldsymbol{\rho}} - V_\infty\cos\zeta_E + \frac{\mu}{bV_\infty}\{(\cos\alpha - 1)\sin\zeta_E\cos(\eta_E - \theta) - \cos\zeta_E\sin\alpha\} \tag{12}$$

Several observations concerning Eq. (12) are discussed below.

The unit vector $\hat{\boldsymbol{\rho}}$ is directed from the observer to the spacecraft. The time-varying parameters ζ_E and η_E define the direction of $\hat{\boldsymbol{\rho}}$. At a given time T, the vector $\hat{\boldsymbol{\rho}}$ will undergo an infinitesimal change for a small displacement of the spacecraft near the planet, assuming that the observer-to-spacecraft distance ρ is very large.

The expression $(-\mathbf{V}_E + \mathbf{V}_P)$ is the velocity of the planet with respect to the observer on earth at the time measurement. If a given time T is considered when the spacecraft is near the planet, then $(-\mathbf{V}_E + \mathbf{V}_P)$ is fixed, independent of the other parameters. Also, the gravitational constant μ of the planet is considered fixed.

The parameter b defines the distance by which the spacecraft will miss the planet. Usually an uncertainty of a few hundred kilometers exists in the estimate of this parameter a few days before the spacecraft passes the planet.

The parameter θ defines the orientation of the spacecraft's trajectory plane near the planet (see Fig. 8). Usually an uncertainty of several degrees will exist in this

parameter, depending on miss distance, a few days before the spacecraft passes the planet.

The parameter V_∞ defines the hyperbolic approach speed of the spacecraft with respect to the planet. A given launch date at earth and arrival date at the planet will almost determine the approach speed precisely, independent of miss distance and near-planet trajectory plane. However, a small uncertainty in the geometry exists. Appendix A gives more detail on the parameter.

The parameter α defines the position of the spacecraft in its hyperbolic orbit at a given time and is a function of μ, V_∞, b, τ (time of periapsis passage), and T (the time at which the spacecraft measurement is taken). Note that for $\alpha = 0$ (when the spacecraft is theoretically an infinite distance away) the expression simplifies to

$$\dot{\rho} = (-\mathbf{V}_E + \mathbf{V}_P) \cdot \hat{\boldsymbol{\rho}} - V_\infty \cos \zeta_E \tag{13}$$

Also, if $\mu = 0$ (no planet mass is present), the expression is the same during the entire encounter period.

In Eq. (12) note that the parameters θ and η_E appear only in the expression as $\cos(\eta_E - \theta)$. The difference of $(\eta_E - \theta)$ can be thought of as the angular orientation of the trajectory plane from some other reference plane. The approach asymptote-to-spacecraft-to-earth plane is a convenient reference plane and is used in the subsequent sections. Figure 9 demonstrates the angular difference of $(\eta_E - \theta)$. In the diagram the vector $\hat{\boldsymbol{\rho}}$ has been translated in position (with the direction unchanged) to a planet-centered coordinate system for convenience instead of the spacecraft-centered system. The parameter can take on positive or negative values, depending on whether η_E is greater or less than θ. Since the equation only depends on $\cos(\eta_E - \theta)$, the equation will yield the same value for $\pm(\eta_E - \theta)$. Thus for every aiming-point orientation of $\theta = \theta_1$, on one side of the asymptote–earth plane, an image aiming-point orientation of $\theta = (2\eta_E - \theta_1)$ exists that will produce the same range rate at *a given time* before the closest approach to the planet. This statement assumes only that upon rotating the trajectory plane the resulting displacement of the spacecraft at a given time T will change the direction from the earth-based observer to the spacecraft by a negligible amount.

B. Angular Measurement Computation

To distinguish which of the two planet-centered trajectory orientations the spacecraft might have, an additional measurement would be a possibility. The measurement chosen in this study is the spacecraft-centered angle between a far-away celestial body and the planet. The far-away celestial body could be the sun, another planet, or a star. To simplify the problem, a star is chosen, since its direction is fixed in space at any given time.[2]

[2]The star Canopus is used in the numerical results presented in Section V.

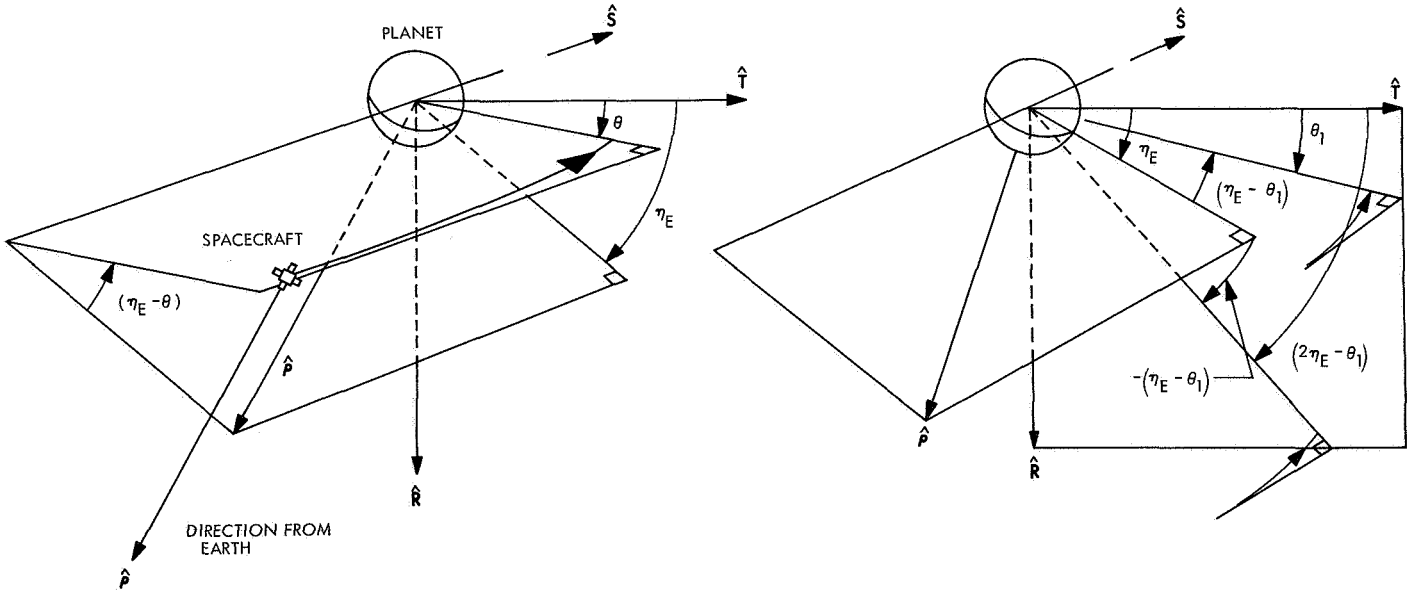

Fig. 9. Description of angular difference $(\eta_E - \theta)$

The direction $\hat{\mathbf{C}}$ from the star to the spacecraft is expressed in the same manner as the earth-to-spacecraft direction in Eqs. (2) and (3). The vector is then expressed as

$$\hat{\mathbf{C}} = (\hat{\mathbf{C}}\cdot\hat{\mathbf{S}})\,\hat{\mathbf{S}} + (\hat{\mathbf{C}}\cdot\hat{\mathbf{T}})\,\hat{\mathbf{T}} + (\hat{\mathbf{C}}\cdot\hat{\mathbf{R}})\,\hat{\mathbf{R}} \qquad (14a)$$

where

$$\left.\begin{aligned} \hat{\mathbf{C}}\cdot\hat{\mathbf{S}} &= -\cos\zeta_C \\ \hat{\mathbf{C}}\cdot\hat{\mathbf{T}} &= +\sin\zeta_C\cos\eta_C \\ \hat{\mathbf{C}}\cdot\hat{\mathbf{R}} &= +\sin\zeta_C\sin\eta_C \end{aligned}\right\} \qquad (14b)$$

Figure 10 shows the graphical explanation of the angles ζ_C and η_C.

When Eqs. (5) and (9) are combined, the direction from the planet to the spacecraft can be expressed as

$$\hat{\mathbf{r}} = -\cos\alpha\,\hat{\mathbf{S}} + \sin\alpha\cos\theta\,\hat{\mathbf{T}} + \sin\alpha\sin\theta\,\hat{\mathbf{R}} \qquad (15)$$

The desired angular measurement β, shown in Fig. 11, can be expressed as

$$\cos\beta = (\hat{\mathbf{C}}\cdot\hat{\mathbf{r}})$$

where $0 \leqq \beta \leqq 180$. Substituting Eqs. (14a), (14b), and (15) into the above expression for β yields

$$\cos\beta = \cos\alpha\cos\zeta_C + \sin\alpha\sin\zeta_C\cos(\eta_C - \theta) \qquad (16)$$

The angles ζ_C and η_C of Eq. (16) define the direction from the star to the spacecraft in an asymptote-oriented coordinate system. For a given launch date and arrival date, these parameters are almost fixed. However, a small uncertainty exists in the values of the parameters because of the uncertainty in the precise direction of the approach asymptote and the precise direction to the star.

Note that η_C and θ of Eq. (16) appear in the angular expression as $\cos(\eta_C - \theta)$, which is the same form for η_E and θ in the range-rate expression of Eq. (12). Thus if η_C is equal to η_E, the angular measurement will not help in determining which of the two trajectory orientations ($\theta = \theta_1$ or $\theta = 2\eta_E - \theta_1$) the spacecraft might have. This would take place if the earth were used in the angular measurement $\hat{\mathbf{C}} = \hat{\boldsymbol{\rho}}$, instead of another body such as a star. Thus one would not choose the earth for one of the bodies in the angular measurement to resolve the trajectory orientation ambiguity. Also, one would not use the earth-to-spacecraft range as a measurement to resolve the ambiguity because of the same type of phenomena. This will be discussed in more detail in Section VI.

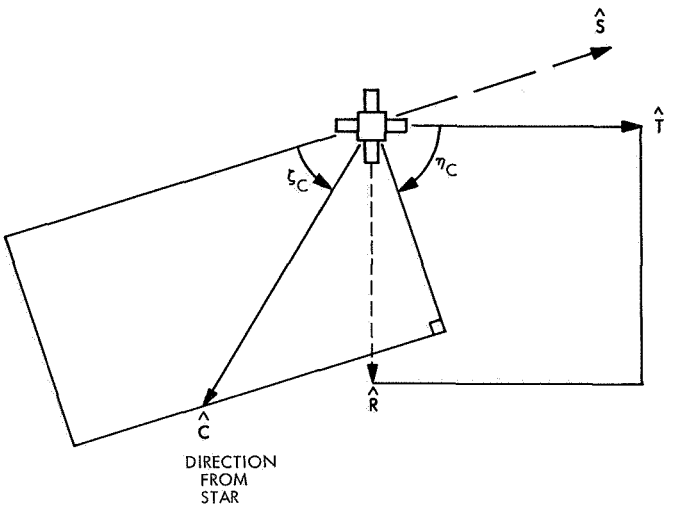

Fig. 10. Description of star's direction

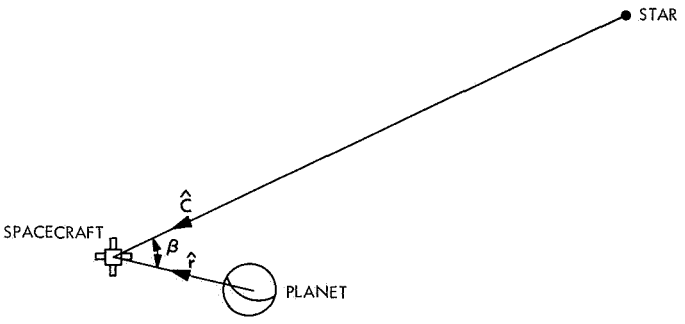

Fig. 11. Description of spacecraft angular measurement

III. Derivation of Partial Derivatives

A. Assumptions

In this section, the partial derivatives of the observables with respect to the independent variables are derived for the orbit-estimation procedure described in Section IV. To simplify the derivation of the partials and to make the task manageable, the following specific assumptions are made concerning the model:

(1) The first assumption is that the observer measuring the range rate is at the center of the earth. This assumption should not affect the conclusions of this study. However, future studies should probably place one or more stations on the earth's surface and should include the station location uncertainties.

(2) The second assumption is that the gravitational constant μ of the planet and the ephemeris positions and velocities of the earth and planet are

known. Again, these assumptions should not affect the conclusions of this study, but for completeness, future studies should include their uncertainties.

(3) The third assumption is that the spacecraft's motion with respect to the target planet is that of two-body motion. Also, the direction of the approach asymptote $\hat{\mathbf{S}}$ is assumed not to change with time; however, an uncertainty in the exact direction of this vector is included in the analysis. These assumptions should be accurate enough for near-planet orbit-determination studies.

(4) The fourth assumption is that the vector $\hat{\boldsymbol{\rho}}$ from earth observer to spacecraft remains *fixed* for displacements of the spacecraft near the planet and also during the total time that the spacecraft approaches the planet. This assumption should affect the accuracy of the partials by only a small amount when the spacecraft is close to the planet. However, the accuracy of this assumption will be degraded the further away the spacecraft is from the planet. The partial derivative of $\dot{\rho}$ with respect to an independent variable, say q, takes the form of

$$\frac{\partial \dot{\rho}}{\partial q} = \frac{\partial \mathbf{V}_{S/E}}{\partial q} \cdot \hat{\boldsymbol{\rho}} + \mathbf{V}_{S/E} \cdot \frac{\partial \hat{\boldsymbol{\rho}}}{\partial q} \tag{17}$$

where

$$\mathbf{V}_{S/E} = -\mathbf{V}_E + \mathbf{V}_P + \mathbf{V}_{S/P}$$

Equation (17) is the result of taking the derivative of Eq. (1). The first part of Eq. (17) will definitely dominate the total partial when the spacecraft is close to the planet and the spacecraft velocity is changing. However, when the spacecraft is far away from the planet, the second part of the expression might dominate the term for the independent variables of b, θ, and τ. Future studies should include a non-fixed direction for $\hat{\boldsymbol{\rho}}$. Modified equations for the start of such a study are given in Section VI. However, in this study $\hat{\boldsymbol{\rho}}$ is assumed to be fixed, which makes

$$\frac{\partial \hat{\boldsymbol{\rho}}}{\partial q} = 0$$

and thus the partial derivative of range rate with respect to the independent variable q will have the form of

$$\frac{\partial \dot{\rho}}{\partial q} = \frac{\partial \mathbf{V}_{S/E}}{\partial q} \cdot \hat{\boldsymbol{\rho}} \tag{18}$$

B. Independent Variables

For the computation of range rate $\dot{\rho}$, the six independent variables are b, θ, V_∞, η_E, ζ_E, and τ, where

b = miss parameter, or semiminor axis of spacecraft hyperbolic orbit with respect to target planet

θ = orientation of spacecraft trajectory plane (planet-centered)

V_∞ = spacecraft hyperbolic excess speed with respect to target planet

τ = time of periapsis passage or closest approach to planet

and the angles η_E and ζ_E define the direction from the approach asymptote $\hat{\mathbf{S}}$ to the earth.

For the angular measurement β, the six independent variables are b, θ, V_∞, η_C, ζ_C, and τ. The angles η_C and ζ_C define the direction from the approach asymptote $\hat{\mathbf{S}}$ to the star.

The velocities $\mathbf{V}_E$ and $\mathbf{V}_P$ are not dependent on the above independent variables and from Eq. (18) the partial derivative of range rate with respect to an independent variable, say q, will thus take the form of

$$\frac{\partial \dot{\rho}}{\partial q} = \frac{\partial \mathbf{V}_{S/P}}{\partial q} \cdot \hat{\boldsymbol{\rho}}$$

or

$$\frac{\partial \dot{\rho}}{\partial q} = \frac{\partial (\mathbf{V}_{S/P} \cdot \hat{\boldsymbol{\rho}})}{\partial q}$$

where $q = b$, θ, V_∞, etc., and $\hat{\boldsymbol{\rho}}$ is a fixed unit vector from the earth-based observer to the spacecraft.

C. Basic Equations

The basic equations by which the partial derivatives can be derived are now reviewed. The equations that give the observables ρ and β are

$$\mathbf{V}_{S/P} \cdot \hat{\boldsymbol{\rho}} = -V_\infty \cos \zeta_E + \frac{\mu}{bV_\infty} \{(\cos \alpha - 1) \sin \zeta_E \cos (\eta_E - \theta) - \cos \zeta_E \sin \alpha\} \tag{19}$$

and

$$\cos \beta = \cos \zeta_C \cos \alpha + \sin \zeta_C \sin \alpha \cos (\eta_C - \theta) \tag{20}$$

where $0 \leq \beta \leq 180$ deg. The equation that relates the time of the observation to the independent variables is

$$n(T - \tau) = -F + e \sin h F \tag{21}$$

where

n = the mean angular motion and is equal to V_∞^3/μ

T = time of the observation

τ = time of closest approach (periapsis passage) between spacecraft and the planet

F = eccentric anomaly of hyperbola

e = the eccentricity of the hyperbolic orbit and is equal to $(a^2 + b^2)^{1/2}/a$

a = the semimajor axis of the hyperbolic orbit and is equal to μ/V_∞^2

The equation that relates b to α, a to α and α to F is

$$a(e \cosh F - 1) = \frac{b^2}{a\left(1 + \frac{b}{a}\sin\alpha - \cos\alpha\right)} = r \tag{22}$$

D. Partial Derivatives

The partial derivatives of the observables $\dot{\rho}$ and β with respect to the independent variables can be expressed as follows:

$$\left.\begin{aligned}
\frac{\partial\dot{\rho}}{\partial b} &= \left(\frac{\partial\dot{\rho}}{\partial b}\right) + \frac{\partial\dot{\rho}}{\partial\alpha}\frac{\partial\alpha}{\partial b} + \frac{\partial\dot{\rho}}{\partial\alpha}\frac{\partial\alpha}{\partial F}\frac{\partial F}{\partial b} \\
\frac{\partial\dot{\rho}}{\partial\theta} &= \left(\frac{\partial\dot{\rho}}{\partial\theta}\right) \\
\frac{\partial\dot{\rho}}{\partial V_\infty} &= \left(\frac{\partial\dot{\rho}}{\partial V_\infty}\right) + \frac{\partial\dot{\rho}}{\partial\alpha}\frac{\partial\alpha}{\partial V_\infty} + \frac{\partial\dot{\rho}}{\partial\alpha}\frac{\partial\alpha}{\partial F}\frac{\partial F}{\partial V_\infty} \\
\frac{\partial\dot{\rho}}{\partial\eta_E} &= -\frac{\partial\dot{\rho}}{\partial\theta} \\
\frac{\partial\dot{\rho}}{\partial\zeta_E} &= \left(\frac{\partial\dot{\rho}}{\partial\zeta_E}\right) \\
\frac{\partial\dot{\rho}}{\partial\tau} &= \frac{\partial\dot{\rho}}{\partial\alpha}\frac{\partial\alpha}{\partial F}\frac{\partial F}{\partial\tau} \\
\frac{\partial\beta}{\partial b} &= \frac{\partial\beta}{\partial\alpha}\frac{\partial\alpha}{\partial b} + \frac{\partial\beta}{\partial\alpha}\frac{\partial\alpha}{\partial F}\frac{\partial F}{\partial b} \\
\frac{\partial\beta}{\partial\theta} &= \left(\frac{\partial\beta}{\partial\theta}\right) \\
\frac{\partial\beta}{\partial V_\infty} &= \frac{\partial\beta}{\partial\alpha}\frac{\partial\alpha}{\partial V_\infty} + \frac{\partial\beta}{\partial\alpha}\frac{\partial\alpha}{\partial F}\frac{\partial F}{\partial V_\infty} \\
\frac{\partial\beta}{\partial\zeta_C} &= \left(\frac{\partial\beta}{\partial\zeta_C}\right) \\
\frac{\partial\beta}{\partial\eta_C} &= -\frac{\partial\beta}{\partial\theta} \\
\frac{\partial\beta}{\partial\tau} &= \frac{\partial\beta}{\partial\alpha}\frac{\partial\alpha}{\partial F}\frac{\partial F}{\partial\tau}
\end{aligned}\right\} \tag{23}$$

where the following partials can be derived by the use of Eqs. (19) through (22):

$$
\begin{aligned}
\left(\frac{\partial \dot{\rho}}{\partial b}\right) &= -\frac{\mu}{b^2 V_\infty}\{\sin\zeta_E \cos(\eta_E - \theta)[\cos\alpha - 1] - \cos\zeta_E \sin\alpha\} \\
\frac{\partial \dot{\rho}}{\partial \alpha} &= -\frac{\mu}{bV_\infty}\{\sin\zeta_E \cos(\eta_E - \theta)\sin\alpha + \cos\zeta_E \cos\alpha\} \\
\frac{\partial \alpha}{\partial b} &= \frac{2b - r\sin\alpha - \dfrac{b^3(r+a)}{a^2 re^2}}{r(b\cos\alpha + a\sin\alpha)} \\
\frac{\partial \alpha}{\partial F} &= -\frac{ae\,b^2 \sinh F}{r^2(b\cos\alpha + a\sin\alpha)} \\
\frac{\partial F}{\partial b} &= -\frac{b\sinh F}{a\,e\,r} \\
\frac{\partial F}{\partial V_\infty} &= -\frac{3aF}{rV_\infty} + (\sinh F)\left(\frac{3a^2e^2 - 2b^2}{r\,a\,e\,V_\infty}\right) \\
\frac{\partial F}{\partial \tau} &= -\frac{V_\infty}{r} \\
\left(\frac{\partial \dot{\rho}}{\partial \theta}\right) &= \frac{\mu}{bV_\infty}\sin\zeta_E \sin(\eta_E - \theta)[\cos\alpha - 1] \\
\left(\frac{\partial \dot{\rho}}{\partial V_\infty}\right) &= -\frac{\mu}{bV_\infty^2}\left\{\sin\zeta_E \cos(\eta_E - \theta)[\cos\alpha - 1] - \cos\zeta_E\left(\sin\alpha - \frac{bV_\infty^2}{\mu}\right)\right\} \\
\frac{\partial \alpha}{\partial V_\infty} &= \frac{2b}{V_\infty}\frac{\partial \alpha}{\partial b} \\
\left(\frac{\partial \dot{\rho}}{\partial \zeta_E}\right) &= \frac{\mu}{bV_\infty}\left\{\cos\zeta_E \cos(\eta_E - \theta)[\cos\alpha - 1] + \sin\zeta_E\left(\sin\alpha + \frac{bV_\infty^2}{\mu}\right)\right\} \\
\frac{\partial \beta}{\partial \alpha} &= \frac{\sin\alpha\cos\zeta_C - \cos\alpha\sin\zeta_C\cos(\eta_C - \theta)}{\sin\beta} \\
\left(\frac{\partial \beta}{\partial \theta}\right) &= -\frac{\sin\alpha\sin\zeta_C\sin(\eta_C - \theta)}{\sin\beta} \\
\left(\frac{\partial \beta}{\partial \zeta_C}\right) &= \frac{\cos\alpha\sin\zeta_C - \sin\alpha\cos\zeta_C\cos(\eta_C - \theta)}{\sin\beta}
\end{aligned}
\qquad (24)
$$

The partial derivatives in Eqs. (23) and (24) that are inside the parentheses have the meaning of the explicit partial differentiation of the observable with respect to the independent variable.

IV. Application of Recursive Estimation Theory

The orbit-determination theory used in this investigation is based on the linear filter theory proposed by Kalman (Ref. 5). The theory is utilized in this investigation by assuming that linearized changes in the observable will result from small changes in the state variables. The covariance matrix and estimated variables are updated at each successive time increment along the spacecraft orbit.

The covariance matrix of the uncertainties of the estimated variables at each time is expressed (Refs. 5, 6) as

$$\mathbf{\Lambda} = \mathbf{\Lambda}_1 - \mathbf{\Lambda}_1 \mathbf{A}^T [\mathbf{A}\,\mathbf{\Lambda}_1 \mathbf{A}^T + \boldsymbol{\lambda}]^{-1} \mathbf{A}\,\mathbf{\Lambda}_1 \tag{25}$$

where $\mathbf{\Lambda}_1$ is the covariance matrix of the variables at the preceding time. The new estimated values for the variables can be expressed as

$$\tilde{\mathbf{q}} = \tilde{\mathbf{q}}_1 + \Delta\tilde{\mathbf{q}} \tag{26}$$

When only range rate is used as an observable, the matrices take the form of

$$\tilde{\mathbf{q}}_1 = \begin{vmatrix} b_1 \\ \theta_1 \\ V_{\infty 1} \\ \eta_{E1} \\ \zeta_{E1} \\ \tau_1 \end{vmatrix}$$

where $\tilde{\mathbf{q}}_1$ is the estimate of the variables at the time T based on previous measurements using range-rate measurements only.

The matrix $\Delta\tilde{\mathbf{q}}$ is the change in the estimated variables based on the current range-rate measurement and is described as

$$\Delta\tilde{\mathbf{q}} = \begin{vmatrix} \Delta b \\ \Delta\theta \\ \Delta V_\infty \\ \Delta\eta_E \\ \Delta\zeta_E \\ \Delta\tau \end{vmatrix}$$

When range-rate and spacecraft angular measurements are used as observables, the matrices take the form of

$$\tilde{\mathbf{q}}_1 = \begin{vmatrix} b_1 \\ \theta_1 \\ V_{\infty 1} \\ \eta_{E1} \\ \zeta_{E1} \\ \zeta_{C1} \\ \eta_{C1} \\ \tau_1 \end{vmatrix} \quad \text{and} \quad \Delta\tilde{\mathbf{q}} = \begin{vmatrix} \Delta b \\ \Delta \\ \Delta V_\infty \\ \Delta\eta_E \\ \Delta\zeta_E \\ \Delta\zeta_C \\ \Delta\eta_C \\ \Delta\tau \end{vmatrix}$$

The matrix $\Delta\tilde{\mathbf{q}}$ is defined as

$$\Delta\tilde{\mathbf{q}} = \mathbf{\Lambda}_1 \mathbf{A}^T [\mathbf{A}\,\mathbf{\Lambda}_1 \mathbf{A}^T + \boldsymbol{\lambda}]^{-1} [\Delta\mathbf{Y}] \tag{27}$$

where $[\Delta\mathbf{Y}]$ is the residual matrix given as

$$[\Delta\mathbf{Y}] = [(\dot{\rho}_n - \dot{\rho})]$$

for utilizing only range-rate measurements, and by

$$[\Delta\mathbf{Y}] = \begin{bmatrix} (\dot{\rho}_n - \dot{\rho}) \\ (\beta_n - \beta) \end{bmatrix} \tag{28}$$

for using range-rate and angular measurements together.

Several quantities used in the preceding equations are defined as follows:

β_n = the theoretical observed spacecraft angular measurement, and its value is determined using the nominal trajectory

β = angular measurement computed from the estimated values of the independent variables

$\dot{\rho}_n$ = the theoretical observed range rate, and its value is determined using the nominal trajectory

$\dot{\rho}$ = range rate computed from the estimated values of the independent variables

$\boldsymbol{\lambda}$ = covariance matrix of the observables. For range-rate measurements, $\boldsymbol{\lambda}$ is a scalar quantity expressed as

$$\boldsymbol{\lambda} = \frac{\sigma_{\dot{\rho}}^2}{\Delta T}$$

For using range-rate and angle measurements together (uncorrelated), $\boldsymbol{\lambda}$ is expressed as

$$\boldsymbol{\lambda} = \frac{1}{\Delta T} \begin{bmatrix} \sigma_{\dot{\rho}}^2 & 0 \\ 0 & \sigma_\beta^2 \end{bmatrix} \tag{29}$$

$\sigma_{\dot{\rho}}$ = the standard deviation of the data noise on the range-rate measurement; in the results the deviation is for a 1-min sample

σ_{ρ} = standard deviation of the angular measurement for a 1-min sample

ΔT = the time between each desired measurement along the orbit in minutes

$\mathbf{A}$ = the matrix of partial derivatives. If only range-rate measurements are used, $\mathbf{A}$ is expressed as

$$\mathbf{A} = \left| \frac{\partial\dot{\rho}}{\partial b} \frac{\partial\dot{\rho}}{\partial\theta} \frac{\partial\dot{\rho}}{\partial V_\infty} \frac{\partial\dot{\rho}}{\partial\eta_E} \frac{\partial\dot{\rho}}{\partial\zeta_E} \frac{\partial\dot{\rho}}{\partial\tau} \right| \tag{30}$$

If range-rate and angular measurements together are considered, $\mathbf{A}$ is expressed as

$$\mathbf{A} = \left| \begin{matrix} \frac{\partial\dot{\rho}}{\partial b} & \frac{\partial\dot{\rho}}{\partial\theta} & \frac{\partial\dot{\rho}}{\partial V_\infty} & \frac{\partial\dot{\rho}}{\partial\eta_E} & \frac{\partial\dot{\rho}}{\partial\zeta_E} & 0 & 0 & \frac{\partial\dot{\rho}}{\partial\tau} \\ \frac{\partial\beta}{\partial b} & \frac{\partial\beta}{\partial\theta} & \frac{\partial\beta}{\partial V_\infty} & 0 & 0 & \frac{\partial\beta}{\partial\zeta_C} & \frac{\partial\beta}{\partial\eta_C} & \frac{\partial\beta}{\partial\tau} \end{matrix} \right| \tag{31}$$

The covariance matrix of the estimated variables has the form of

$$\Lambda = \begin{vmatrix} \sigma_b^2 & \rho_1\sigma_b\sigma_\theta & & & & & \rho_5\sigma_b\sigma_\tau \\ \rho_1\sigma_b\sigma_\theta & \sigma_\theta^2 & \cdot & & & & \cdot \\ \cdot & \cdot & \sigma_{V_\infty}^2 & \cdot & & & \cdot \\ & & \cdot & \sigma_{\eta_E}^2 & \cdot & & \cdot \\ & & & \cdot & \sigma_{\zeta_E}^2 & & \cdot \\ \rho_5\sigma_b\sigma_\tau & & & & \cdot & & \sigma_\tau^2 \end{vmatrix} \tag{32}$$

if only range-rate measurements are considered, and has the form of

$$\Lambda = \begin{vmatrix} \sigma_b^2 & \rho_1\sigma_b\sigma_\theta & & \cdot & & & \cdot & \rho_7\sigma_b\sigma_\tau \\ \rho_1\sigma_b\sigma_\theta & \sigma_\theta^2 & \cdot & \cdot & \cdot & & \cdot & \cdot \\ \cdot & \cdot & \sigma_{V_\infty}^2 & \cdot & \cdot & \cdot & \cdot & \cdot \\ \cdot & \cdot & \cdot & \sigma_{\eta_E}^2 & \cdot & \cdot & \cdot & \cdot \\ \cdot & \cdot & \cdot & \cdot & \sigma_{\zeta_E}^2 & \cdot & \cdot & \cdot \\ \cdot & \cdot & \cdot & \cdot & \cdot & \sigma_{\zeta_C}^2 & \cdot & \cdot \\ \cdot & \cdot & \cdot & \cdot & \cdot & \cdot & \sigma_{\eta_C}^2 & \cdot \\ \rho_7\sigma_b\sigma_\tau & \cdot & \cdot & \cdot & \cdot & \cdot & \cdot & \sigma_\tau^2 \end{vmatrix} \tag{33}$$

if range-rate and angular measurements together are considered. The variances of the independent variables are the elements of the diagonal of the matrix.

To simplify the problem, noise will not be added directly to the range-rate and angular measurements. However, an uncertainty in the measurements will be assumed. In other words, the values for the observed range rate and spacecraft angle will be computed using the nominal trajectory with no noise added; however, in the matrix manipulations an uncertainty in the measurements will be assumed. These uncertainties are contained in the λ matrix. The result of this simplification is that the estimated variables will converge to their proper values faster and more smoothly than if noise had been added. However, the conclusions of the study should not be affected.

One reason for using a recursive filter theory in this investigation, instead of other estimation procedures, is the reduction in machine time for running the various cases. Inverting matrices, such as 6×6 or 8×8, requires much machine time for many computations along the trajectory. By using the recursive filter theory, the maximum matrix size that has to be inverted is a 1×1 using range-rate measurements with six independent variables to be estimated, and a 2×2 using the range-rate and angular measurements together with eight independent variables to be estimated.

V. Numerical Results

The numerical results presented in this section were taken from a double-precision orbit-estimation program utilizing the IBM 1620 digital computer. The program uses the estimation procedure and equations given in Sections III and IV. The program is started 10 days prior to the spacecraft's closest approach to the planet and incremented in time. The time increments were selected such that the changes in the partial derivatives were less than 50%.

A. Example Trajectory

The example trajectory used in the results is a ballistic trajectory from earth to Mars. The approach characteristics selected at Mars are typical of a launch date in the middle of February 1969, with an arrival date at Mars at the beginning of August 1969. This selection is representative of the *Mariner* Mars 1969 flyby mission to be conducted by the Jet Propulsion Laboratory. The nominal values used for the independent variables are as follows:

$b = 7000$ km (impact parameter)

$\theta = 25$ deg (orientation of trajectory plane)

$V_\infty = 7$ km/sec (approach speed)

$\eta_E = 30$ deg (orientation of approach asymptote, earth-to-spacecraft plane)

$\zeta_E = 160$ deg (angle between approach asymptote and earth-to-spacecraft vector)

$\eta_C = 260$ deg (orientation of approach asymptote, Canopus-to-spacecraft plane)

$\zeta_C = 100$ deg (angle between approach asymptote and Canopus-to-spacecraft vector)

$\tau = 0$ hr (the nominal time of spacecraft closest approach to the planet, designated as 0 hr GMT)

The parameters V_∞, η_E, ζ_E, η_C, and ζ_C define the hyperbolic excess velocity at Mars and the angles between the earth and the star Canopus. For a given launch date at earth and arrival date at Mars, the parameters are approximately determined and thus only a small uncertainty will exist. A larger uncertainty will exist in the parameters b and θ, which define how the spacecraft will pass the planet, and τ, the precise time of arrival.

B. Initial Uncertainty of Independent Variables

As mentioned previously the starting time for the estimation program was selected to be 10 days before the spacecraft's closest approach to the planet. Also at this time, an initial covariance matrix was selected for the uncertainties of the independent variables. It was assumed that there was no correlation between the independent variables at the initial time. The initial covariance matrix for both range-rate and angular measurements is

$$\Lambda_0 = \begin{vmatrix} \sigma_{b0}^2 & 0 & 0 & 0 & 0 & 0 & 0 & 0 \\ 0 & \sigma_{\theta 0}^2 & 0 & 0 & 0 & 0 & 0 & 0 \\ 0 & 0 & \sigma_{V_\infty 0}^2 & 0 & 0 & 0 & 0 & 0 \\ 0 & 0 & 0 & \sigma_{\eta_E 0}^2 & 0 & 0 & 0 & 0 \\ 0 & 0 & 0 & 0 & \sigma_{\zeta_E 0}^2 & 0 & 0 & 0 \\ 0 & 0 & 0 & 0 & 0 & \sigma_{\zeta_C 0}^2 & 0 & 0 \\ 0 & 0 & 0 & 0 & 0 & 0 & \sigma_{\eta_C 0}^2 & 0 \\ 0 & 0 & 0 & 0 & 0 & 0 & 0 & \sigma_{\tau 0}^2 \end{vmatrix} \tag{34}$$

For this problem the following initial standard deviations were assumed for the parameters:

$$\begin{aligned} \sigma_{b0} &= 1000.0 \text{ km} \\ \sigma_{\theta 0} &= 10.0 \text{ deg} \\ \sigma_{V_\infty 0} &= 1.0 \text{ m/sec} \\ \sigma_{\eta_E 0} &= 0.1 \text{ deg} \\ \sigma_{\zeta_E 0} &= 0.01 \text{ deg} \\ \sigma_{\zeta_C 0} &= 0.01 \text{ deg} \\ \sigma_{\eta_C 0} &= 0.1 \text{ deg} \\ \sigma_{\tau 0} &= 6.0 \text{ min} \end{aligned} \tag{35}$$

The precise values used above could be debated, but the result of the incorrect convergence of θ will not be altered as the standard deviations of Eqs. (35) are changed.

C. Initial Estimated Values of Parameters

The initial estimated values of the independent variables at 10 days prior to closest approach were arbitrarily perturbed from the nominal values by approximately one standard deviation. The nominal value of a parameter corresponds to its actual value in the model. The estimated value corresponds to what it is thought to be. The initial values of the parameters are as follows:

$$\begin{aligned} b_I &= 8000.0 \\ V_{\infty I} &= 7.001 \text{ km/sec} \\ \eta_{EI} &= 30.1 \text{ deg} \\ \zeta_{EI} &= 160.01 \text{ deg} \\ \zeta_{CI} &= 100.01 \text{ deg} \\ \eta_{CI} &= 260.1 \text{ deg} \\ \tau_I &= 6.0 \text{ min} \end{aligned}$$

Several initial values for θ were used in the study.

D. Standard Deviations of Observables

The two observables used in the study are earth-to-spacecraft range rate and the spacecraft-centered angle between the star Canopus and the target planet. For comparison, results are presented for two standard deviations $\sigma_{\dot{\rho}}$ of the data noise on the range-rate measurement. These are 0.001 m/sec and 0.01 m/sec for a 1-min sample.[3] For the angular measurement, a standard deviation σ_β of 0.01 deg is used for a 1-min sample.[4] The covariance

[3]The standard deviation of the data noise is expected to be within this range for future planetary missions.

[4]This value was estimated after conversing with a few people involved in approach guidance at the Jet Propulsion Laboratory.

matrix for the observables has the following form if both the range-rate and angular measurements (uncorrelated) are used:

$$\lambda = \frac{1}{\Delta T}\begin{bmatrix} \sigma^2_{\dot{\rho}} & 0 \\ 0 & \sigma^2_{\beta} \end{bmatrix}$$

The quantity ΔT is the time in minutes by which the program is incremented along the spacecraft trajectory. The partial derivatives used in the Λ matrix of Section IV are computed at every time increment ΔT along the trajectory. The time increments used in the program vary from 1440 min at 10 days out, when the partial derivatives change very little, to about 0.2 min at closest approach, when the partial derivatives are erratic. A constant 1-min or smaller time increment ΔT is not used along the whole trajectory because of the excess time required for the machine calculations.

E. Identification of Trajectory Runs

The results of the orbit-determination program for the example trajectory are shown graphically in Figs. 12 through 61 at the end of this section. Figures 12 and 13 show the nominal values of range rate and angular measurement with time. The range rate shown on Fig. 12 is that attributed to the gravitational influence of Mars, i.e., $\mathbf{V}_{S/P} \cdot \hat{\boldsymbol{\rho}}$ given in Eq. (19). Figures 14–27 show the partial derivatives of range rate and the angular measurement with respect to the independent variables for the nominal trajectory.

Figure 28 shows the initial aiming points for three cases plotted in Figs. 29 through 60. Figures 29–44 show the estimation and standard deviations of the independent variables for a range-rate data noise of 0.001 m/sec ($\sigma_{\dot{\rho}}$) for a 1-min sample. Figures 45–60 show the same for a range-rate data noise of 0.01 m/sec. The subscript labels 1, 2, and 3 on the plots in these figures correspond to cases 1, 2, and 3 shown in Fig. 28 and are identified as follows:

(1) In case 1, the initial estimated value of θ is equal to 23 deg at 10 days prior to planet closest approach, and only range-rate measurements are used. It is shown that for this case the value of θ will converge correctly to its nominal value of 25 deg. Other variables will also converge to their nominal values.

(2) In case 2, the initial estimated value of θ is equal to 38 deg at 10 days prior to planet closest approach, and again only range-rate measurements are used. However, for this case it is shown that the estimated value of θ will converge to an incorrect image value of 35 deg. The other variables will converge to their nominal values.

(3) In case 3, the initial estimated value of θ is again 38 deg at 10 days prior to planet closest approach, but for this case both range-rate and angular measurements are used. This time it is shown that the estimated value of θ will converge to its correct value of 25 deg. Again the other variables will converge to their nominal values.

Note that the effect of the smaller data noise on range rate is to make convergence of the various parameters start a few hours earlier. Also, the effect of including the angular measurement with range rate is to make convergence of the parameters start a few days earlier; this effect is probably optimistic, since the model used does not contain noise in the measurement or biases in the measurement equipment. Figure 61 shows the estimated values of θ as a function of time for several initial values of θ and a range-rate data noise of 0.01 m/sec.

F. Discussion of Ambiguity in Convergence of Orientation of the Trajectory Plane

Special attention is called to Figs. 29 and 30, 45 and 46, and 61. These figures show the estimated values of θ and the standard deviation as a function of time for various initial values of θ. Note that correct convergence results for case 1 (θ_1) of Figs. 29 and 30, and 45 and 46.[5] Case 1 corresponds to an initial estimated value of θ equal to 23 deg (at 10 days prior to closest approach) using range rate as an observable. Note that for case 2 (θ_2), where the initial value of θ is 38 deg, incorrect convergence results to a value of 35 deg instead of 25 deg. This value of 35 deg corresponds to the image aiming point $(2\eta_E - \theta_N)$, where $\eta_E = 30$ deg and $\theta_N = 25$ deg for the example problem. Both range-rate and the angular measurement are then used for case 3 (θ_3), using the same initial value for θ of 38 deg that was used for case 2. Note that correct convergence results for this case. Another point of interest in Figs. 29 and 45 is the symmetry of the convergence of θ as a function of time for cases 1 (θ_1) and 2 (θ_2). Note that one appears to be the mirror image of the other.

[5]Convergence is assumed when the estimated parameter, such as θ, approaches a value with a consistently decreasing value for the standard deviation of its uncertainty.

The bounds on the initial values of θ for which convergence to the nominal or image aiming points will occur is the next point of interest. Several initial values for θ were run using an initial standard deviation of 10 deg and using only the range-rate measurements with a data noise of 0.01 m/sec. These are plotted in Fig. 61. Initial values of the other variables and their standard deviations were not altered. For the cases run, note that the initial θ values of 38, 30, 27, and 25 deg approximately converge to the incorrect image value of 35 deg. The initial θ values of 35, 32, and 22 deg converge to the correct value of 25 deg. The time-varying standard deviations of all the cases are about the same as that of cases 1 and 2 of Fig. 46. Also note in Fig. 61 that it is possible for the initial estimated value of θ (25 deg) to be almost correct and still converge to the incorrect image solution (35 deg). It is not clear why this takes place. However, from Fig. 61, once the estimated value of θ crosses the approximate mid-point ($\theta = 30$ deg) between the image and the nominal θ, the parameter then seems to eventually converge to the other solution.

The estimates of η_E and η_C of Figs. 35, 41, 51, and 57 did not improve, since the standard deviation of θ did not become less than the *a priori* standard deviations of η_E and η_C (0.1 deg). The angles η_E and η_C are linked with θ by the expressions $\cos(\eta_E - \theta)$ and $\cos(\eta_C - \theta)$ of Eqs. (19) and (20).

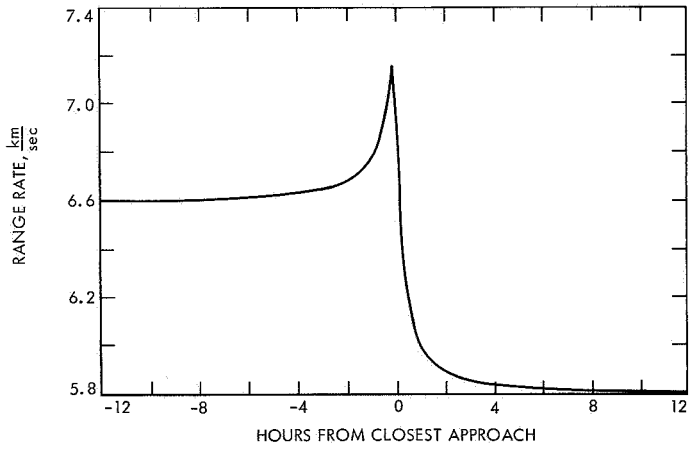

Fig. 12. Nominal range rate vs time from closest approach

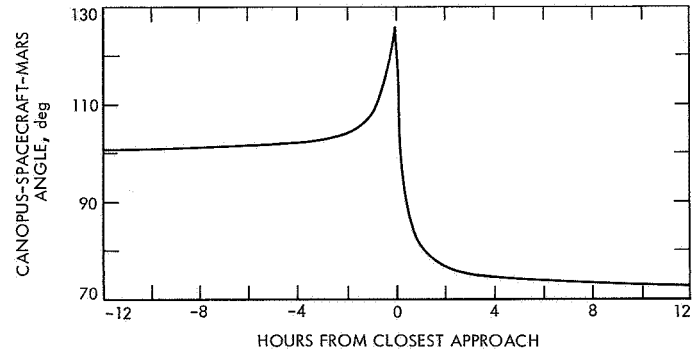

Fig. 13. Nominal Canopus–spacecraft–Mars angle (angular measurement) vs time from closest approach

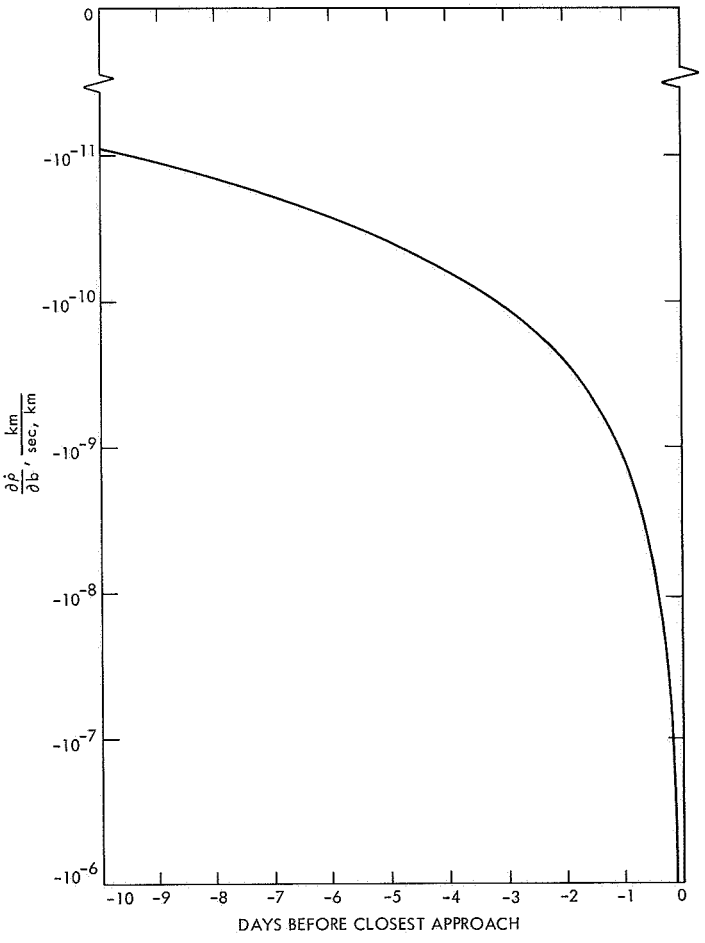

Fig. 14. Partial derivative of range rate with respect to impact parameter *b* vs days before closest approach

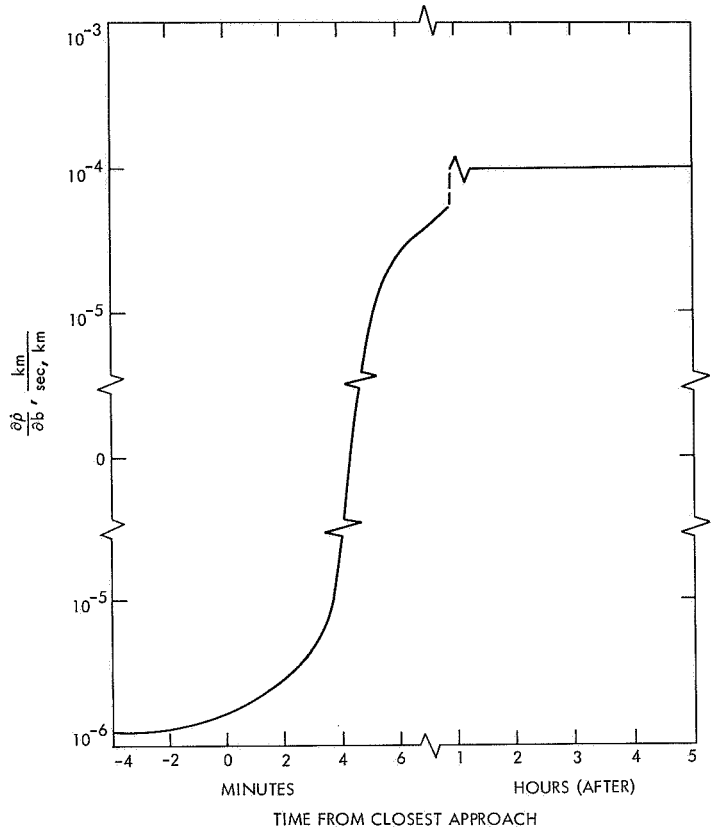

Fig. 15. Partial derivative of range rate with respect to impact parameter *b* vs time near closest approach

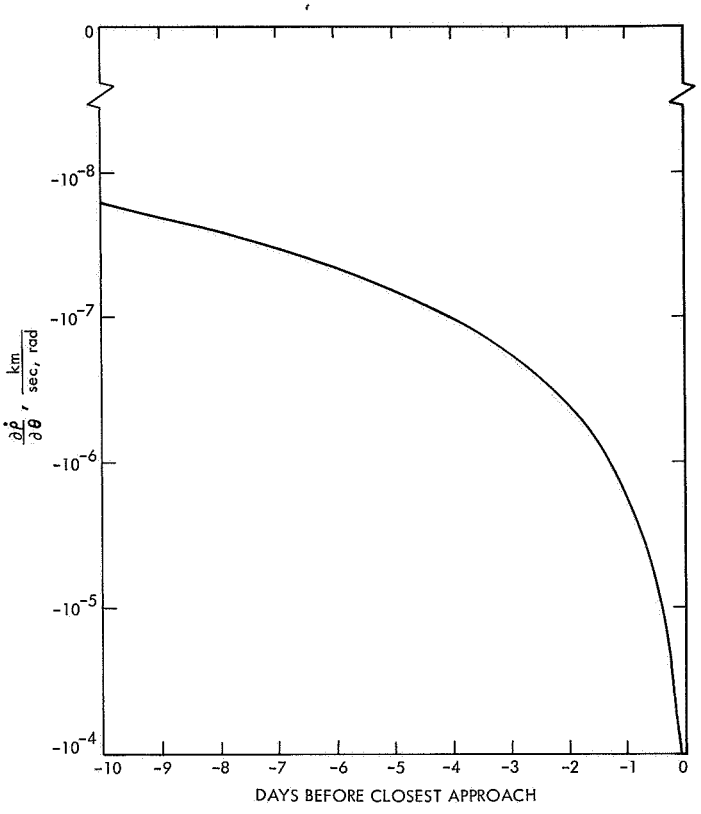

Fig. 16. Partial derivative of range rate with respect to trajectory-plane orientation θ vs days before closest approach

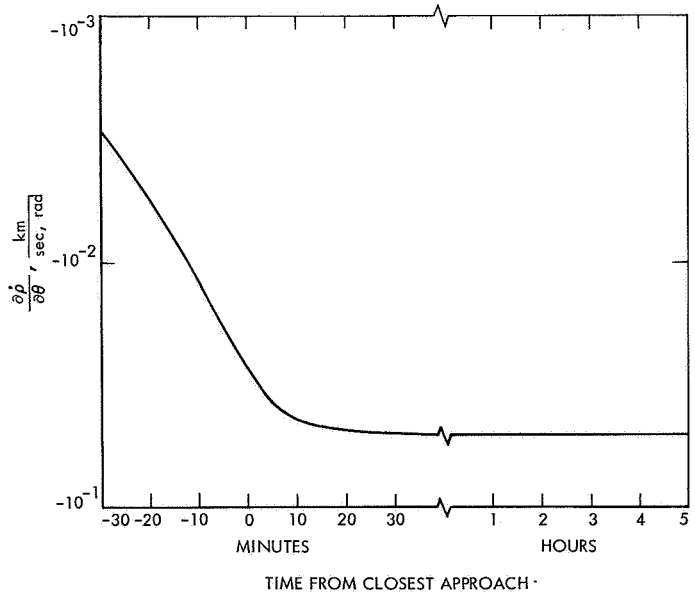

Fig. 17. Partial derivative of range rate with respect to trajectory-plane orientation θ vs time near closest approach

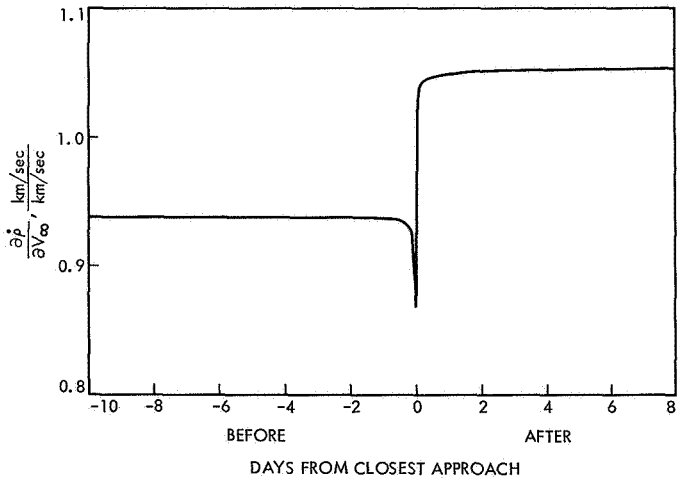

Fig. 18. Partial derivative of range rate with respect to hyperbolic excess speed V_∞ vs time from closest approach

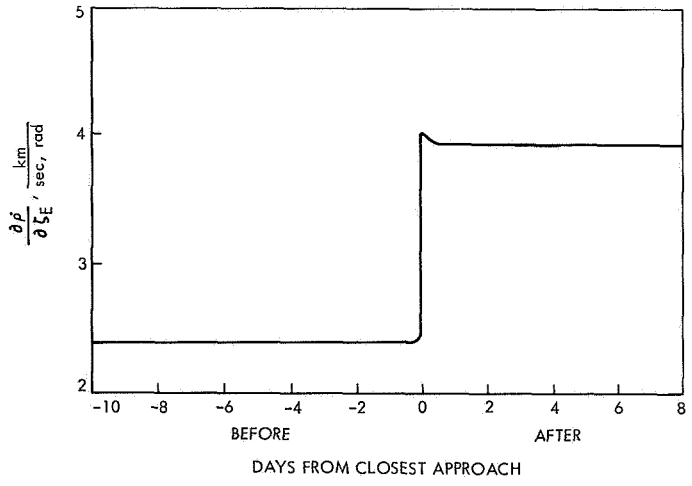

Fig. 19. Partial derivative of range rate with respect to angle ζ_E vs time from closest approach

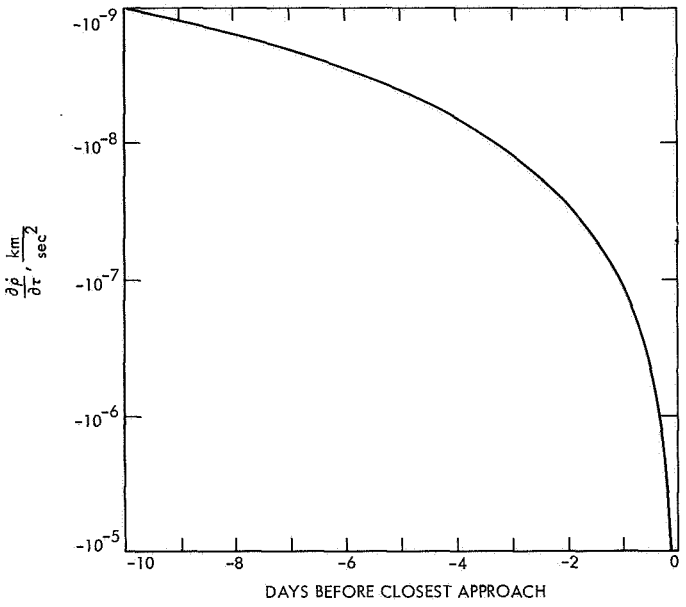

Fig. 20. Partial derivative of range rate with respect to time of periapsis passage τ vs days before closest approach

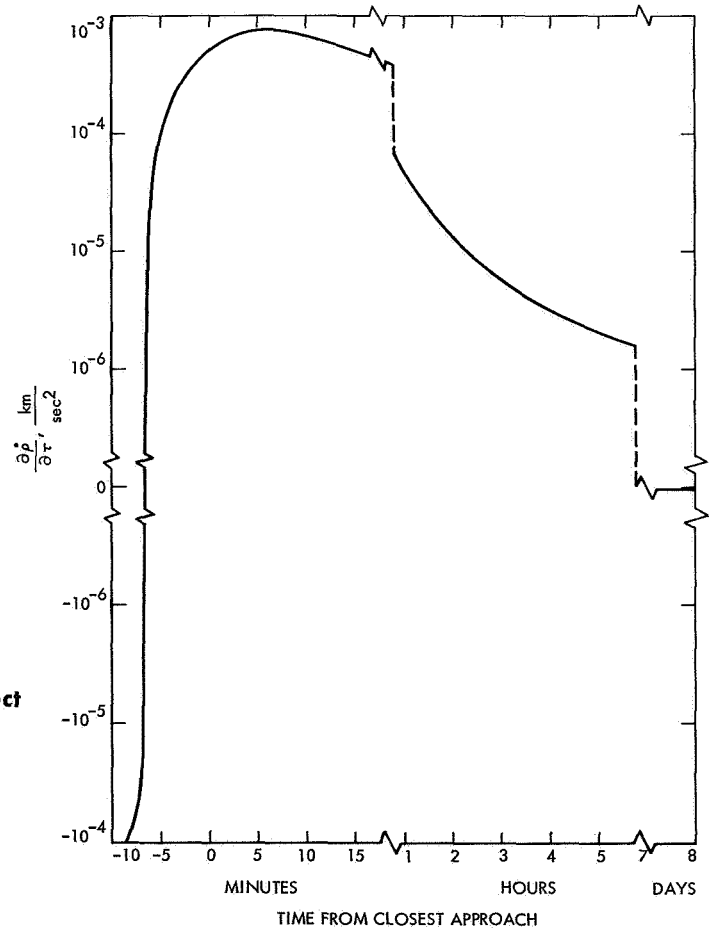

Fig. 21. Partial derivative of range rate with respect to time of periapsis passage τ vs time near closest approach

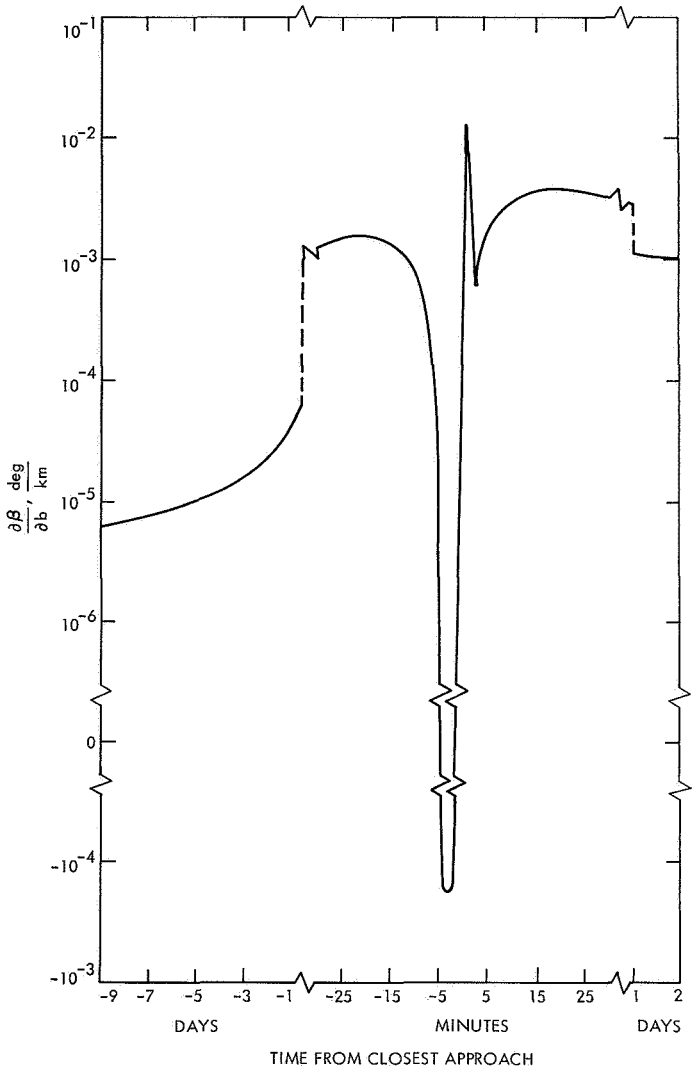

Fig. 22. Partial derivative of angular measurement with respect to impact parameter *b* vs time from closest approach

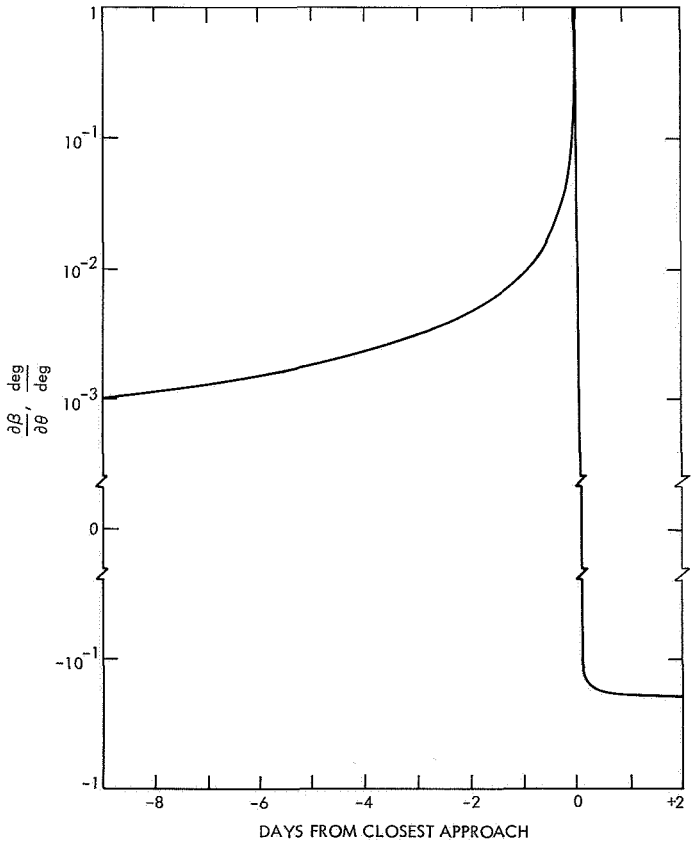

Fig. 23. Partial derivative of angular measurement with respect to trajectory-plane orientation θ vs time from closest approach

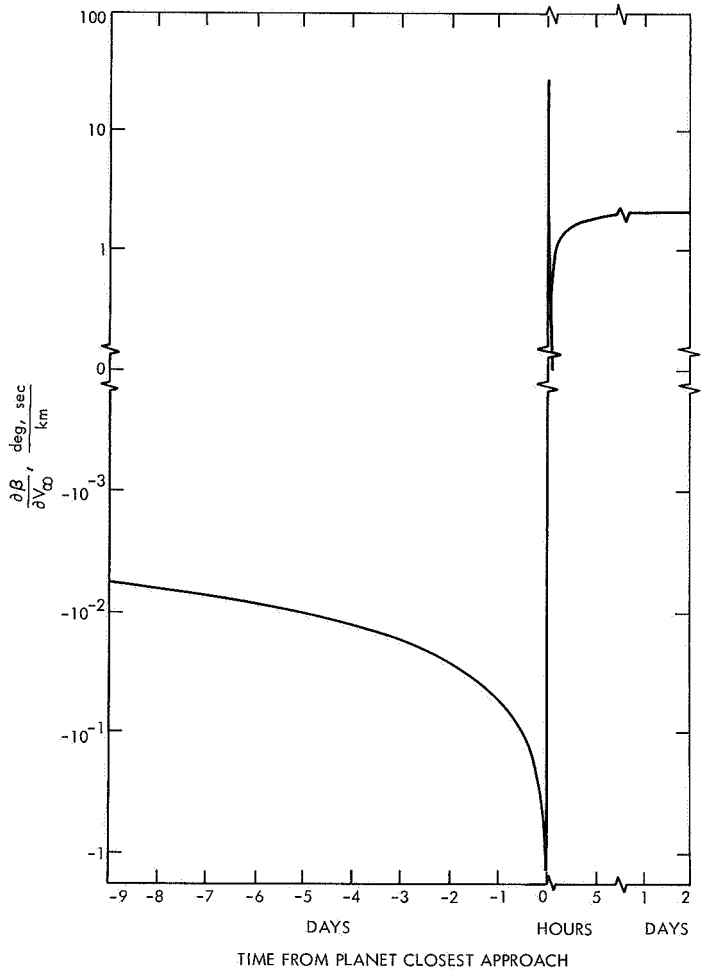

Fig. 24. Partial derivative of angular measurement with respect to hyperbolic excess speed V_∞ vs time from closest approach

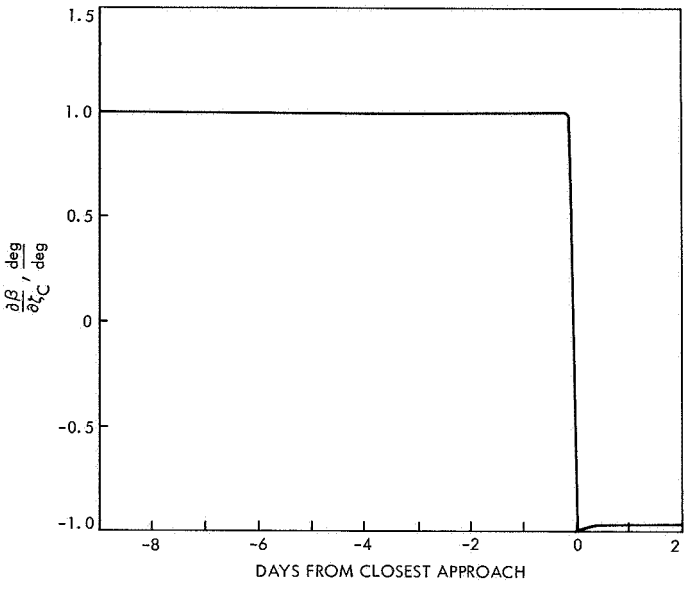

Fig. 25. Partial derivative of angular measurement with respect to angle ζ_C vs time from closest approach

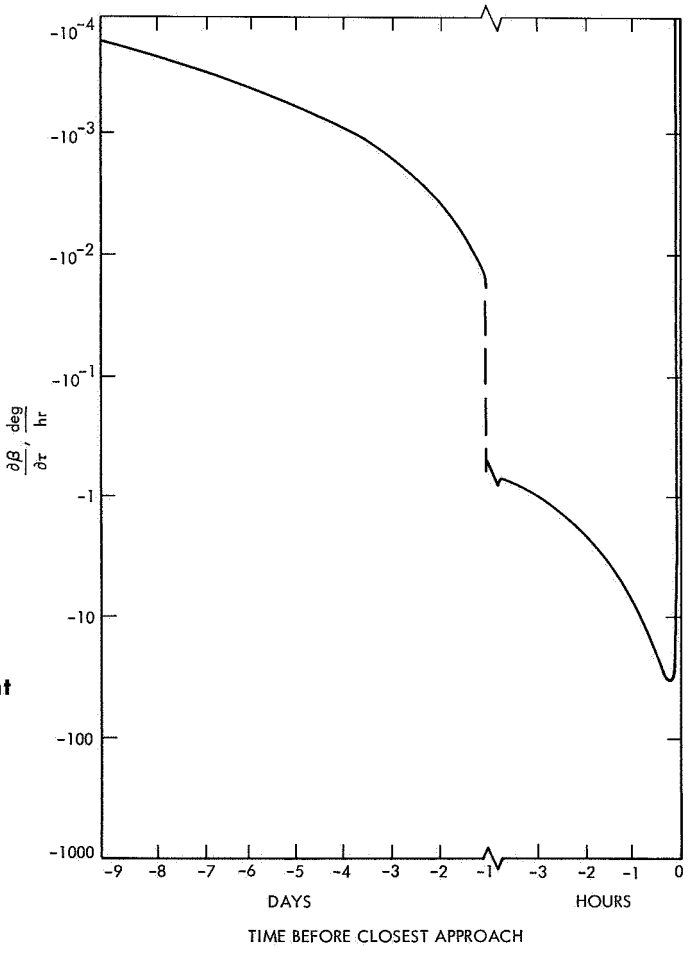

Fig. 26. Partial derivative of angular measurement with respect to time of periapsis passage τ vs time before closest approach

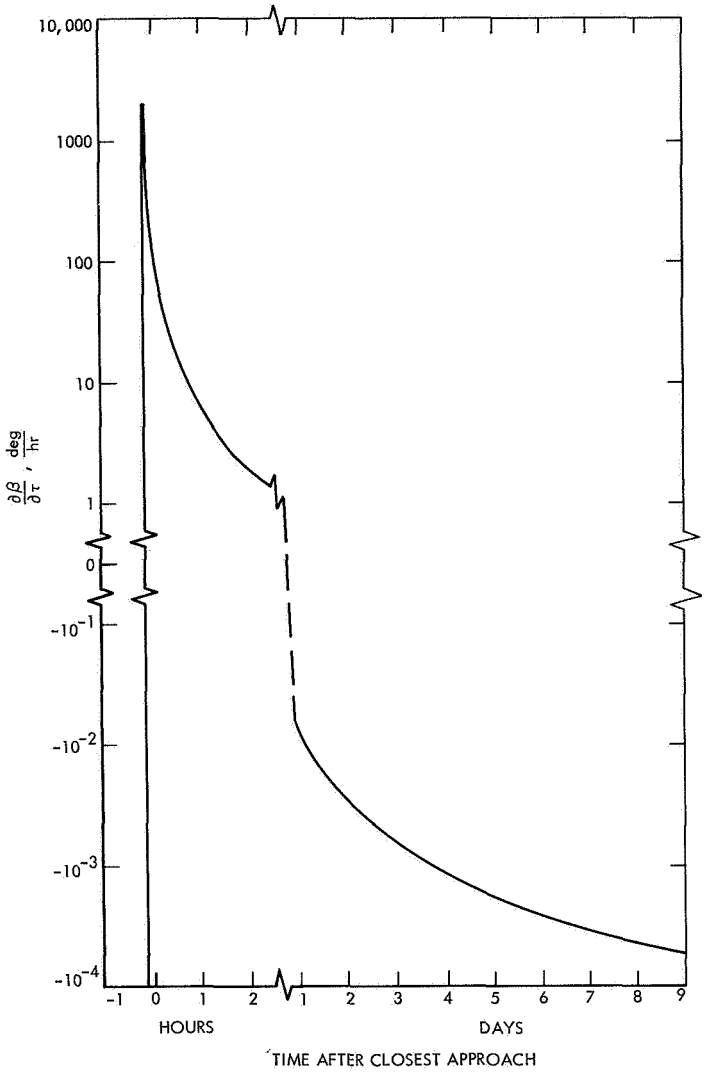

Fig. 27. Partial derivative of angular measurement with respect to time of periapsis passage τ vs time after closest approach

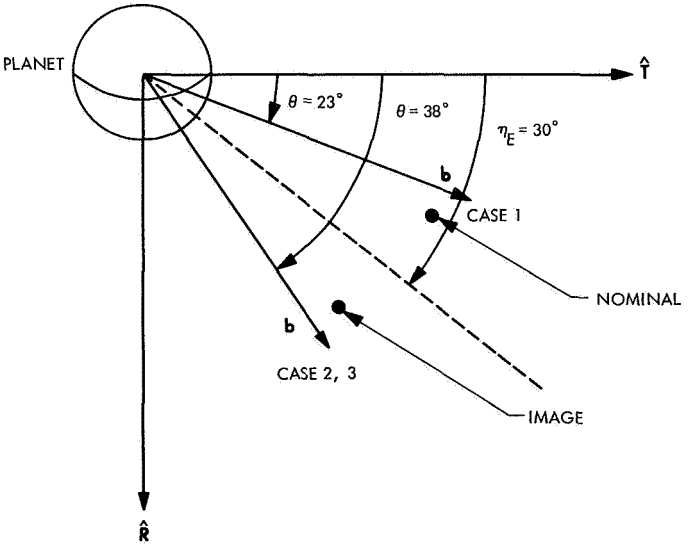

Fig. 28. Initial aiming points for three cases plotted in Figs. 29–60

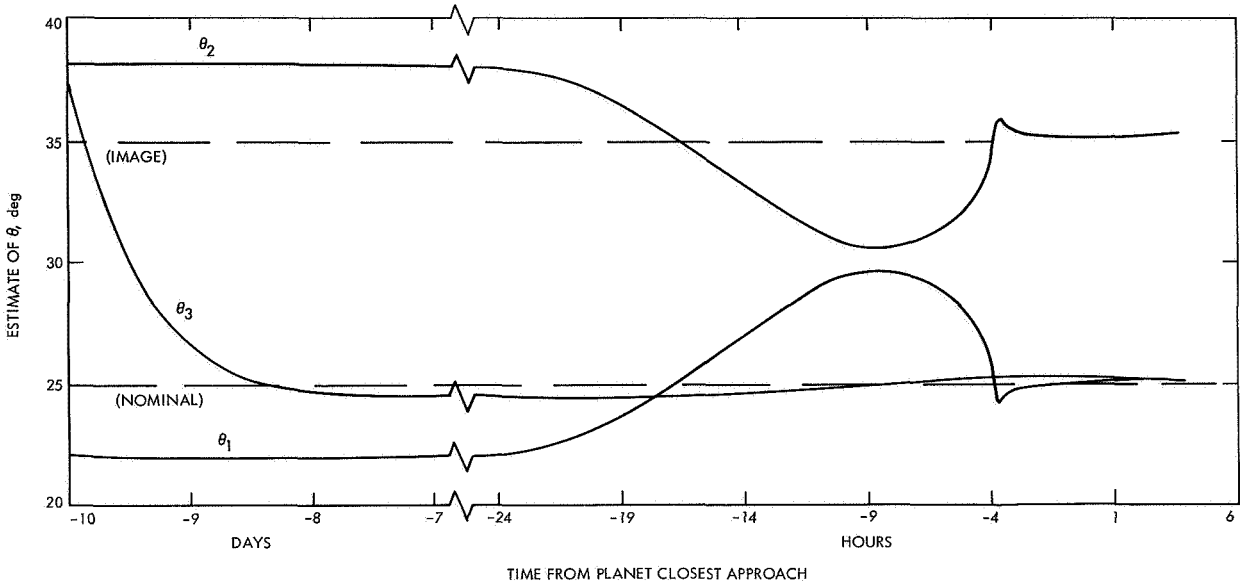

Fig. 29. Estimate of trajectory-plane orientation θ vs time from closest approach for $\sigma_{\dot{\rho}} = 0.001$ m/sec

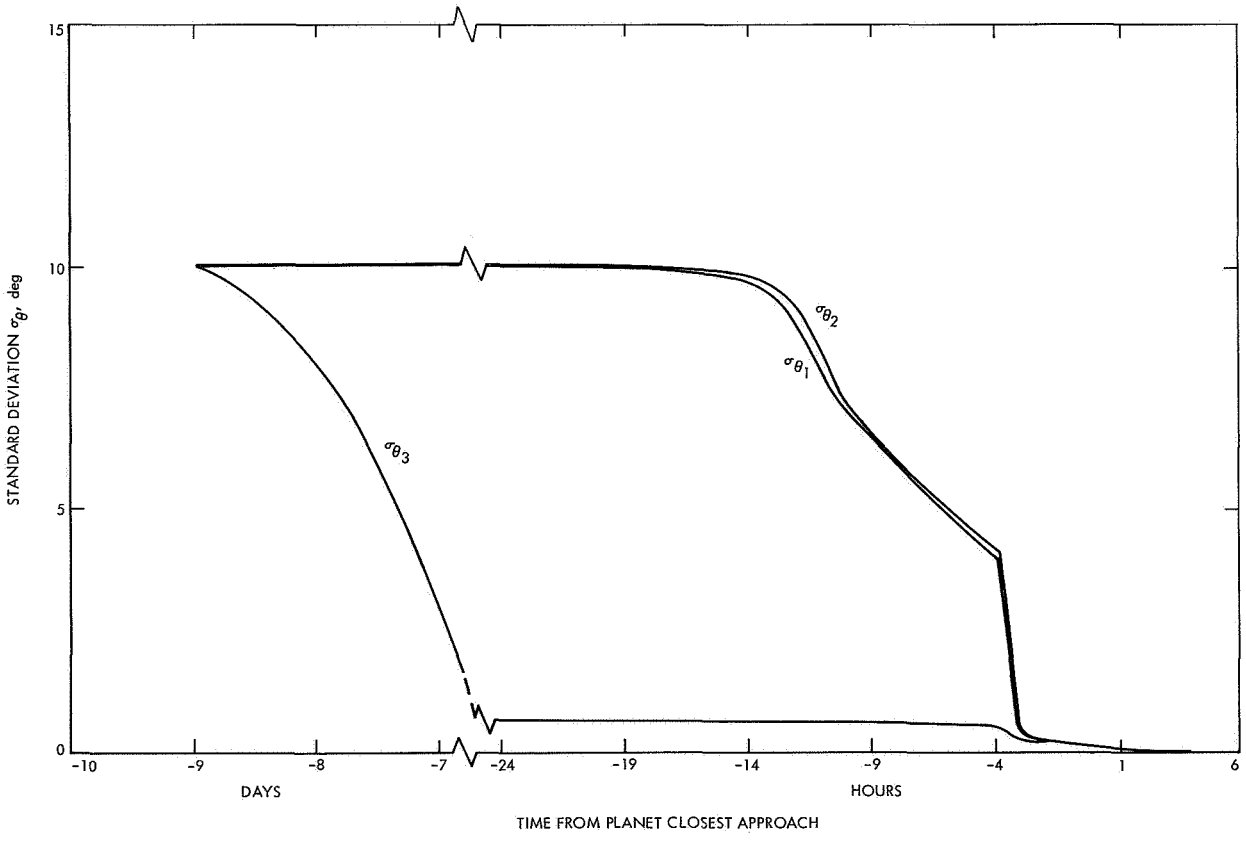

Fig. 30. Standard deviation of trajectory-plane orientation θ vs time from closest approach for $\sigma_{\dot{\rho}} = 0.001$ m/sec

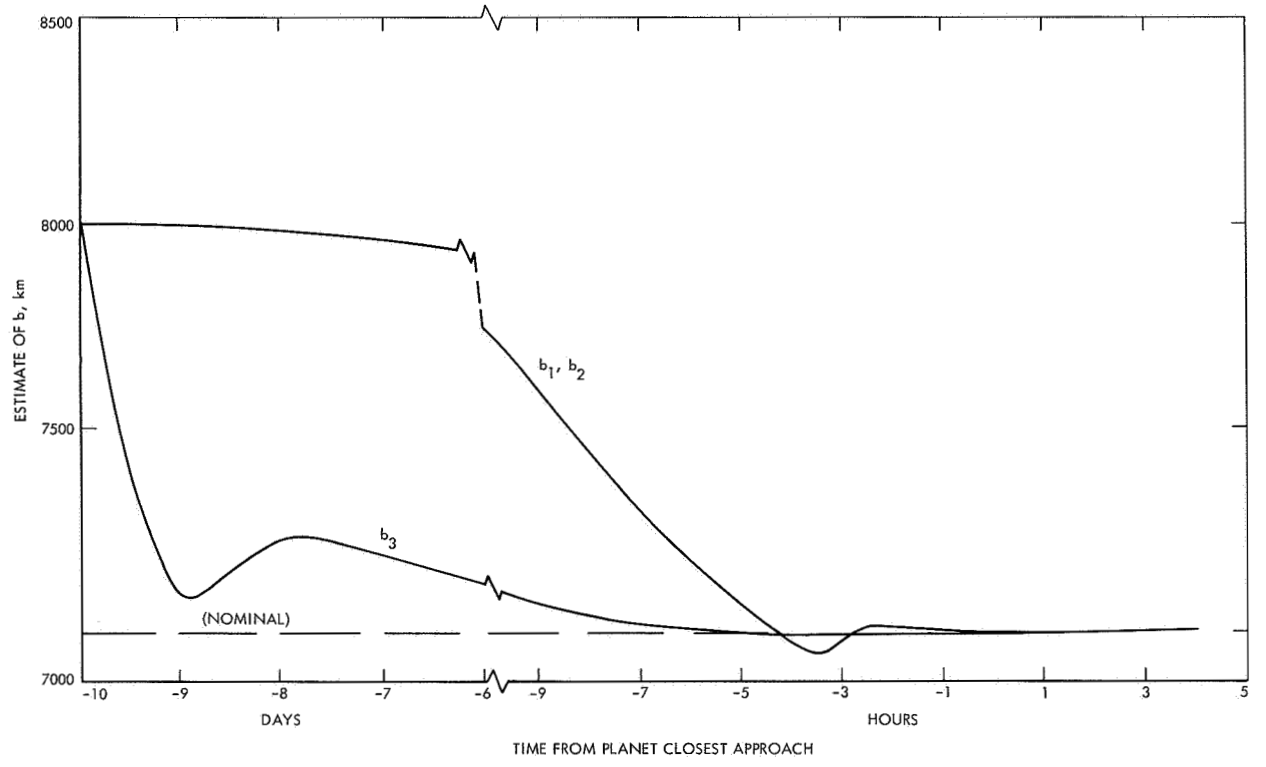

Fig. 31. Estimate of impact parameter *b* vs time from closest approach for $\sigma_{\dot{\rho}}^{\cdot} = 0.001$ m/sec

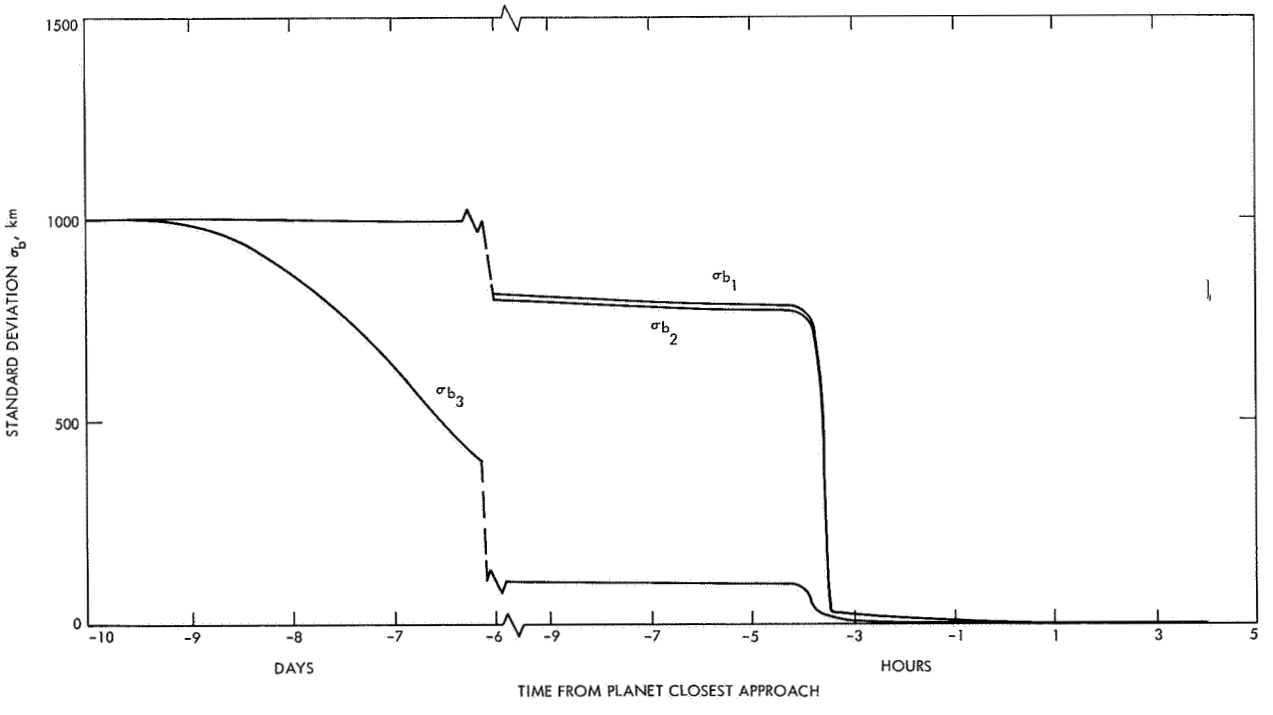

Fig. 32. Standard deviation of impact parameter *b* vs time from closest approach for $\sigma_{\dot{\rho}}^{\cdot} = 0.001$ m/sec

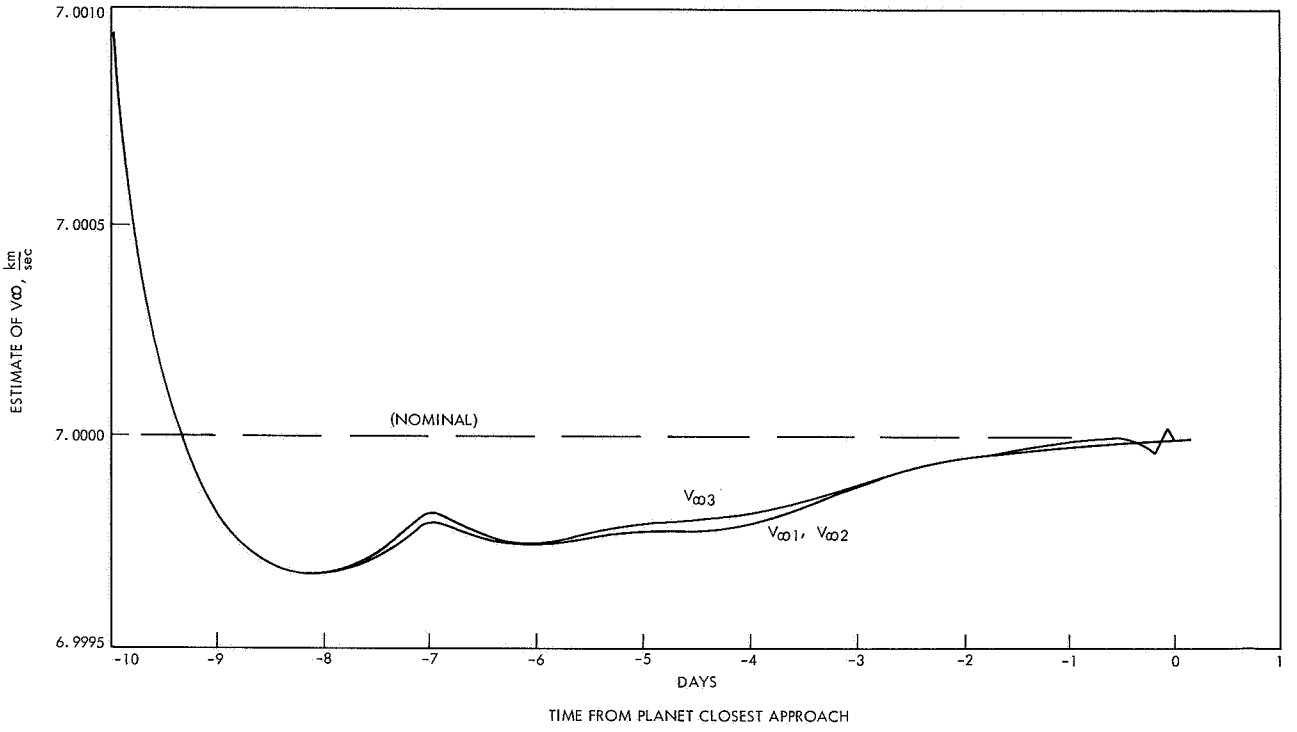

Fig. 33. Estimate of hyperbolic excess speed V_∞ vs time from closest approach for $\sigma_{\dot{\rho}}^{\bullet} = 0.001$ m/sec

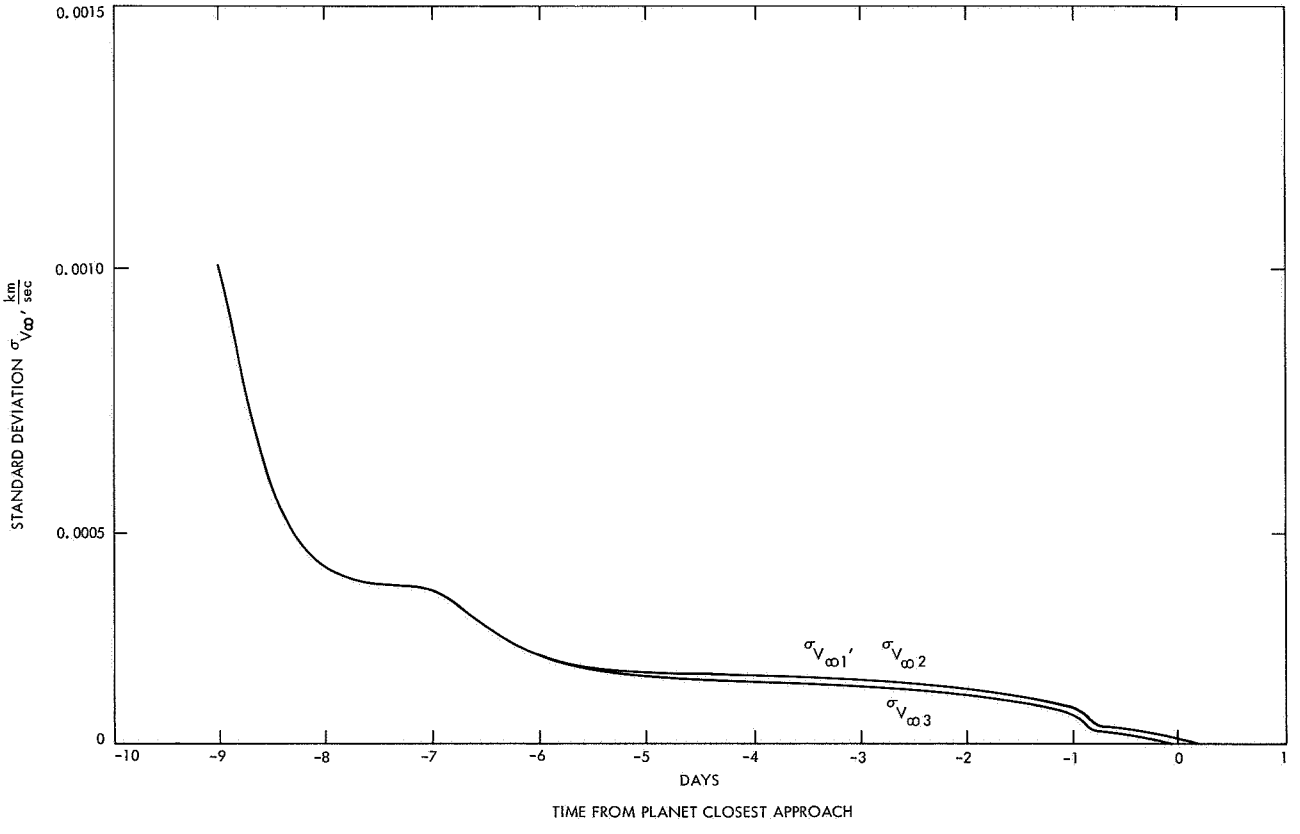

Fig. 34. Standard deviation of hyperbolic excess speed V_∞ vs time from closest approach for $\sigma_{\dot{\rho}}^{\bullet} = 0.001$ m/sec

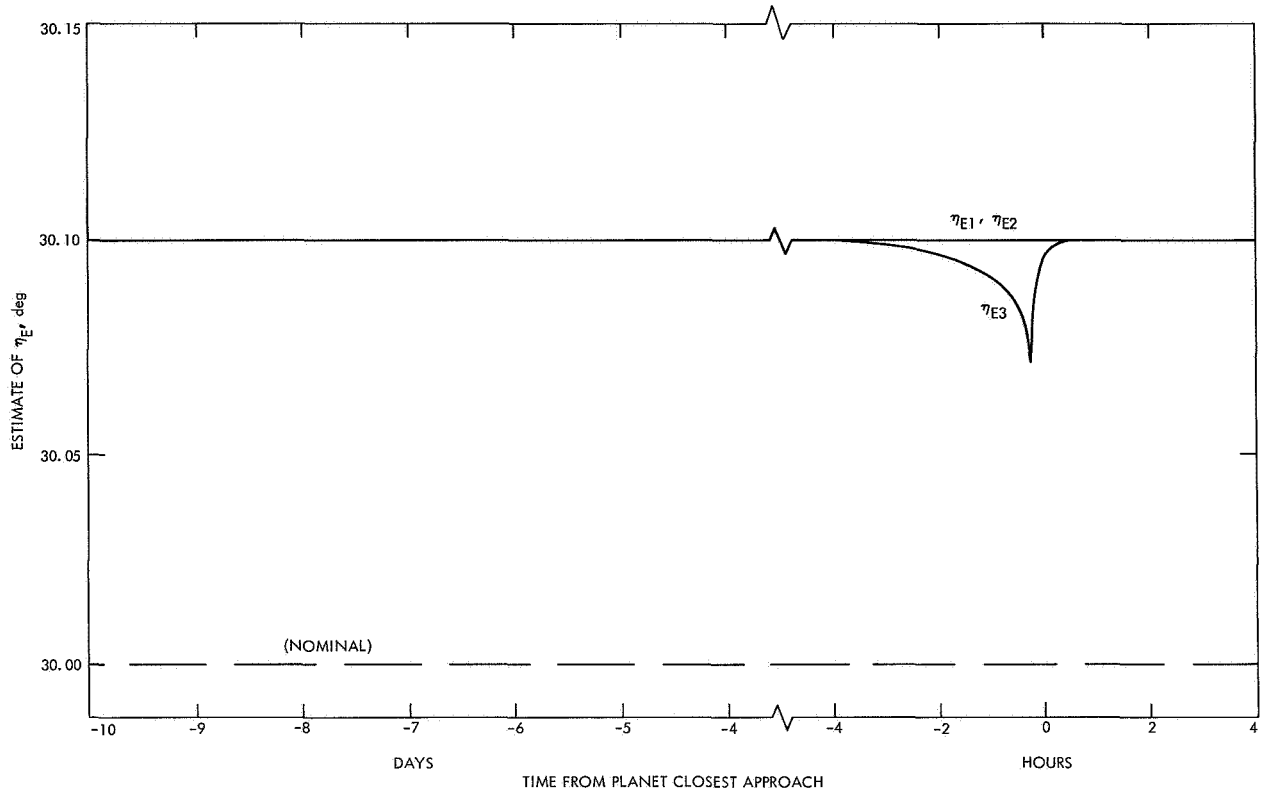

Fig. 35. Estimate of parameter η_E vs time from closest approach for $\sigma_{\dot{\rho}} = 0.001$ m/sec

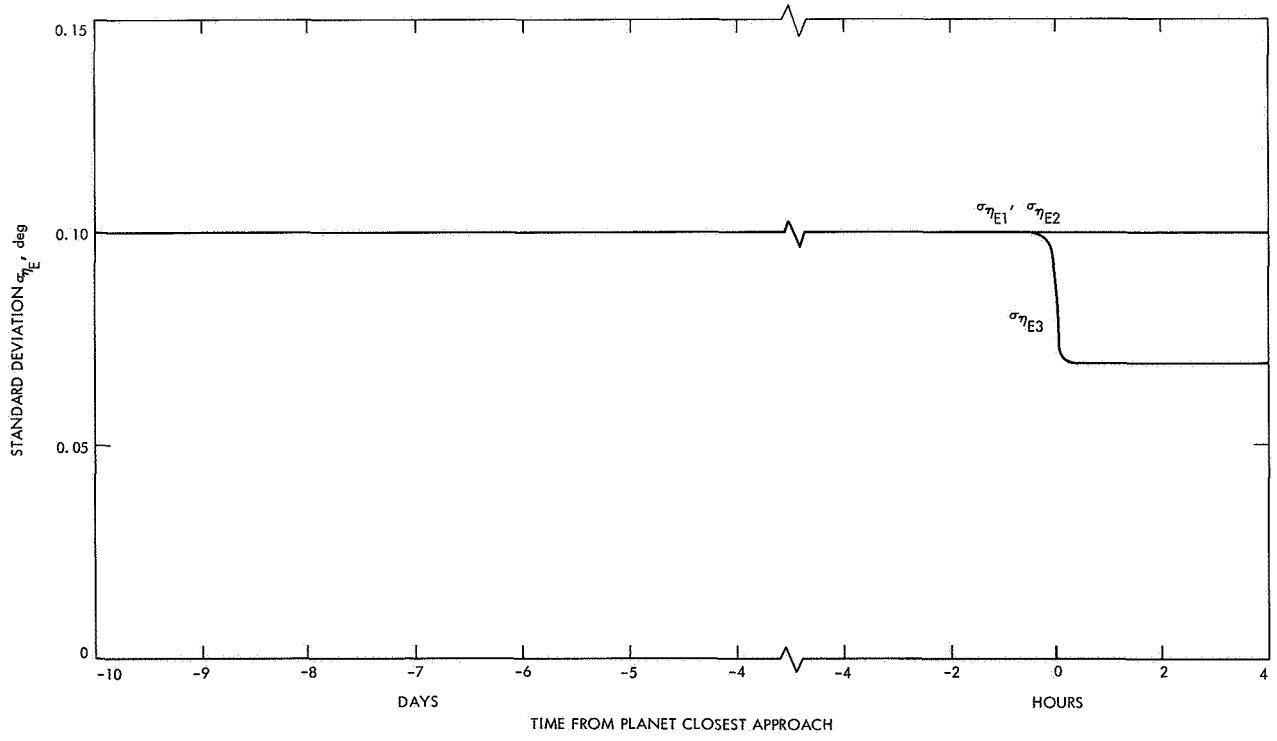

Fig. 36. Standard deviation of parameter η_E vs time from closest approach for $\sigma_{\dot{\rho}} = 0.001$ m/sec

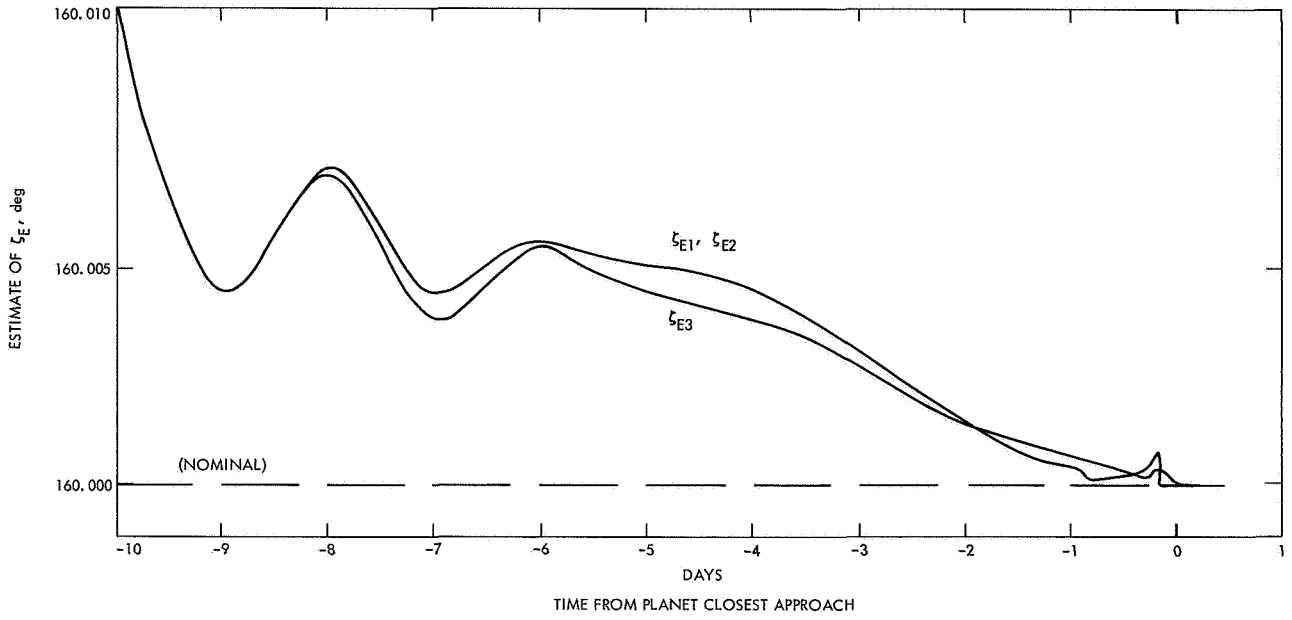

Fig. 37. Estimate of parameter ζ_E vs time from closest approach for $\sigma_{\dot{\rho}} = 0.001$ m/sec

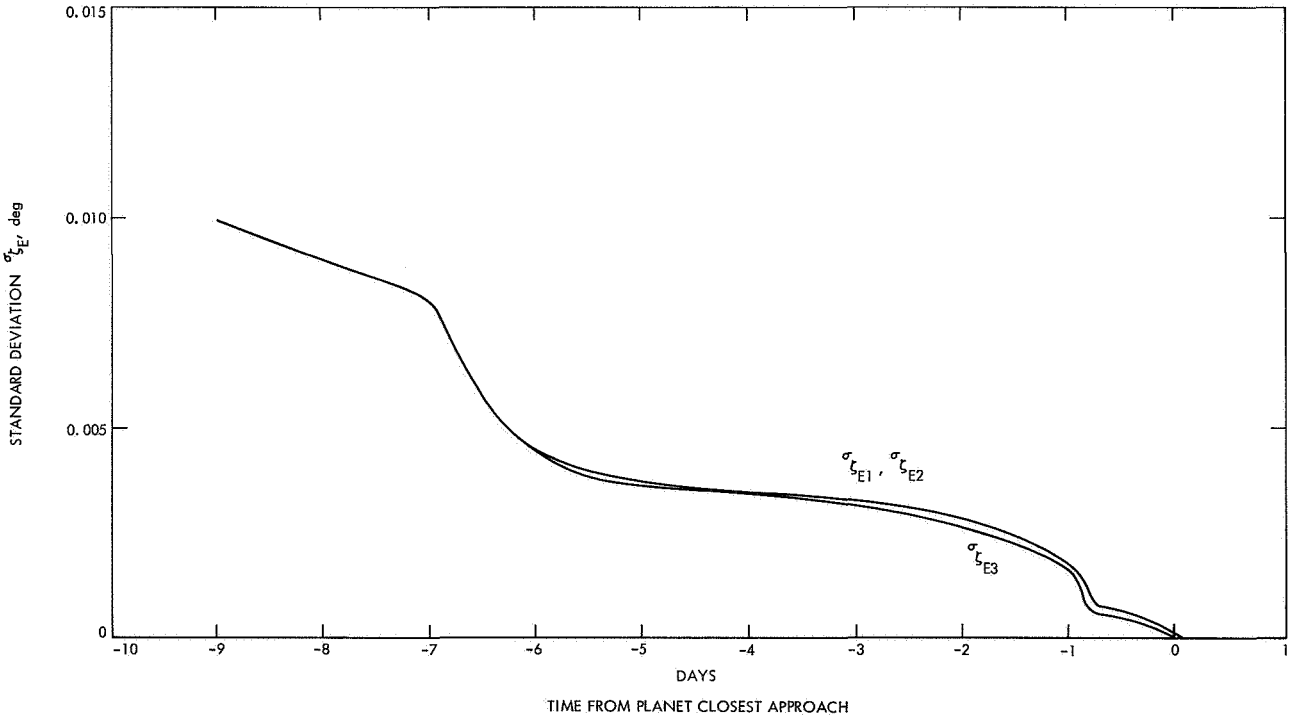

Fig. 38. Standard deviation of parameter ζ_E vs time from closest approach for $\sigma_{\dot{\rho}} = 0.001$ m/sec

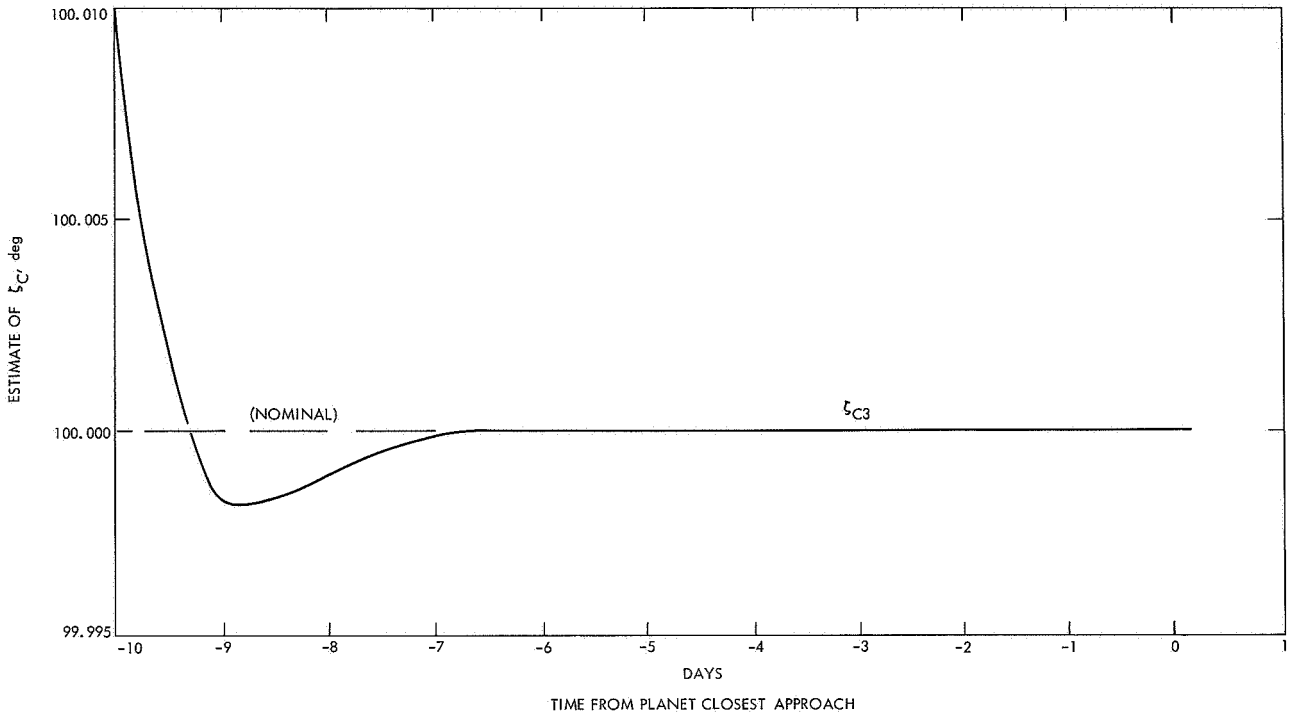

Fig. 39. Estimate of parameter ζ_C vs time from closest approach for $\sigma_{\dot{\rho}} = 0.001$ m/sec

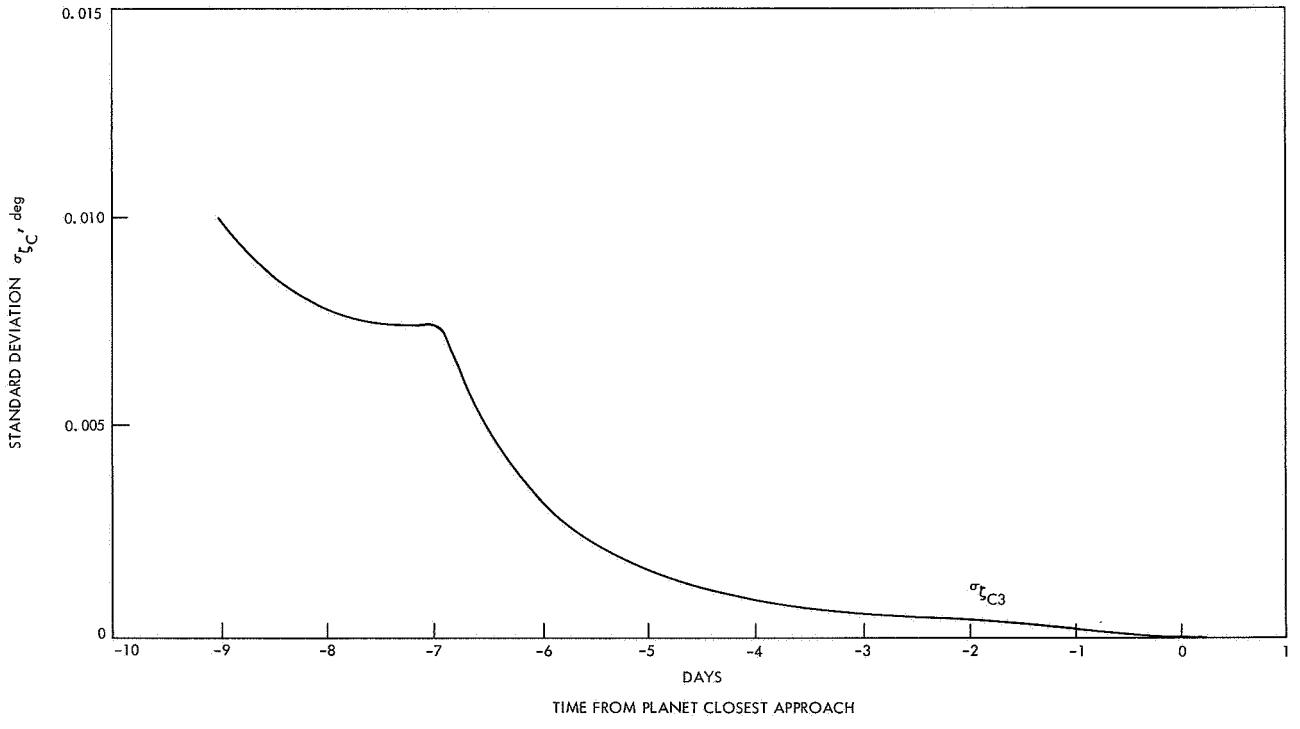

Fig. 40. Standard deviation of parameter ζ_C vs time from closest approach for $\sigma_{\dot{\rho}} = 0.001$ m/sec

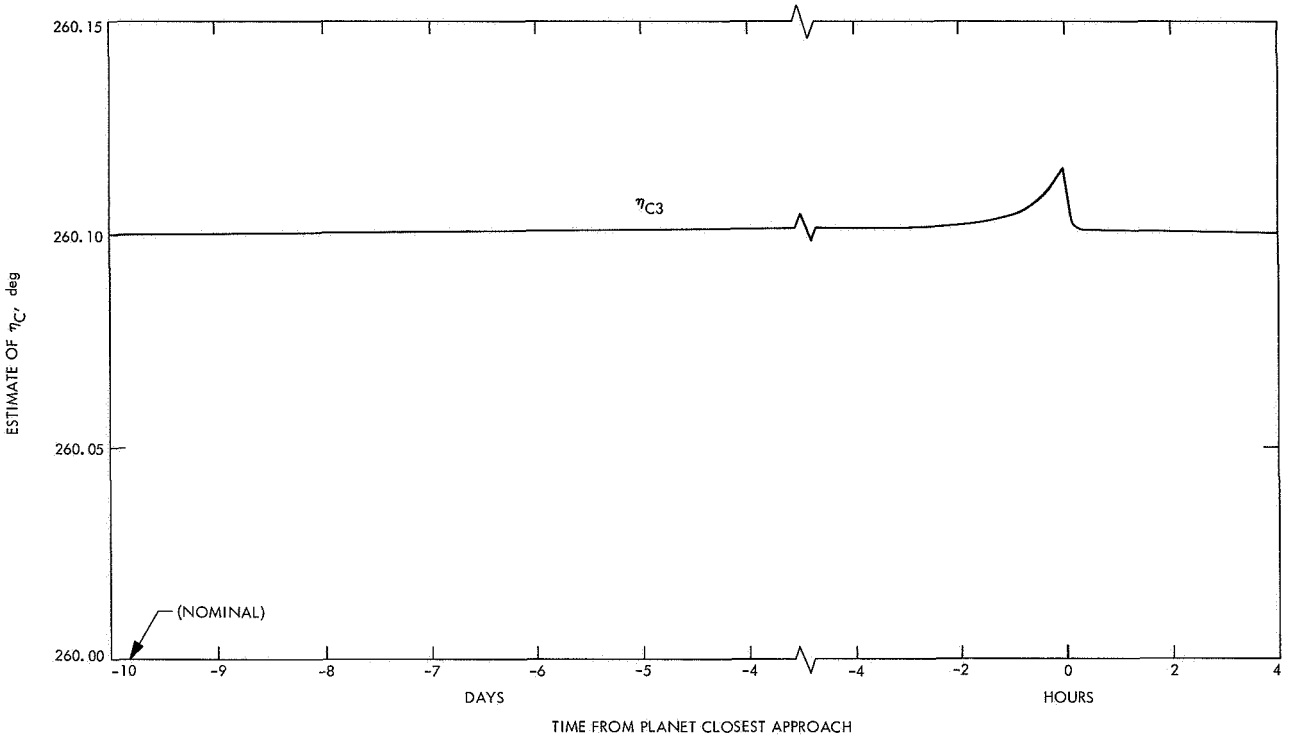

Fig. 41. Estimate of parameter η_C vs time from closest approach for $\sigma_{\dot{\rho}} = 0.001$ m/sec

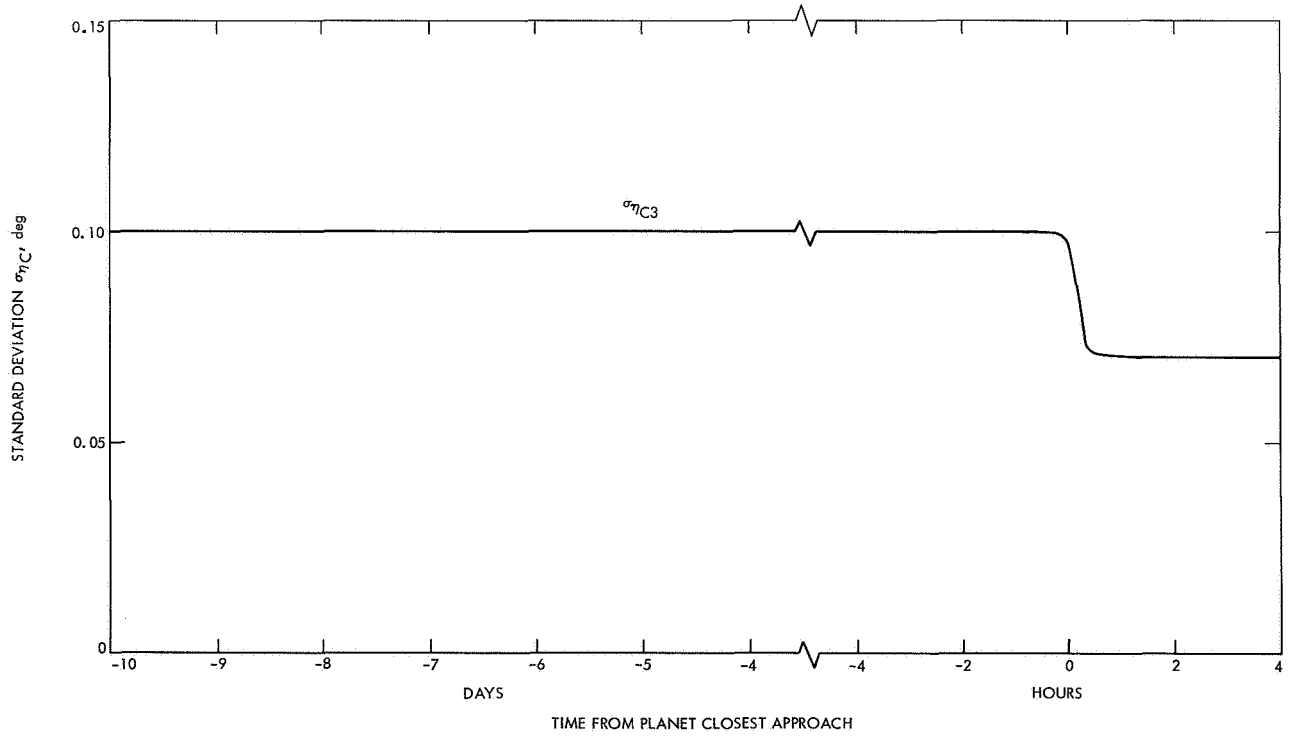

Fig. 42. Standard deviation of parameter η_C vs time from closest approach for $\sigma_{\dot{\rho}} = 0.001$ m/sec

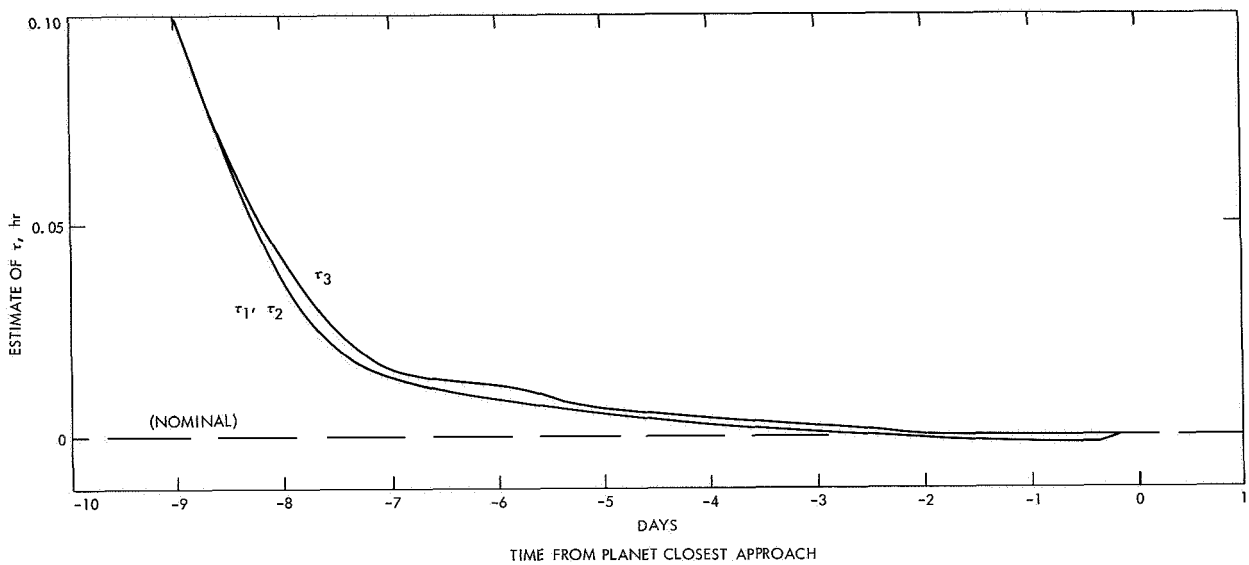

Fig. 43. Estimate of time of periapsis passage τ vs time from closest approach for $\sigma_{\dot{\rho}}^{\cdot} = 0.001$ m/sec

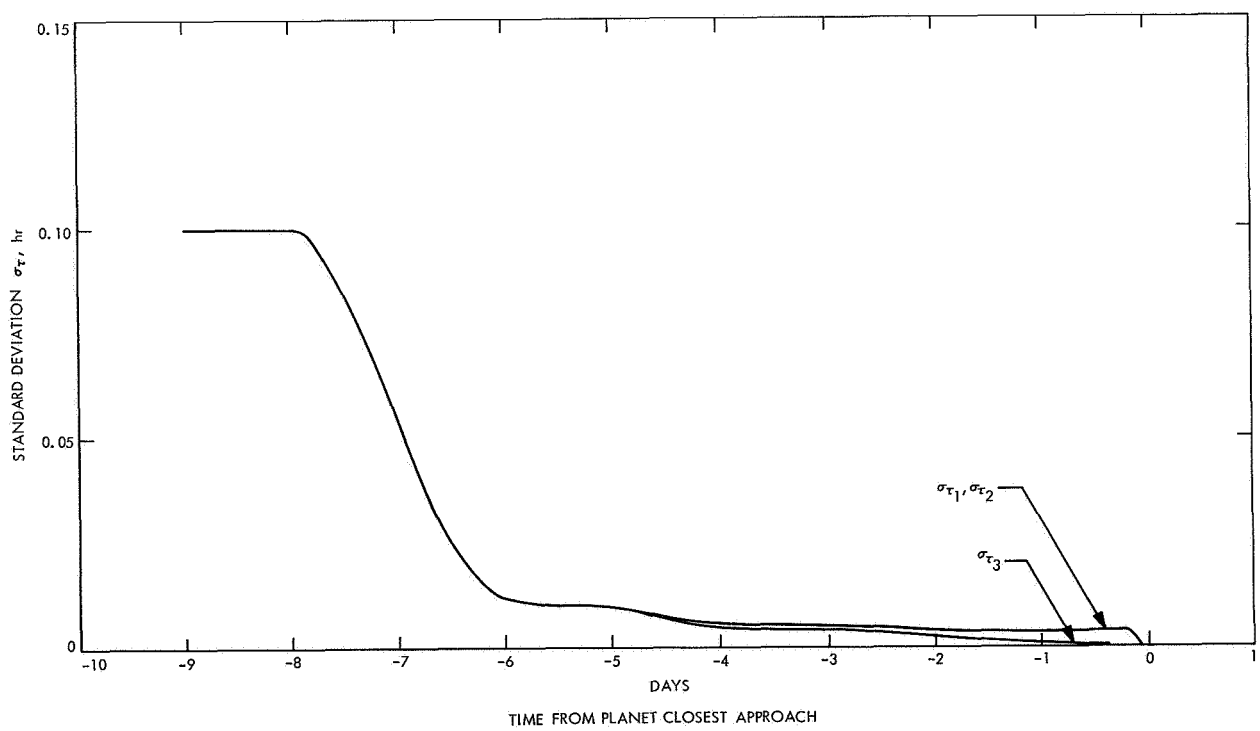

Fig. 44. Standard deviation of time of periapsis passage τ vs time from closest approach for $\sigma_{\dot{\rho}}^{\cdot} = 0.001$ m/sec

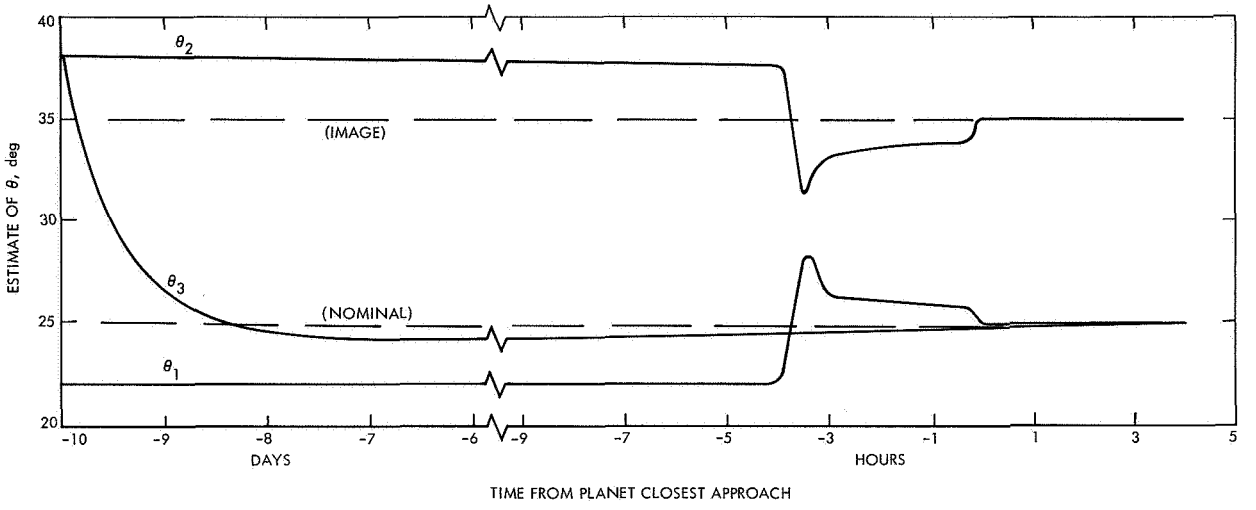

Fig. 45. Estimate of trajectory-plane orientation θ vs time from closest approach for $\sigma_{\dot{\rho}} = 0.01$ m/sec

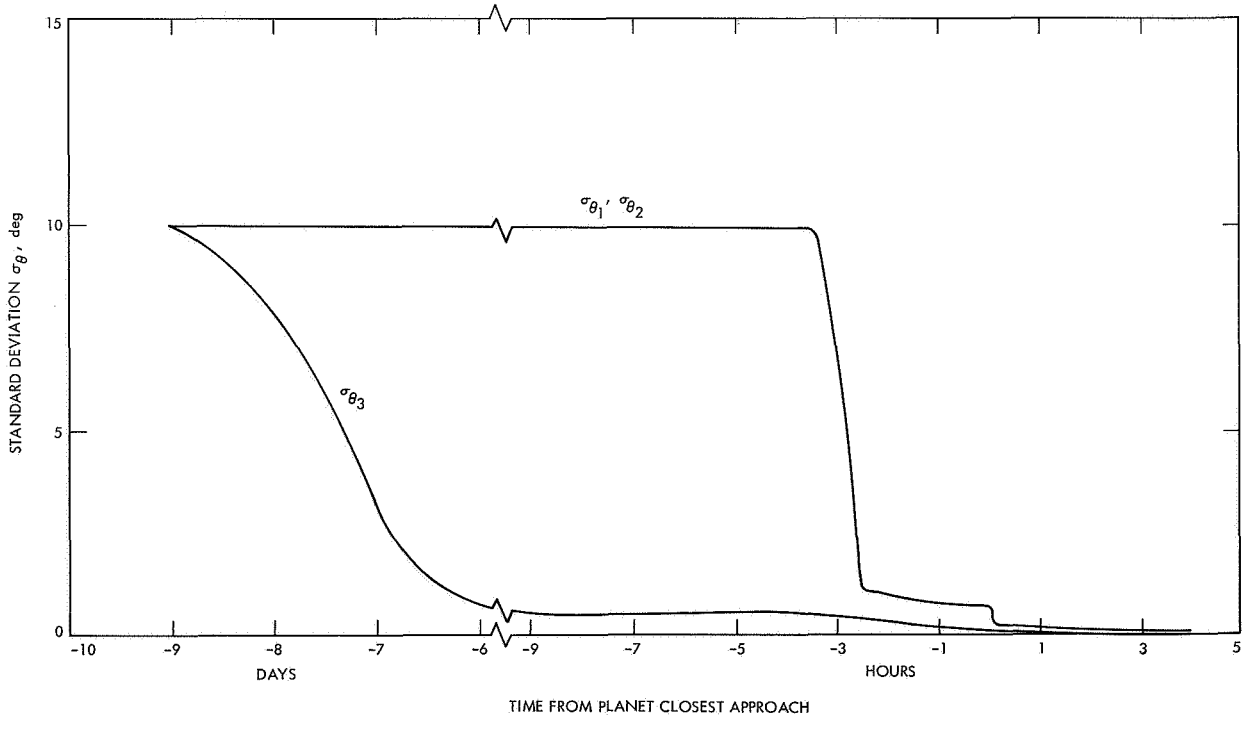

Fig. 46. Standard deviation of trajectory-plane orientation θ vs time from closest approach for $\sigma_{\dot{\rho}} = 0.01$ m/sec

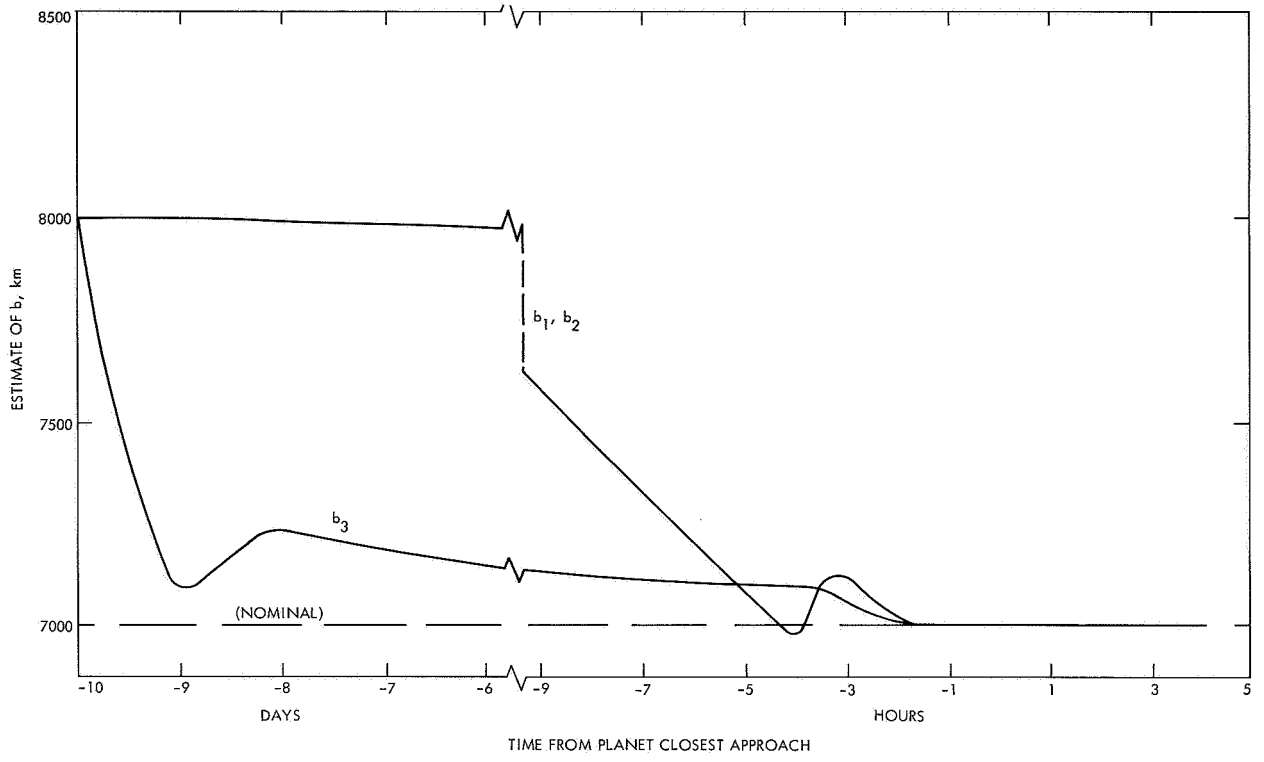

Fig. 47. Estimate of impact parameter *b* vs time from closest approach for $\sigma_{\dot{\rho}}^{\cdot} = 0.01$ m/sec

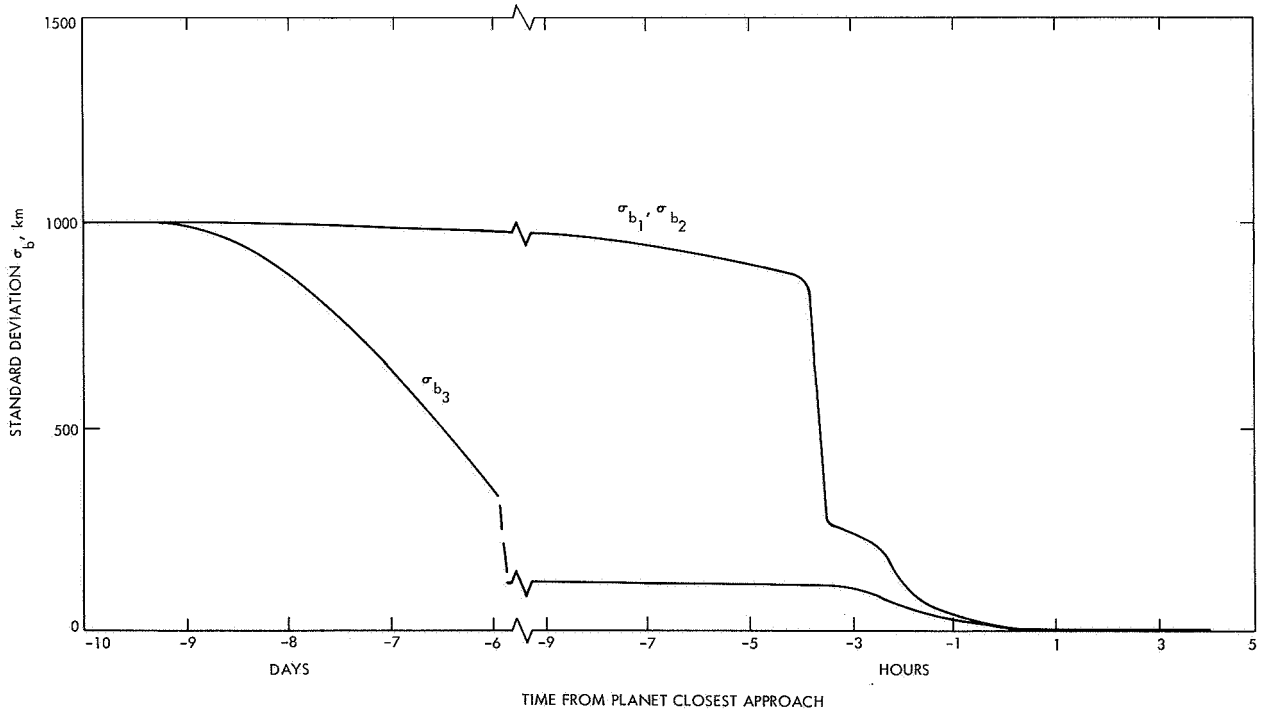

Fig. 48. Standard deviation of impact parameter *b* vs time from closest approach for $\sigma_{\dot{\rho}}^{\cdot} = 0.01$ m/sec

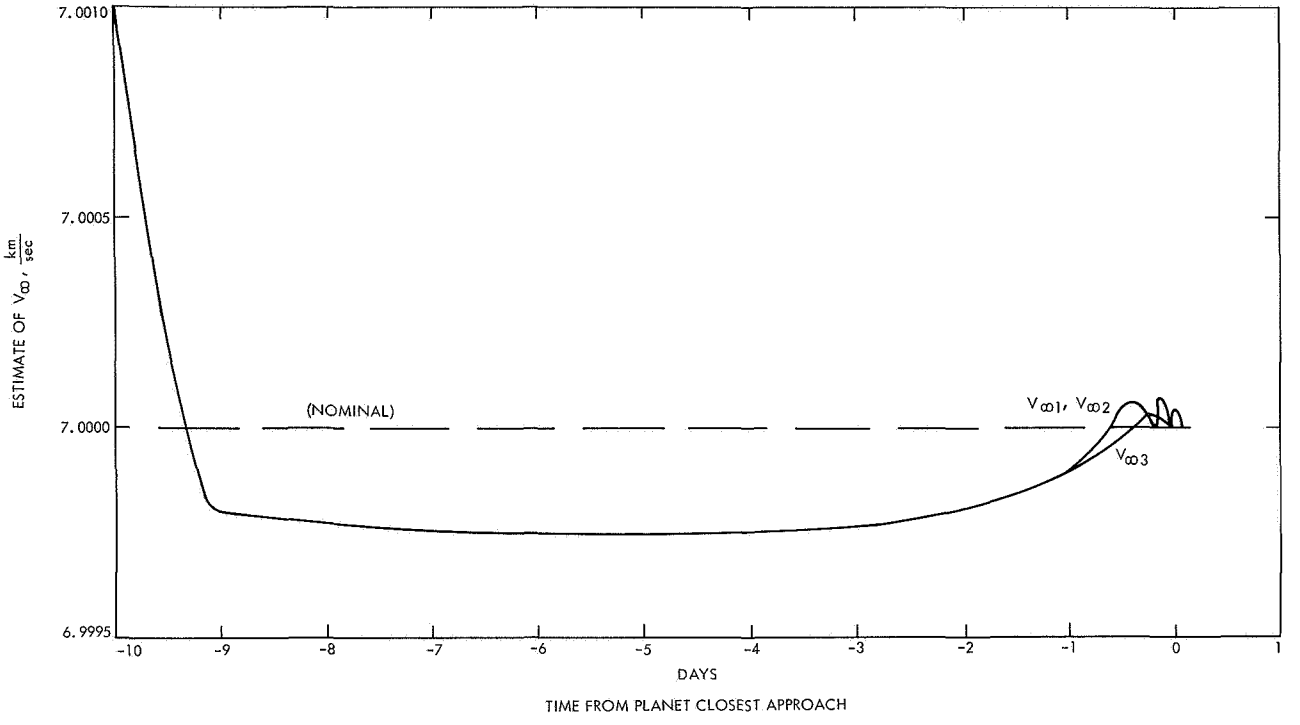

Fig. 49. Estimate of hyperbolic excess speed V_{∞} vs time from closest approach for $\sigma_{\dot{\rho}}^{*} = 0.01$ m/sec

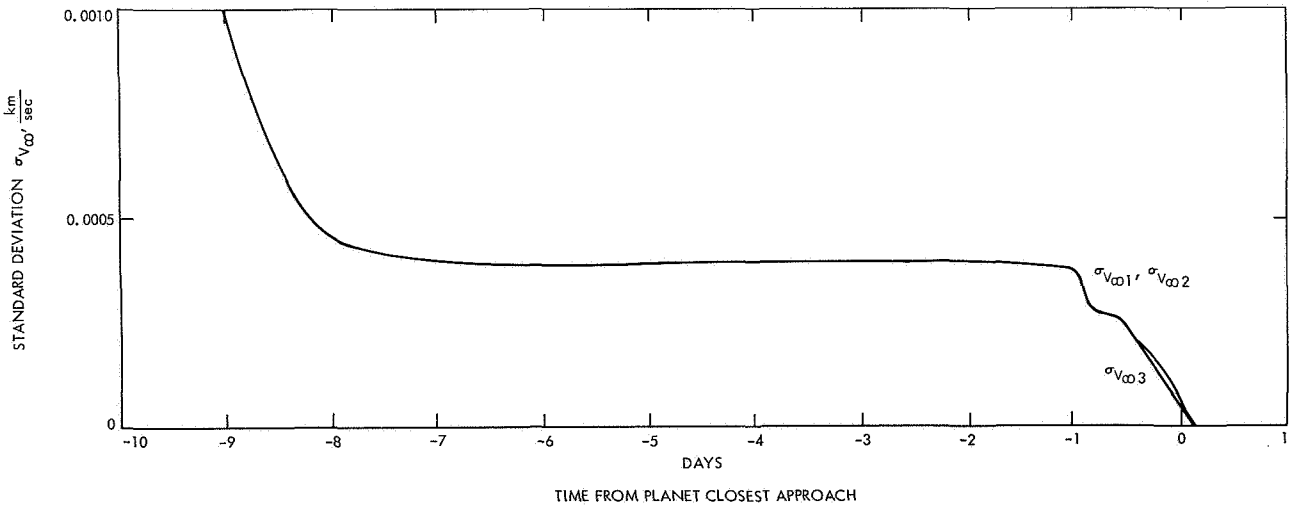

Fig. 50. Standard deviation of hyperbolic excess speed V_{∞} vs time from closest approach for $\sigma_{\dot{\rho}}^{*} = 0.01$ m/sec

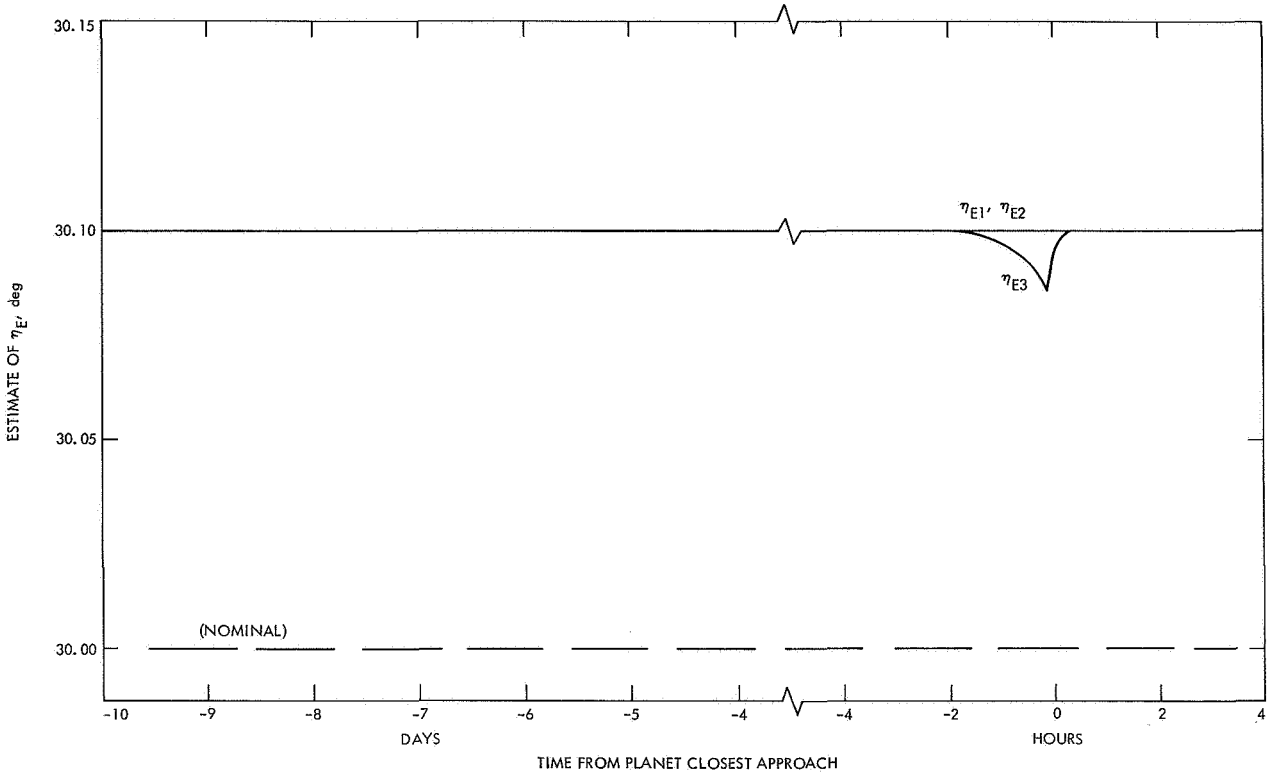

Fig. 51. Estimate of parameter η_E vs time from closest approach for $\sigma_{\dot{\rho}} = 0.01$ m/sec

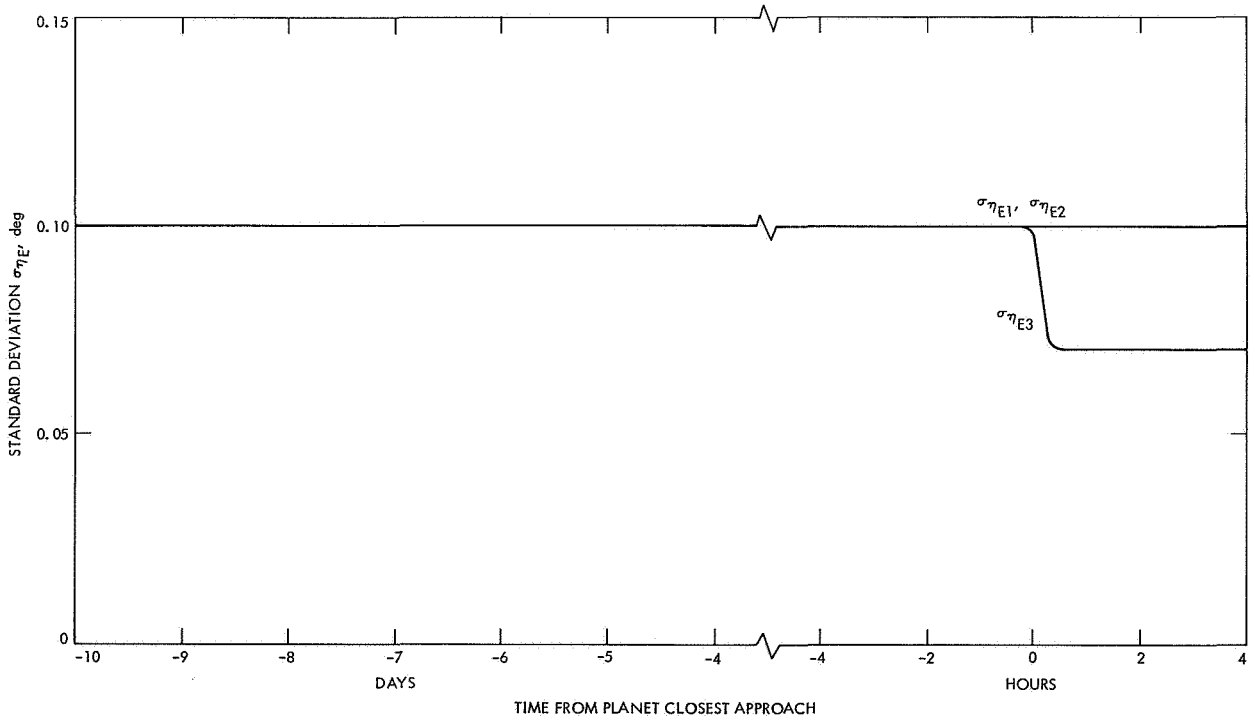

Fig. 52. Standard deviation of parameter η_E vs time from closest approach for $\sigma_{\dot{\rho}} = 0.01$ m/sec

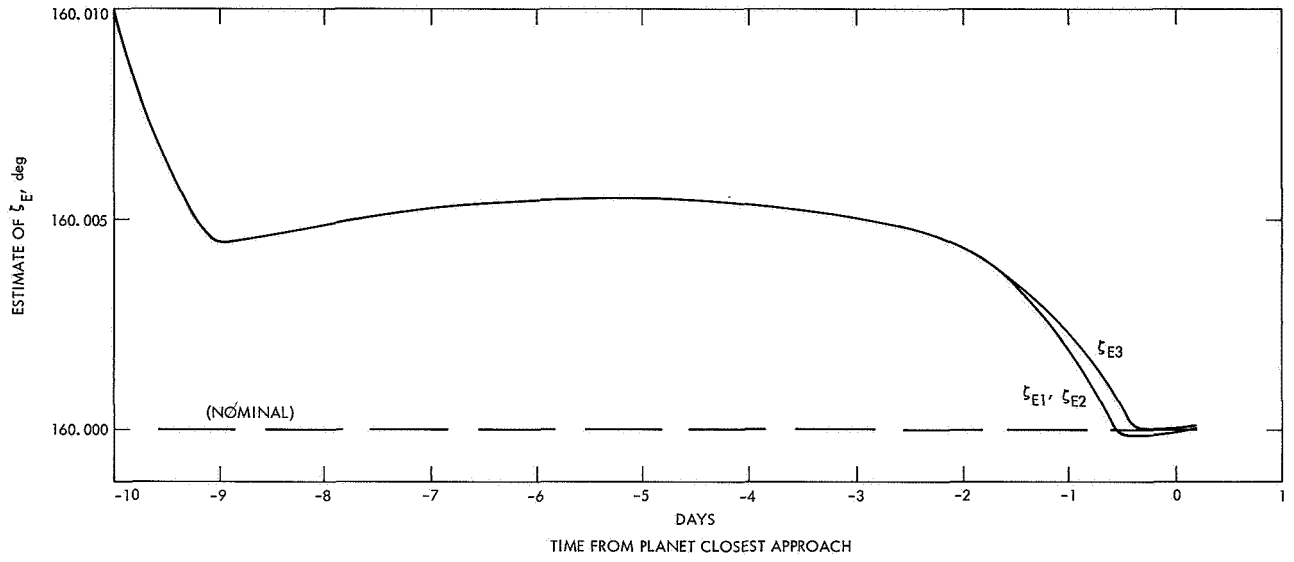

Fig. 53. Estimate of parameter ζ_E vs time from closest approach for $\sigma_{\dot{\rho}} = 0.01$ m/sec

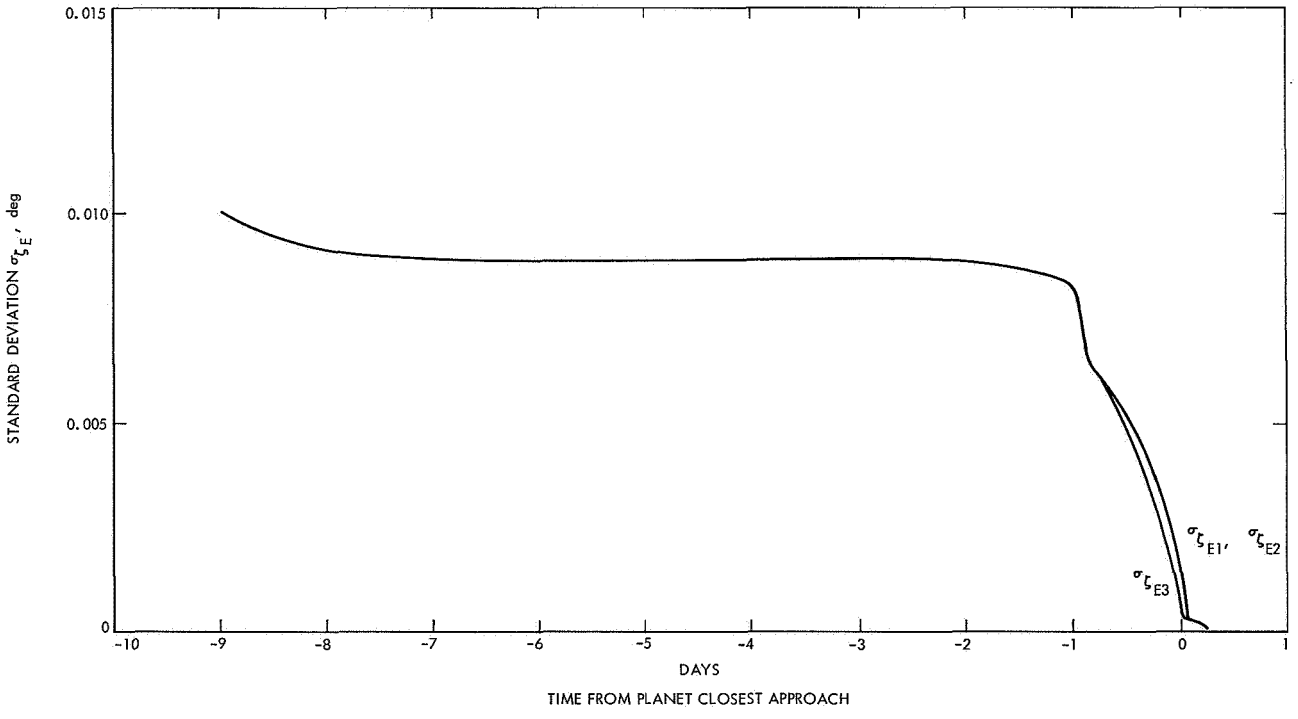

Fig. 54. Standard deviation of parameter ζ_E vs time from closest approach for $\sigma_{\dot{\rho}} = 0.01$ m/sec

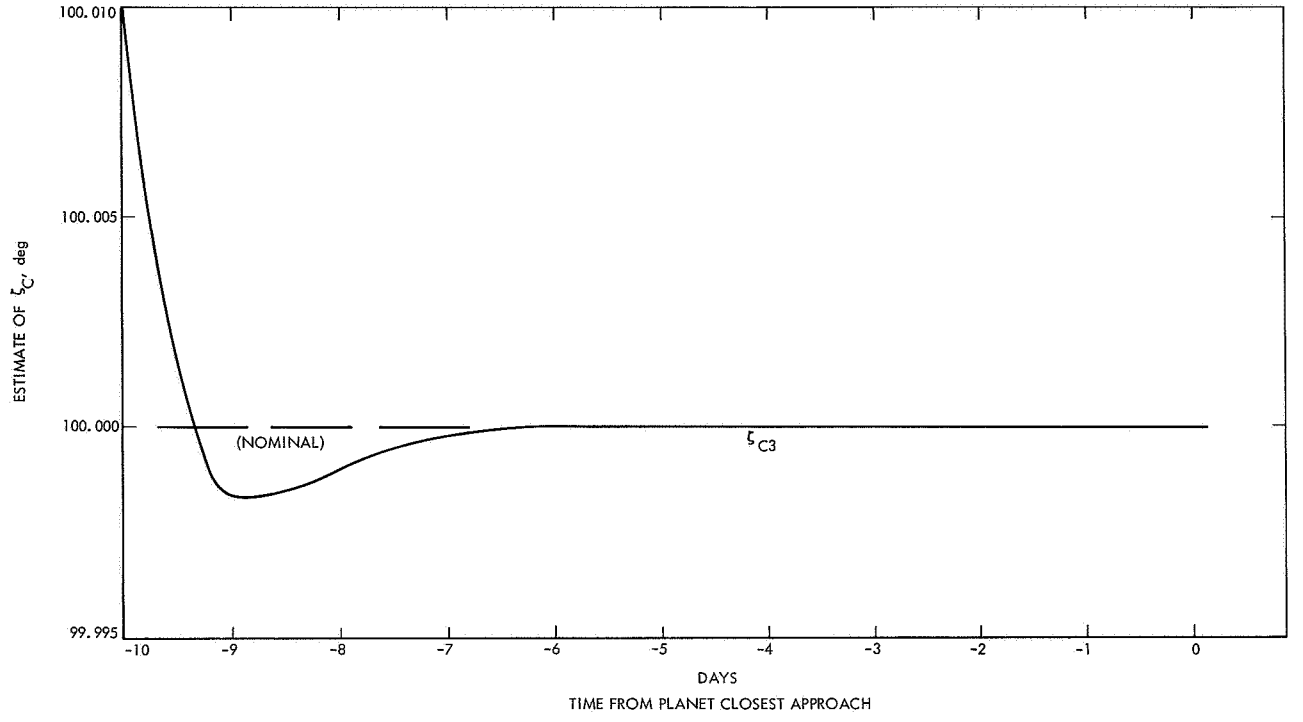

Fig. 55. Estimate of parameter ζ_C vs time from closest approach for $\sigma_{\dot{\rho}} = 0.01$ m/sec

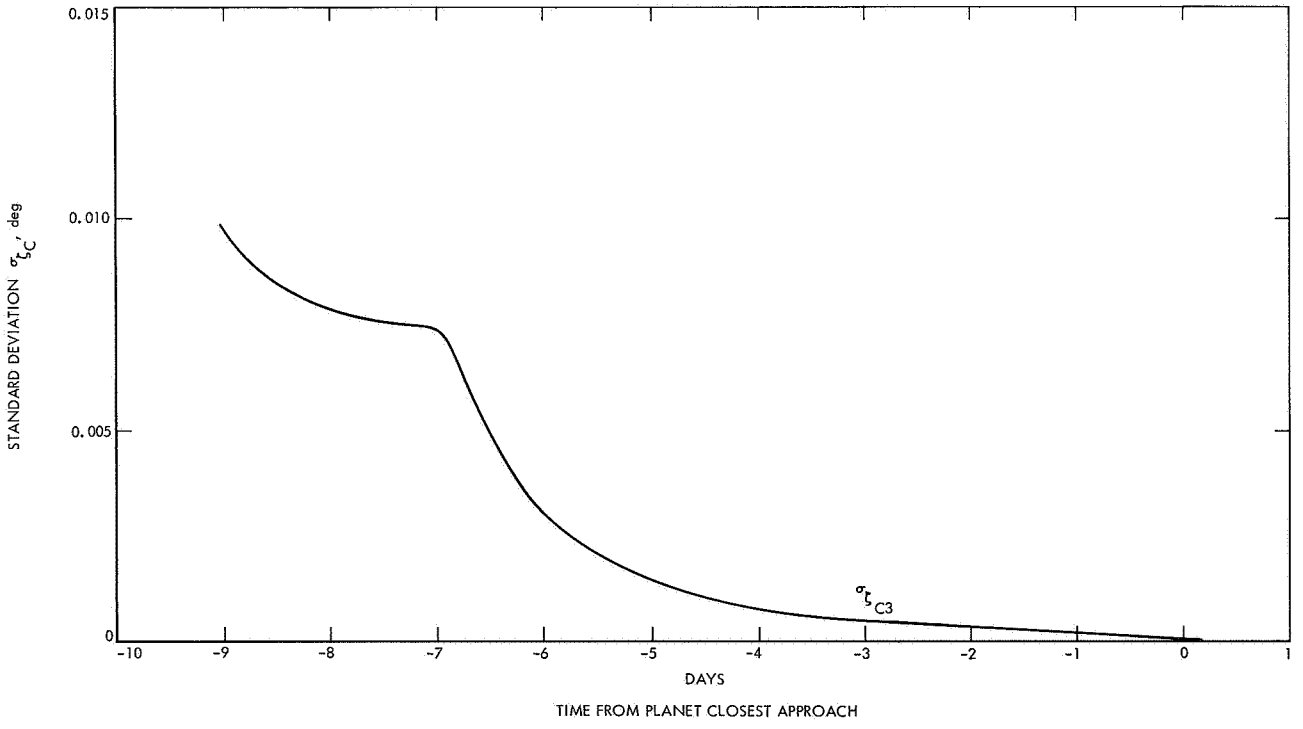

Fig. 56. Standard deviation of parameter ζ_C vs time from closest approach for $\sigma_{\dot{\rho}} = 0.01$ m/sec

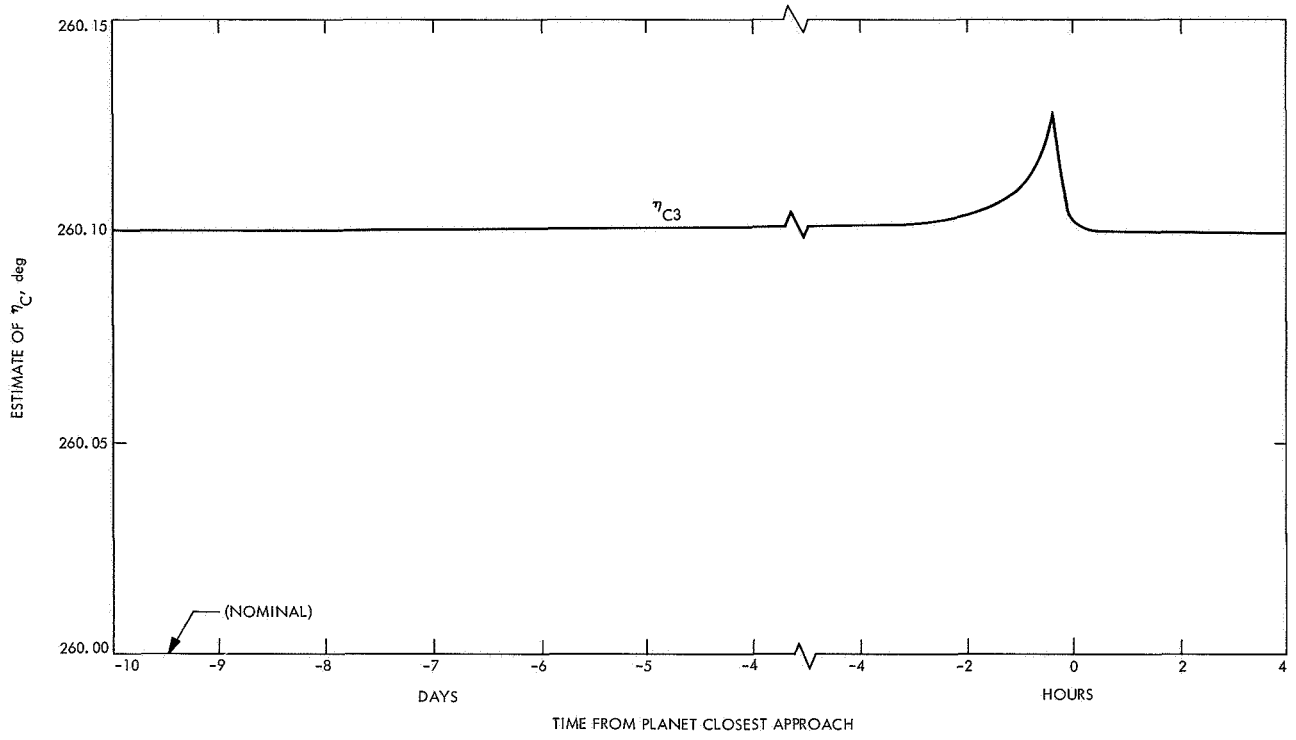

Fig. 57. Estimate of parameter η_C vs time from closest approach for $\sigma_{\dot{\rho}}^{*} = 0.01$ m/sec

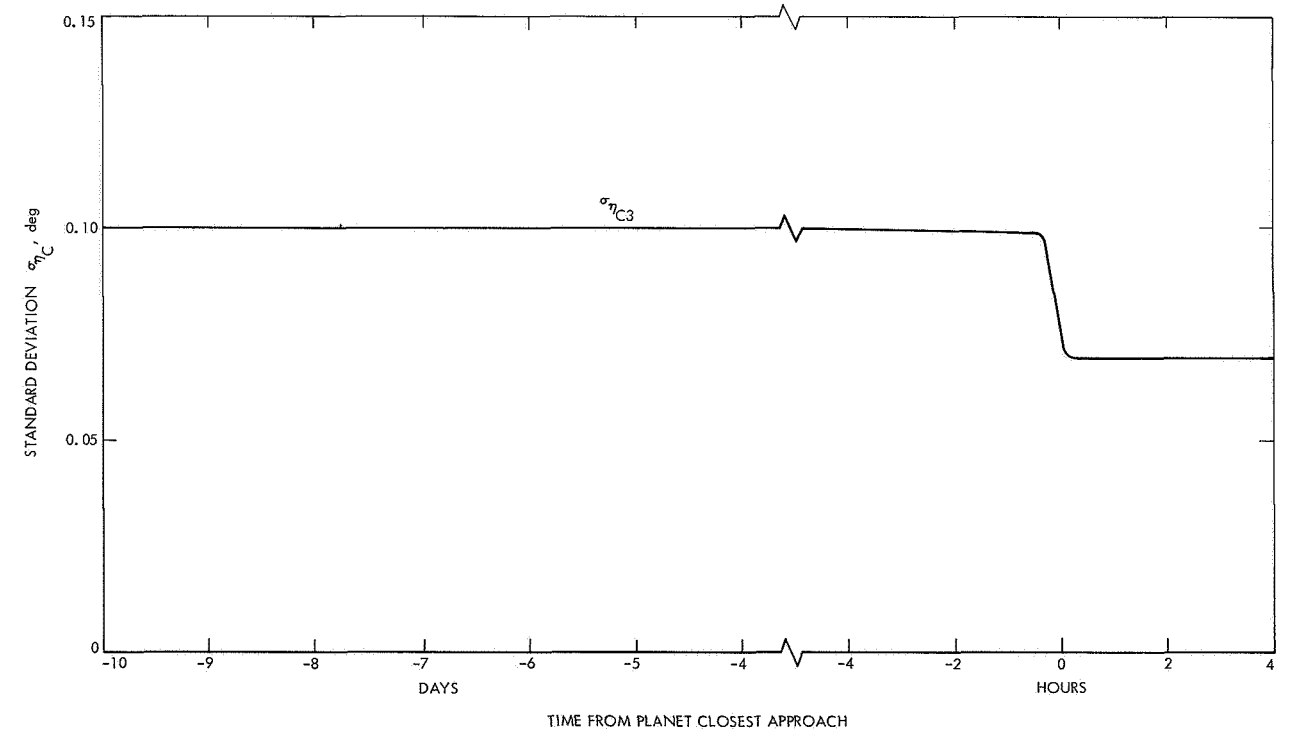

Fig. 58. Standard deviation of parameter η_C vs time from closest approach for $\sigma_{\dot{\rho}}^{*} = 0.01$ m/sec

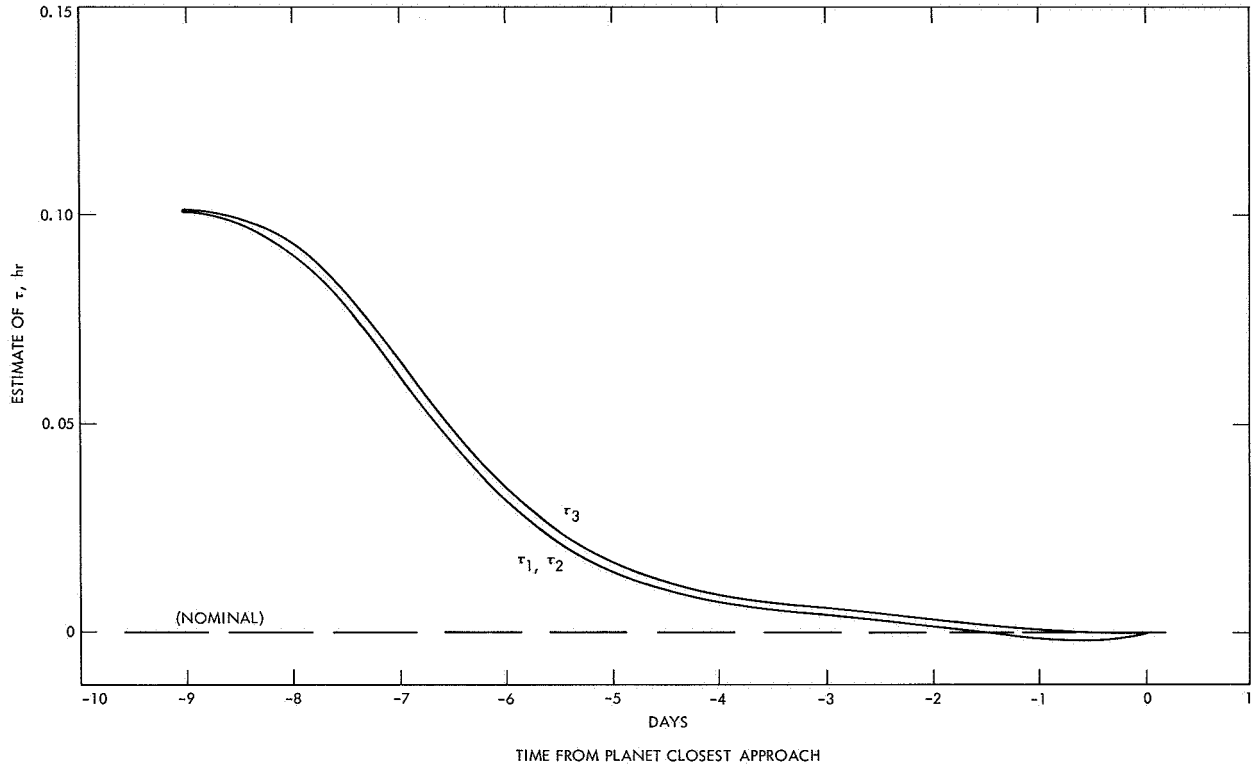

Fig. 59. Estimate of time of periapsis passage τ vs time from closest approach for $\sigma_{\dot{\rho}}^{\bullet} = 0.01$ m/sec

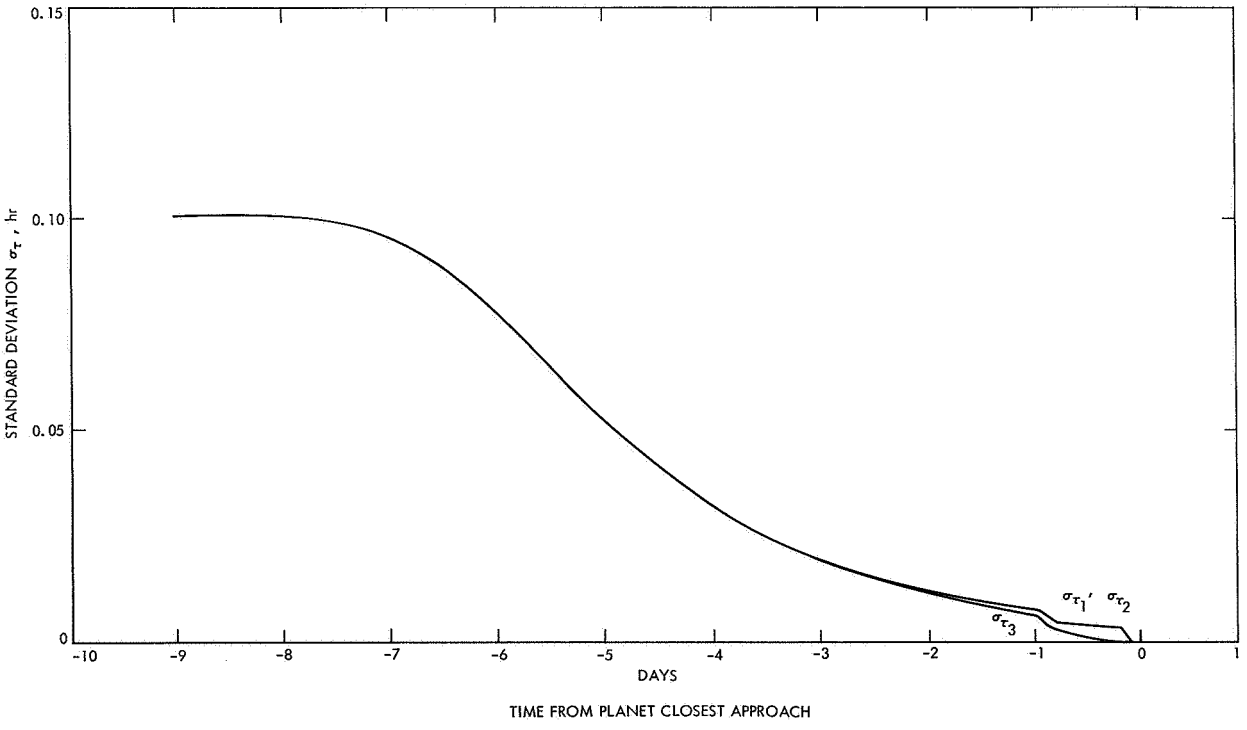

Fig. 60. Standard deviation of time of periapsis passage τ vs time from closest approach for $\sigma_{\dot{\rho}}^{\bullet} = 0.01$ m/sec

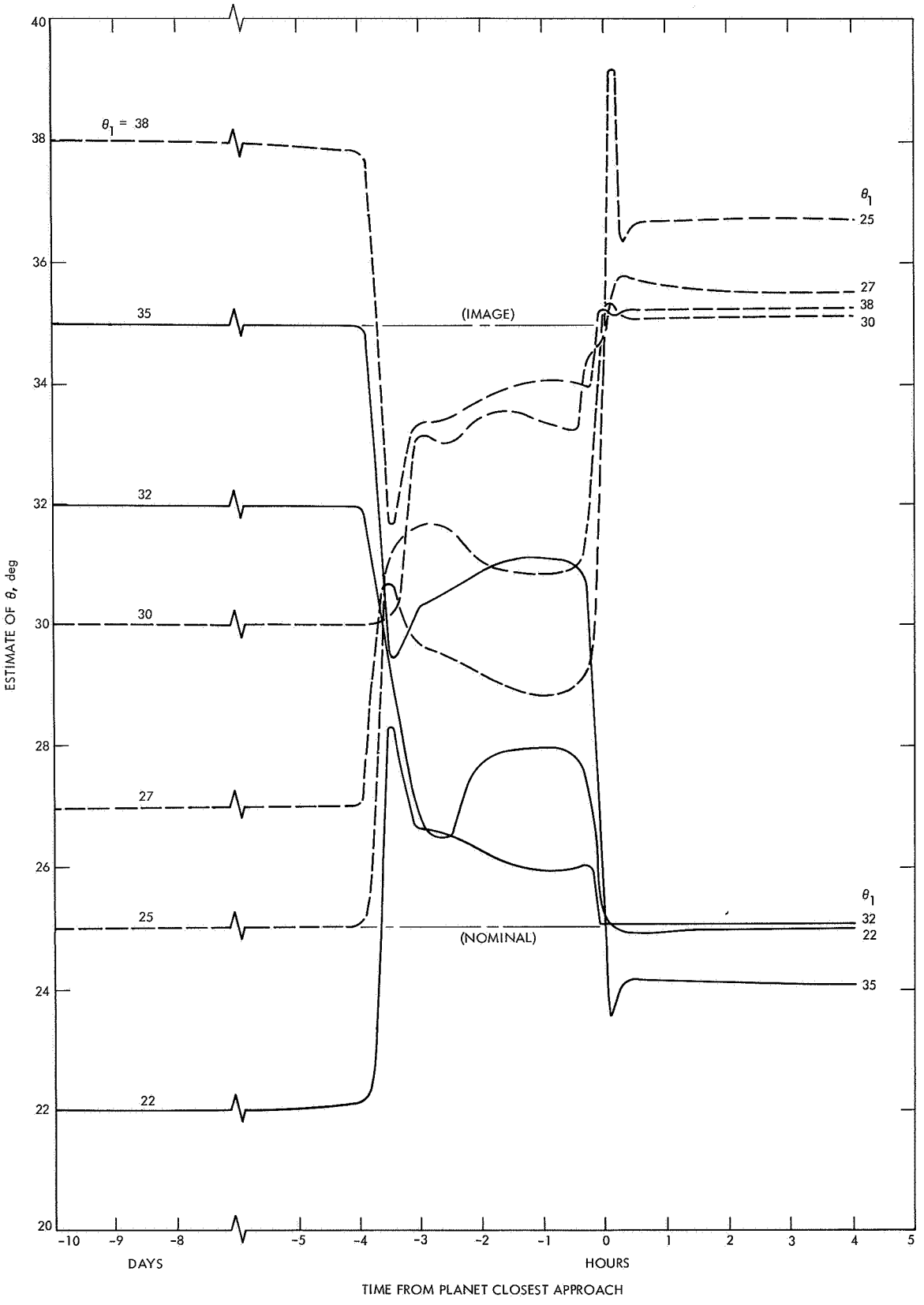

Fig. 61. Estimate of trajectory-plane orientation θ vs time for various initial estimates using $\sigma_{\dot{\rho}} = 0.01$ m/sec

VI. Extension of Range-Rate Equation

A. Derivation of New Range-Rate Equation

In Section II the equation for range rate from earth to the spacecraft was shown to be

$$\dot{\rho} = (-\mathbf{V}_E + \mathbf{V}_P + \mathbf{V}_{S/P}) \cdot \hat{\boldsymbol{\rho}} \tag{36}$$

The unit vector from earth to the spacecraft was expressed as

$$\hat{\boldsymbol{\rho}} = -\cos\zeta_E \hat{\mathbf{S}} + \sin\zeta_E \cos\eta_E \hat{\mathbf{T}} + \sin\zeta_E \sin\eta_E \hat{\mathbf{R}}$$

For the example problem, $\hat{\boldsymbol{\rho}}$ was considered to be fixed for small displacements of the spacecraft near the planet and also as the spacecraft approached the planet. Thus the parameters ζ_E and η_E were fixed. In order to consider a $\hat{\boldsymbol{\rho}}$ that is not fixed, the form of the range-rate equation will be changed to reveal more insight into the geometry. Range rate can then be expressed as

$$\dot{\rho} = \frac{(-\mathbf{V}_E + \mathbf{V}_P + \mathbf{V}_{S/P})}{\rho} \cdot \hat{\boldsymbol{\rho}} \tag{37}$$

The vector $\boldsymbol{\rho}$ is defined as

$$\boldsymbol{\rho} = \mathbf{R}_P + \mathbf{r} \tag{38}$$

where

$\mathbf{R}_P$ = vector from the earth-based observer to the planet at a given time T

$\mathbf{r}$ = radius vector from the planet to the spacecraft at the given time T

From Eq. (15),

$$\mathbf{r} = -r\cos\alpha \hat{\mathbf{S}} + r\sin\alpha\cos\theta \hat{\mathbf{T}} + r\sin\alpha\sin\theta \hat{\mathbf{R}}$$

The vector from the earth to the planet is expressed in a similar manner to that of Eq. (3), which is

$$\mathbf{R}_P = (\mathbf{R}_P \cdot \hat{\mathbf{S}})\hat{\mathbf{S}} + (\mathbf{R}_P \cdot \hat{\mathbf{T}})\hat{\mathbf{T}} + (\mathbf{R}_P \cdot \hat{\mathbf{R}})\hat{\mathbf{R}} \tag{39a}$$

where

$$\left.\begin{aligned} \mathbf{R}_P \cdot \hat{\mathbf{S}} &= R_P\{-\cos\zeta_P\} \\ \mathbf{R}_P \cdot \hat{\mathbf{T}} &= R_P\{\sin\zeta_P\cos\eta_P\} \\ \mathbf{R}_P \cdot \hat{\mathbf{R}} &= R_P\{\sin\zeta_P\sin\eta_P\} \end{aligned}\right\} \tag{39b}$$

and

$$R_P = |\mathbf{R}_P|$$

The parameters ζ_P and η_P define the direction from the observer to the planet at a given time T. These differ slightly from ζ_E and η_E, which define the direction from observer to spacecraft. Let

$$\left.\begin{aligned} V_S &= (-\mathbf{V}_E + \mathbf{V}_P) \cdot \hat{\mathbf{S}} \\ V_T &= (-\mathbf{V}_E + \mathbf{V}_P) \cdot \hat{\mathbf{T}} \\ V_R &= (-\mathbf{V}_E + \mathbf{V}_P) \cdot \hat{\mathbf{R}} \end{aligned}\right\} \tag{40}$$

Making the substitutions of Eqs. (10), (15), (38), (39b), and (40) into (37) yields

$$\begin{aligned} \dot{\rho} = &-\frac{V_S}{\rho}(R_P\cos\zeta_P + r\cos\alpha) \\ &+ \frac{V_T}{\rho}(R_P\sin\zeta_P\cos\eta_P + r\sin\alpha\cos\theta) \\ &+ \frac{V_R}{\rho}(R_P\sin\zeta_P\sin\eta_P + r\sin\alpha\sin\theta) \\ &- \frac{R_P}{\rho}V_\infty\cos\zeta_P \\ &+ \frac{R_P}{\rho}\frac{\mu}{bV_\infty}\{\sin\zeta_P\cos(\eta_P - \theta)[\cos\alpha - 1] - \cos\zeta_P\sin\alpha\} \end{aligned} \tag{41}$$

Notice that Eq. (41) has a similar form to the simplified range-rate Eq. (12), except ζ_P and η_P replace ζ_E and η_E. The parameters ζ_P and η_P vary slightly with time, but only depend on the position of the planet with respect to earth. Moving or displacing the spacecraft in space does not affect these two parameters. For the new expression of Eq. (41), $\dot{\rho}$ is dependent on θ by expressions other than $\cos(\eta_P - \theta)$. Thus the time history of $\dot{\rho}$ past the planet will no longer have the precise identical values for $\pm(\eta_P - \theta)$ for every approach direction of the trajectory; however, they will be very close. As the direction of the approach asymptote is varied, the closeness of the two range-rate histories for $\pm(\eta_P - \theta)$ will vary. This will be discussed further in Section VI-B.

The range ρ from the earth to the spacecraft given in Eq. (41) can be expressed as follows:

$$\begin{aligned} \rho &= [\boldsymbol{\rho} \cdot \boldsymbol{\rho}]^{1/2} \\ \rho &= [(\mathbf{R}_P + \mathbf{r}) \cdot (\mathbf{R}_P + \mathbf{r})]^{1/2} \\ \rho &= [R_P^2 + r^2 + 2\mathbf{r} \cdot \mathbf{R}_P]^{1/2} \end{aligned}$$

Substituting Eqs. (15) and (39) into the above expression yields

$$\rho = [R_P^2 + r^2 + 2r R_P \cos\alpha \cos\zeta_P + 2r R_P \sin\alpha \sin\zeta_P \cos(\eta_P - \theta)]^{1/2} \tag{42}$$

Notice in Eq. (42), for earth-to-spacecraft range ρ, that θ only appears in the form $\cos(\eta_P - \theta)$. Thus the range ρ history *will* have the same values for $\pm(\eta_P - \theta)$. Thus if range is used as an observable, a problem similar to that encountered for range rate will occur in determining whether $\theta = \theta_1$, or $\theta = 2\eta_P - \theta_1$.

B. Survey of Various Directions of the Approach Asymptote $\hat{S}$

Upon surveying the effects on range rate of various approach directions of the spacecraft at the planet, it was found that if the approach asymptote $\hat{S}$, direction from earth to planet $\mathbf{R}_P$, and velocity of planet with respect to earth $(-\mathbf{V}_E + \mathbf{V}_P)$ are all coplanar, $\dot{\rho}$ will again depend on θ only in the form of $\cos(\eta_P - \theta)$. The coplanar relationship desired is demonstrated in Fig. 62. The requirement for the coplanar relationship is

$$\tan\eta_P = \frac{(-\mathbf{V}_E + \mathbf{V}_P)\cdot\hat{R}}{(-\mathbf{V}_E + \mathbf{V}_P)\cdot\hat{T}} = \frac{V_R}{V_T} \tag{43}$$

where $0 \leq \eta_P \leq 2\pi$. Recall that η_P is defined as the angle from the $\hat{T}$ axis to the projection of $\mathbf{R}_P$ onto the $\hat{R}, \hat{T}$ plane. If the value for V_T in Eq. (43) is substituted into Eq. (41), the result is

$$\begin{aligned}\dot{\rho} = &-\frac{V_S}{\rho}(R_P\cos\zeta_P + r\cos\alpha) \\ &+ \frac{V_R}{\rho\sin\eta_P}[R_P\sin\zeta_P + r\sin\alpha\cos(\eta_P - \theta)] \\ &- \frac{R_P V_\infty \cos\zeta_P}{\rho} \\ &+ \frac{R_P}{\rho}\frac{\mu}{bV_\infty}\{\sin\zeta_\rho\cos(\eta_P - \theta)[\cos\alpha - 1] - \cos\zeta_P\sin\alpha\}\end{aligned} \tag{44}$$

The result derived is the range rate from earth to the spacecraft when the following three vectors are coplanar: (1) the instantaneous radius vector $\mathbf{R}_P$ from earth to the planet; (2) the instantaneous velocity of the planet with respect to earth $(-\mathbf{V}_E + \mathbf{V}_P)$; (3) the direction of the approach asymptote $\hat{S}$ of the spacecraft at the planet.

At the time T when the coplanar relationship exists, note from Eq. (44) that $\dot{\rho}$ is only dependent on θ by the function of $\cos(\eta_P - \theta)$. Thus at this time T, $\dot{\rho}$ will have the same value for $\pm(\eta_P - \theta)$. The parameter ζ_P will be identically the same for any value of η_P or θ at a given time T.

If the coplanar relationship exists during the entire approach of the spacecraft to the planet, then at *any* time T, $\dot{\rho}$ will have the same value for $\pm(\eta_P - \theta)$, since η_P will then be constant. This coplanar relationship will exist at *any* time T if: (1) the velocity of the planet with respect to earth $(-\mathbf{V}_E + \mathbf{V}_P)$ is constant; or (2) if the change of this velocity with time remains in the same plane, i.e., the plane that contains the instantaneous velocity and the planet-to-earth vector. Both of these conditions are approximately satisfied. The velocity of the planet with respect to the earth $(-\mathbf{V}_E + \mathbf{V}_P)$ will change very little over a time interval of a few days; the small velocity change that does occur over this time interval will be nearly directed in the plane that contains the instantaneous velocity $(-\mathbf{V}_E + \mathbf{V}_P)$ and the earth-to-planet direction. The latter should be true if the inclinations of the heliocentric trajectory planes of the earth, the spacecraft, and the target planet are separated by only a few degrees, which is usually the case for low-energy ballistic trajectories to most of the planets.

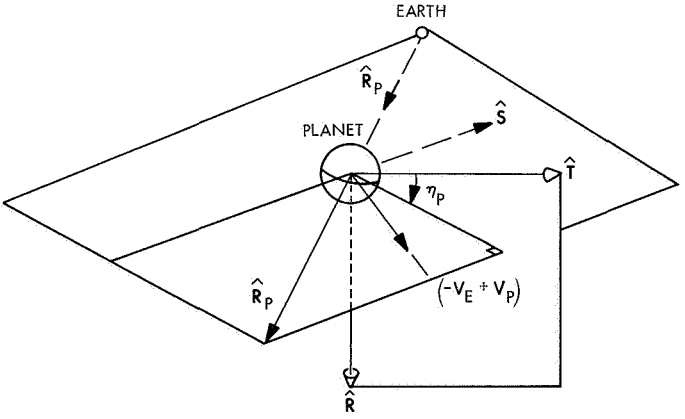

Fig. 62. Description of coplanar relationship

VII. Conclusions and Extensions of Work

A. Conclusions

The analytical study presented in this report may be summarized as follows:

1. Simple analytical equations are derived for the range rate of the spacecraft with respect to the earth during the planetary approach phase. Also, simple analytical equations are derived for a spacecraft-centered angle between a body and the target planet. These expressions enable various orbit-determination studies to be easily performed.

2. The geometrical symmetry of the earth-to-spacecraft range-rate time history was pointed out for trajectory-plane orientations on either side of the plane that contains the earth, the planet, and the direction of the approach asymptote of the near-planet trajectory. The assumption made is that the radius vector from earth to spacecraft remains constant during the planetary approach. An extension of the analysis is shown in Section VI where the earth-to-spacecraft radius varies with aiming point and with time.

3. Prior to this investigation, it was thought that the spacecraft range and range-rate time history past the planet was unique for every planet-centered trajectory-plane orientation or inclination chosen.

4. The range-rate partial derivatives are derived for the case where the observer is located at the center of the earth, and the earth-to-spacecraft position vector is fixed during the approach phase and for displacements of the spacecraft as a result of rotating the trajectory plane.

From the numerical results presented in Sections V and VI, the following conclusions can be drawn:

1. Under the assumptions that the observer is located at the center of the earth and the spacecraft position vector relative to the earth is fixed, an orbit-determination program using range rate as an observable can converge to the incorrect image solution of the trajectory orientation θ when the initial estimated value of θ is such that the *a priori* dispersions of θ encompass both the image and the nominal values of θ.

2. The incorrect convergence can take place regardless of the size of the standard deviation of the data noise.

3. By adding another observable, such as a spacecraft-centered angle between a star and the target planet, the program will converge to the correct nominal orientation of the trajectory plane.

4. If the earth-to-spacecraft radius is not fixed near the target planet, then the earth-to-spacecraft range-rate time history will no longer be identical for $\pm(\eta_P - \theta)$, equal values of the trajectory orientation selected about the earth, planet, and approach-asymptote plane.

5. An orbit-determination program might still converge to the incorrect trajectory orientation, however, since the differences are small. This is an area for further study.

6. A special direction of the approach asymptote at the planet could still exist, however, which would again make the range-rate time history identical for equal values of the trajectory-plane orientation $\pm(\eta_P - \theta)$ symmetric about the earth, planet, and approach-asymptote plane. This approach direction must be such that the approach asymptote, the planet-to-earth vector, and the velocity of the planet with respect to earth are all coplanar. This situation occurs for specific trajectories to Mars in 1971. However, possible convergence to the incorrect trajectory orientation has not been demonstrated for this special situation and is also an area for further study.

7. The geometrical symmetry of the earth-to-spacecraft range ρ was pointed out with the trajectory-plane orientation $\pm(\eta_P - \theta)$ on either side of the plane that contains the earth, the planet, and the direction of the approach asymptote with respect to the planet. Thus the earth-to-spacecraft range was discarded as an additional observable in this investigation, since no additional knowledge would be gained in knowing which of the two trajectory planes the spacecraft might be on.

B. Recommendations for Further Study

The estimation of the trajectory orientation and the study of its incorrect convergence should be performed using a more precise model. The author considers this report to be only the first step. Additional steps to obtain a more precise model are as follows:

1. Include a non-fixed direction from earth to the spacecraft when the spacecraft is near the target planet. Preliminary equations for this step are derived in Section VI.

2. Examine various directions of the spacecraft's approach asymptote at the target planet. One special direction to examine is that in which the approach asymptote, the planet-to-earth vector, and the velocity of planet with respect to earth are all coplanar.[6]

[6]This geometrical relationship exists for typical trajectories from earth to Mars in 1971.

3. Include one or more rotating observers on the surface of the earth instead of putting the observer at the center of the earth.

4. Include additional orbit-determination uncertainties in the study, such as an uncertainty in the gravitational constant of the planet, ephemeris uncertainties of the planet, station-location uncertainties of the observer on the surface of the earth, and the inclusion of data noise on the observables.

If incorrect convergence still results for the trajectory-plane orientation after including the above changes to the model, additional observables can be utilized to alleviate the situation as was done in this report. Another possible method of alleviating the situation might be to start the estimation procedure near both the image and the nominal trajectory orientation and to compare the sum of the square of the residuals for the two converged cases. The converged trajectory with the lowest sum of the square of the residuals would then be assumed to be the correct one, since for this case the calculated trajectory would agree more nearly with the observed trajectory.[7]

[7]This method was suggested by several engineers at the Jet Propulsion Laboratory. Its feasibility is being studied by K. Russell.

Appendix A

Description of Approach Asymptote and Hyperbolic Excess Velocity

According to the two-body problem, the path of one body with respect to another due to the mutual gravitational attraction of the two bodies is an ellipse, parabola, or a hyperbola. If the motion of a small body (such as a spacecraft) originates outside the gravitational influence of the other body (such as a planet), the path of the spacecraft with respect to the planet will be that of a hyperbola with the planet located at the focus. The incoming asymptote of this hyperbolic path is called the approach asymptote. The speed of the spacecraft with respect to the planet as it enters the gravitational influence of the planet is called the hyperbolic excess speed. At this time the direction of the spacecraft velocity with respect to the planet is along the approach asymptote.

The direction and magnitude of the hyperbolic excess velocity is determined by subtracting the heliocentric velocity vector of the spacecraft at that time from the heliocentric velocity of the planet as shown in Fig. A-1. If $\mathbf{V}_\infty = \mathbf{V} - \mathbf{V}_P$, where $V_\infty = |\mathbf{V}_\infty|$, then $\hat{\mathbf{S}}$ is defined as

$$\hat{\mathbf{S}} = \frac{\mathbf{V}_\infty}{V_\infty}$$

The velocities of the spacecraft with respect to the sun and planet at arrival are uniquely determined for a given launch date at earth and arrival date at the planet. This is true because the heliocentric path of the spacecraft is uniquely determined by two radii from the sun to spacecraft and the total transit time between the two points (Lambert's theorem). The two radii correspond to the heliocentric position vectors of the earth and planet at launch and arrival, respectively.

Fixing the heliocentric trajectory of the spacecraft will then determine the heliocentric velocity $\mathbf{V}$ of the spacecraft anywhere along its path. At a given time the velocity of the planet $\mathbf{V}_P$ is known. Thus the hyperbolic excess velocity, $\mathbf{V}_\infty = \mathbf{V} - \mathbf{V}_P$, of the spacecraft with respect to the target planet is uniquely determined by the launch date at earth and arrival date at the planet. A small uncertainty in this velocity will exist due to the various perturbing influences and uncertainties. The hyperbolic excess velocity is almost constant, independent of which side of the planet the spacecraft will pass. Changing the flyby pass will change the heliocentric position of the spacecraft at arrival by only a fraction of a percent. This small change will alter the spacecraft heliocentric velocity at arrival and thus the hyperbolic excess velocity by an infinitesimal amount.

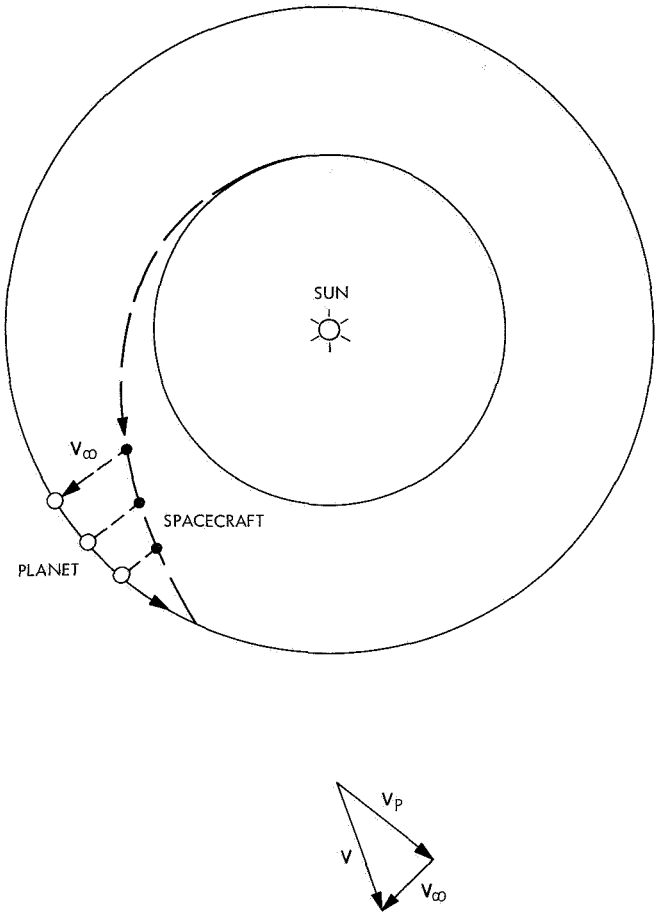

Fig. A-1. Description of approach asymptote and hyperbolic excess velocity

Appendix B

Derivation of Radius Equation

The radius of the spacecraft from the target planet can be expressed in terms of the target-centered angle α from the approach-asymptote direction to the spacecraft. This angle is more convenient than true anomaly ν in the presentation of the results. The hyperbolic conic equation for planet-to-spacecraft radius is

$$r = \frac{b^2}{a(1 + e\cos\nu)} \tag{B-1}$$

From Fig. B-1

$$\nu = \alpha - \gamma \tag{B-2}$$

The angle γ is equal to the true anomaly ν of the spacecraft when the spacecraft is an infinite distance away ($r \to \infty$). Making this substitution into Eq. (B-1) yields

$$\cos\gamma = -\frac{1}{e} \tag{B-3}$$

where $(0 \leq \gamma \leq \pi)$. Thus

$$\sin\gamma = \sqrt{1 - \cos^2\gamma} \tag{B-4}$$

Substituting Eq. (B-3) into (B-4) yields

$$\sin\gamma = \sqrt{\frac{e^2 - 1}{e}} \tag{B-5}$$

Substituting Eqs. (B-2), (B-3), and (B-5) into (B-1) yields

$$r = \frac{b^2}{a(1 + \sqrt{e^2 - 1}\sin\alpha - \cos\alpha)} \tag{B-6}$$

From analytical geometry

$$c^2 = a^2 + b^2 \tag{B-7}$$

Also

$$c = ae \tag{B-8}$$

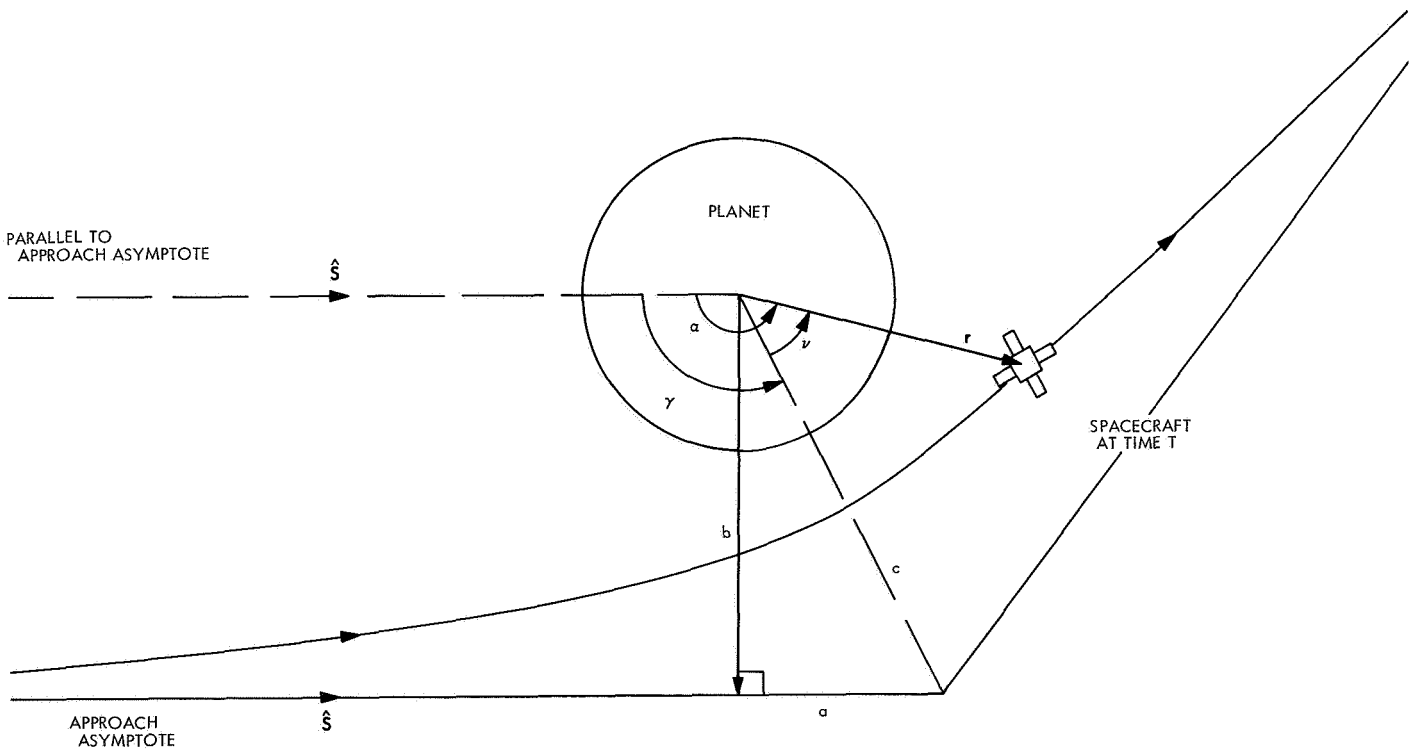

Fig. B-1. Definition of hyperbolic elements

Substituting Eq. (B-8) into B-7) yields

$$\sqrt{e^2 - 1} = \frac{b}{a} \tag{B-9}$$

Substituting Eq. (B-9) into (B-6) yields

$$r = \frac{b^2}{a\left(1 + \frac{b}{a}\sin\alpha - \cos\alpha\right)} \tag{B-10}$$

References

1. Trask, D. W., "DSIF Data Types and Tracking Modes," in *The Deep Space Network*, Space Programs Summary 37-33, Vol. III, pp. 6–7, Jet Propulsion Laboratory, Pasadena, Calif., May 31, 1966.
2. Breckenridge, W. G., "Approach Guidance Accuracy Studies," in *Supporting Research and Advanced Development*, Space Programs Summary 37-23, Vol. 14, pp. 32–36, Jet Propulsion Laboratory, Pasadena, Calif., Oct. 31, 1963.
3. Gates, C. R., and Gordon, H. J., *Planetary Approach Guidance*, Technical Report 32-631, Jet Propulsion Laboratory, Pasadena, Calif., June 30, 1964.
4. Kizner, W., *A Method of Describing Miss Distances for Lunar and Interplanetary Trajectories*, External Publication 674, Jet Propulsion Laboratory, Pasadena, Calif., Aug. 1, 1959.
5. Kalman, R. E., "A New Approach to Linear Filtering and Prediction Problems," *Trans. ASME, Ser. D: J. Basic Eng.*, Vol. 82, pp. 35–50, 1960.
6. Anderson, J. D., *Theory of Orbit Determination—Part II, Estimation Formulas*, Technical Report 32-498, Jet Propulsion Laboratory, Pasadena, Calif., Oct. 1, 1963.

Bibliography

Anderson, J. D., "Trajectory Determination From Observational Data," *Science and Technology Series*, Vol. 9, pp. 133–158, 1966.

Bollman, W. E., "The Engineering Design of Interplanetary Ballistic Trajectories," AIAA Paper 63-414, presented at Yale University, Aug. 19–21, 1963.

Brouwer, D., and Clemence, G. M., *Celestial Mechanics*, Academic Press, New York and London, 1961.

Clarke, V. C., Bollman, W. E., Roth, R. Y., and Scholey, W. J., *Design Parameters for Ballistic Interplanetary Trajectories, Part I. One Way Transfers to Mars and Venus*, Technical Report 32-77, Jet Propulsion Laboratory, Pasadena, Calif., Jan. 16, 1963.

Warner, M. R., Nead, M. W., and Hudson, R. H., *The Orbit Determination Program of the Jet Propulsion Laboratory*, Technical Memorandum 33-168, Jet Propulsion Laboratory, Pasadena, Calif., Mar. 18, 1964.